UNIVERSITY OF WARMIA AND MAZURY IN OLSZTYN

Technical Sciences

18(4) 2015

PUBLISHER UWM

OLSZTYN 2015

The Technical Sciences is indexed and abstracted in BazTech (http://baztech.icm.edu.pl) and in IC Journal Master List (http://journals.indexcopernicus.com)

The Journal is also available in electronic form on the web sites
http://www.uwm.edu.pl/techsci (subpage Issues)
http://wydawnictwo.uwm.edu.pl (subpage Czytelnia)

The print edition is the primary version of the Journal

PL ISSN 1505-4675

Address
ul. Jana Heweliusza 14
10-718 Olsztyn-Kortowo, Poland
tel.: +48 89 523 36 61
fax: +48 89 523 34 38
e-mail: wydawca@uwm.edu.pl

Ark. wyd. 7,4, ark. druk. 6,0, nakład 85 egz.
Druk – Zakład Poligraficzny UWM w Olsztynie
zam. nr 76

Contents

Biosystem Engineering

Civil Engineering

Geodesy and Cartography

Information Technology

Technical Sciences 18(4), 2015, 237–246

ASSESSMENT OF CEREAL SEED SHAPE WITH THE USE OF SPHERICITY FACTORS

Zdzisław Kaliniewicz, Justyna Biedulska, Beata Jadwisieńczak

Department of Heavy Duty Machines and Research Methodology
University of Warmia and Mazury in Olsztyn

Received 8 June 2014; accepted 10 November 2015; available on line 24 November 2015.

Key words: seeds, dimensions, mass, shape, correlations.

Abstract

Shape is one of the key discriminating factors in seeds. It plays a major role in seed cleaning and sorting, and it influences the bulk behavior of seeds. The shape of seeds can be described with the use of sphericity factors. In this study, the thickness, width, length and mass of principal cereal seeds (wheat, rye, barley, oats and triticale) were determined. The geometric parameters of seeds were used to calculate five sphericity factors for each seed type. The results of measurements and calculations were processed statistically by analysis of variance, correlation analysis and linear regression analysis. In the group of the analyzed cereal seeds, the lowest values were noted for sphericity factor K_5 in the range of 0.046 to 0.275, and the highest values – for sphericity factor K_3 in the range of 0.359 to 0.650. The shape of cereal seeds was mostly highly correlated with: thickness in barley seeds, width in wheat seeds, width and thickness in rye and triticale seeds, and length in oat seeds. All of the analyzed sphericity factors can be used interchangeably to describe the shape of cereal seeds, and the relationships between those factors can be described with linear equations.

Symbols

K_1 – sphericity factor describing the ratio of seed thickness to seed length,
K_2 – sphericity factor describing the ratio of seed width to seed length,
K_3 – sphericity factor describing the ratio of geometric mean diameter to seed length,
K_4, K_5 – sphericity factors describing the ratio of seed thickness and seed width to seed length,
L – seed length, mm,
T – seed thickness, mm,
W – seed width, mm.

Correspondence: Zdzisław Kaliniewicz, Katedra Maszyn Roboczych i Metodologii Badań, Uniwersytet Warmińsko-Mazurski, ul. Oczapowskiego 11/B112, 10-719 Olsztyn, phone: +48 89 523 39 34, e-mail: zdzislaw.kaliniewicz@uwm.edu.pl

Introduction

Cereals are the most common crops in Poland and worldwide. Cereal seeds can be used for sowing crop plants, for energy production and, above all, as raw materials for animal feed and food production. Cereal production involves various processes, including sowing, harvest, transport, cleaning, sorting, storage and processing. A sound knowledge of the physical properties of processed materials is required at every stage of the production process and during modeling (HEBDA, MICEK 2007, ZDYBEL et al. 2009, BOAC et al. 2010, KUSIŃSKA et al. 2010, KALKAN, KARA 2011, MARKOWSKI et al. 2013, SOLOGUBIK et al. 2013).

Shape is one of the key discriminating factors in seeds, which enables to distinguish one type of seeds from another. It plays a major role in seed cleaning and sorting, and it influences the bulk behavior of seeds (seed shape determines the angle of repose). Seed shape can be described in three ways: by comparing a seed to a geometric figure, by calculating the shape factor, and with the use of virtual models (FRĄCZEK, WRÓBEL 2006). In the simplified method, the shape of a seed is compared to a geometric figure. The most common seed shapes include spherical, ellipsoid, lenticular, pyramidal and polyhedral (GROCHOWICZ 1994, FRĄCZEK, WRÓBEL 2006). More detailed evaluations of seed shape involve virtual models which are developed with the use of parametric equations or by modeling real-world objects in virtual space (JAIN, BAL 1997, MABILLE, ABECASSIS 2003, FRĄCZEK, WRÓBEL 2006, MIESZKALSKI, SOŁODUCHA 2008). Virtual models preserve shape features characteristic of a given species, but they require specialist applications and are, therefore, rarely used. The shape of seeds is generally described with the use of shape factors of varied complexity (FRĄCZEK, WRÓBEL 2006). The formulas of shape factors are based primarily on the geometric parameters of seeds. The greater the similarity between the described parameters, the more likely the shape factor is to approximate 1% or 100%. Since the value of the sphericity factor describing ideally spherical seeds and cuboid seeds is the same, FRĄCZEK and WRÓBEL (2006) proposed to describe the shape of seeds by determining the sphericity factor and the type of geometric figure which most closely resembles the analyzed seeds.

In the literature, various mathematical formulas are given for describing the sphericity factors of seeds (MOHSENIN 1986, GROCHOWICZ 1994, FRĄCZEK, WRÓBEL 2006, TYLEK 2010). For this reason, the results presented by different authors cannot always be reliably compared.

The objective of this study was to determine the range of variation in five sphericity factors of cereal seeds, to determine the effect of seed dimensions and seed mass on sphericity factors, and to determine the relationships between the analyzed sphericity factors.

Materials and Methods

The experimental material comprised seeds of primary cereals (wheat var. Nawra, rye var. Dańkowskie Złote, barley var. Skarb, oats var. Kasztan and triticale var. Atletico), harvested in north-eastern Poland. The relative moisture content of the evaluated seeds was determined on a drying scale with a 50/WH halogen lamp at: wheat – 12.8%, rye – 12.5%, barley – 12.6%, oats – 11.4% and triticale – 13.2%. The survey sampling method was used to randomly select 120 seeds from seed samples of 2 kg each. Standard error of the estimate did not exceed 0.25 mm for the three basic seed dimensions and 2.5 mg for seed mass.

Basic dimensions were determined using an MWM 2325 workshop microscope (length and width) to the nearest 0.02 mm and a thickness gauge to the nearest 0.01 mm, and seed mass was determined on a WAA 100/C/2 weighing scale to the nearest 0.1 mg. The measurements were performed according to the method described by KALINIEWICZ et al. (2011).

The shape of every type of seeds was described by determining the following sphericity factors (MOHSENIN 1986, GROCHOWICZ 1994, TYLEK 2010):

$$K_1 = \frac{T}{L} \tag{1}$$

$$K_2 = \frac{W}{L} \tag{2}$$

$$K_3 = \frac{(T \cdot W \cdot L)^{\frac{1}{3}}}{L} \tag{3}$$

$$K_4 = \frac{T + W}{2L} \tag{4}$$

$$K_5 = \frac{T \cdot W}{L^2} \tag{5}$$

The results of measurements and calculations were processed in the Statistica 10.0 program by one-way ANOVA, correlation analysis and linear regression analysis (RABIEJ 2012) at a significance level of 0.05.

Results and Discussion

The physical parameters of the analyzed cereal seeds are presented in Table 1. The average seed mass of the analyzed cereal varieties was compared with that of other cereal varieties (MABILLE, ABECASSIS 2003, HEBDA, MICEK 2005, 2007, KOCIUBA et al. 2007, ZDYBEL et al. 2009, CACAK-PIETRZAK et al. 2010, CHRZĄSTEK et al. 2010) to reveal that rye seeds were characterized by low plumpness, wheat, barley and triticale seeds – by average plumpness, and oat seeds – by high plumpness. Oat seeds were longest, and wheat seeds were shortest. Thickness and width were highest in barley and lowest in rye seeds. A comparison of the average dimensions of seeds of the analyzed cereal varieties with those of other varieties (MABILLE, ABECASSIS 2003, SEGIT et al. 2003, HEBDA, MICEK 2005, 2007, SADOWSKA, ŻABIŃSKI 2009, ZDYBEL et al. 2009, BOAC et al. 2010, KALKAN, KARA 2011, MARKOWSKI et al. 2013, SOLOGUBIK et al. 2013) revealed similar relationships to those noted in an analysis of seed mass. A comparison of the dimensions of seeds of the same wheat variety demonstrated that the analyzed material was characterized by higher plumpness than that studied by GEODECKI and GRUNDAS (2003).

Table 1

Statistical parameters of the distribution of the physical characteristics of cereal seeds

Seed type	Physical parameter	Value of parameter			Standard deviation
		min.	max	mean	
wheat	thickness [mm]	2.44	3.34	2.87	0.209
	width [mm]	2.52	3.95	3.29	0.305
	length [mm]	5.59	8.29	6.73	0.394
	mass [mg]	26.7	61.4	44.41	8.908
Rye	thickness [mm]	1.75	2.95	2.39	0.245
	width [mm]	1.83	3.43	2.65	0.276
	length [mm]	5.40	9.13	7.49	0.678
	mass [mg]	10.9	46.8	28.67	6.937
Barley	thickness [mm]	2.11	3.38	2.87	0.223
	width [mm]	2.92	4.40	3.84	0.294
	length [mm]	7.37	10.65	9.03	0.653
	mass [mg]	23.4	66.4	45.29	8.620
Oats	thickness [mm]	2.05	2.95	2.55	0.151
	width [mm]	2.44	3.66	3.15	0.249
	length [mm]	7.34	13.70	10.39	1.201
	mass [mg]	16.0	54.4	38.57	8.023
Triticale	thickness [mm]	1.88	3.41	2.70	0.331
	width [mm]	2.07	3.96	3.23	0.382
	length [mm]	5.91	9.27	7.57	0.602
	mass [mg]	14.9	64.5	40.04	11.670

The statistical distribution of sphericity factors characterizing seeds of the analyzed cereal varities is presented in Table 2. The highest mean values of sphericity factors were noted in wheat seeds, and the lowest – in oat seeds. Sphericity factor K_1 ranged from 0.185 to 0.488. Statistically significant differences in the values of K_1 were not observed only in rye and barley seeds. In seeds of rye var. Dańkowskie Złote, the value of factor K_1 was nearly identical to that reported for this variety by FRĄCZEK and WRÓBEL (2006). In seeds of the analyzed cereal varieties, the values of factor K_1 were similar to those noted in other varieties. Considerable similarities were observed in relation to seeds of wheat var. Nawra and Roma (FRĄCZEK, WRÓBEL 2006), seeds of barley var. Skarb, Rastik (SADOWSKA, ŻABIŃSKI 2009) and Rodion (HEBDA, MICEK 2005), and seeds of oat var. Kasztan and Dukat (HEBDA, MICEK 2005). The mean value of the sphericity factor for seeds of wheat var. Nawra was similar to that reported in lentils var. Anita and beans var. Atena (FRĄCZEK, WRÓBEL 2006).

Table 2

Statistical parameters of the distribution of the sphericity factors of cereal seeds

Seed type	Sphericity factor	Value of sphericity factor			Standard deviation
		min.	max	mean	
Wheat	K_1	0.368	0.488	0.426[a]	0.025
	K_2	0.375	0.601	0.489[a]	0.038
	K_3	0.520	0.650	0.592[a]	0.024
	K_4	0.375	0.529	0.458[a]	0.028
	K_5	0.141	0.275	0.209[a]	0.025
Rye	K_1	0.252	0.437	0.319[c]	0.028
	K_2	0.284	0.456	0.354[c]	0.032
	K_3	0.425	0.579	0.483[d]	0.026
	K_4	0.277	0.441	0.337[d]	0.027
	K_5	0.077	0.194	0.114[d]	0.019
Barley	K_1	0.256	0.393	0.318[c]	0.027
	K_2	0.358	0.496	0.426[b]	0.031
	K_3	0.451	0.573	0.513[c]	0.025
	K_4	0.307	0.436	0.372[c]	0.027
	K_5	0.092	0.188	0.136[c]	0.020
Oats	K_1	0.185	0.361	0.248[d]	0.029
	K_2	0.244	0.381	0.306[d]	0.028
	K_3	0.359	0.507	0.423[e]	0.027
	K_4	0.217	0.361	0.277[e]	0.027
	K_5	0.046	0.130	0.076[e]	0.015
Triticale	K_1	0.250	0.433	0.358[b]	0.035
	K_2	0.278	0.524	0.427[b]	0.040
	K_3	0.411	0.596	0.534[b]	0.032
	K_4	0.264	0.463	0.392[b]	0.034
	K_5	0.069	0.211	0.154[b]	0.027

a, *b*, *c*, *d*, *e* – different letters denote statistically significant differences between the values of a given sphericity factor in the analyzed cereal species.

The value of sphericity factor K_2 ranged from 0.244 to 0.601. Similar values of K_2 (statistically non-significant differences) were observed in barley and triticale seeds. The values of K_2 were highly similar in seeds of the following cereal varieties:

– wheat var. Nawra – wheat var. Roma (FRĄCZEK, WRÓBEL 2006) and Ceralio (MARKOWSKI et al. 2013),

– rye var. Dańkowskie Złote – rye var. Amilo (ZDYBEL et al. 2009),

– barley var. Skarb – barley var. Rastik (SADOWSKA, ŻABIŃSKI 2009).

The value of factor K_2 noted in this study was practically identical to that determined by FRĄCZEK and WRÓBEL (2006) who analyzed the shape of seeds of the same rye variety.

In the literature, K_3 is the most widely used sphericity factor. In the group of the analyzed factors, K_3 was characterized by the highest values in the range of 0.359 to 0.650. All of the analyzed cereal species differed significantly in their values of K_3. The value of K_3 describing seeds of wheat var. Nawra was similar to that reported in wheat var. Korweta (MARKOWSKI et al. 2013) and Bayraktar-2000 (KALKAN, KARA 2011) and in seeds of the African star apple (OYELADE et al. 2005). In seeds of barley var. Skarb, the value of factor $K3$ was similar to that reported in seeds of barley var. Scarlett (SOLOGUBIK et al. 2013), blond psyllium (AHMADI et al. 2012) and flaxseed (PRADHAN et al. 2010). In seeds of oat var. Kasztan, the value of K_3 was similar to that reported in edible squash (PAKSOY, AYDIN 2004).

Sphericity factor K_4 ranged from 0.217 (oat seeds) to 0.529 (wheat seeds). Seeds of all cereal species analyzed in this study differed significantly in values of K_4. Similar relationships between seed types were observed in respect of K_5 which was characterized by the lowest values in the group of the evaluated sphericity factors. K_5 ranged from 0.046 (oat seeds) to 0.275 (wheat seeds).

An analysis of linear correlations between physical parameters (dimensions and mass) and sphericity factors (Tab. 3) revealed that seed shape was most highly correlated with the following parameters:

– thickness in barley seeds,

– width in wheat seeds,

– width and thickness in rye and triticale seeds,

– length in oat seeds.

Parameters which had a negligible effect on sphericity factors were: length in wheat and triticale seeds, width and thickness in oat seeds, and mass in rye seeds. In all cases, the value of the sphericity factor increased with seed thickness and decreased with a rise in seed length. The above results from the applied formulas, and it indicates that the dimensions of cereal seeds do not increase proportionally with an increase in their plumpness. The relationships between the analyzed sphericity factors and physical parameters were similar, which suggests that the evaluated factors can be applied interchangeably to cereal seeds. Nonetheless, the seed shape of other cereal species justifies the use of factors whose formulas account for all three dimensions, namely factors K_3, K_4 and K_5.

Table 3

Coefficients of linear correlation between selected physical parameters and sphericity factors of cereal seeds

Seed type	Physical parameter	Correlation coefficient for:				
		K_1	K_2	K_3	K_4	K_5
Wheat	thickness	**0.609**	**0.421**	**0.560**	**0.549**	**0.557**
	width	**0.370**	**0.781**	**0.670**	**0.685**	**0.670**
	length	**-0.222**	-0.083	-0.159	-0.153	-0.159
	mass	**0.356**	**0.543**	**0.514**	**0.520**	**0.515**
Rye	thickness	**0.543**	**0.246**	**0.440**	**0.427**	**0.429**
	width	**0.244**	**0.564**	**0.446**	**0.456**	**0.433**
	length	**-0.332**	**-0.329**	**-0.362**	**-0.364**	**-0.371**
	mass	**0.181**	0.127	0.174	0.168	0.159
Barley	thickness	**0.611**	**0.474**	**0.579**	**0.566**	**0.569**
	width	**0.272**	**0.533**	**0.415**	**0.433**	**0.408**
	length	**-0.505**	**-0.421**	**-0.489**	**-0.484**	**-0.494**
	mass	**0.323**	**0.372**	**0.367**	**0.368**	**0.357**
Oats	thickness	0.154	0.010	0.096	0.088	0.103
	width	**-0.383**	0.097	-0.175	-0.154	**-0.190**
	length	**-0.851**	**-0.734**	**-0.853**	**-0.847**	**-0.845**
	mass	**-0.350**	-0.106	**-0.251**	**-0.245**	**-0.267**
Triticale	thickness	**0.761**	**0.508**	**0.697**	**0.682**	**0.691**
	width	**0.515**	**0.748**	**0.690**	**0.697**	**0.681**
	length	-0.032	-0.044	-0.036	-0.042	-0.044
	mass	**0.538**	**0.518**	**0.579**	**0.575**	**0.576**

Values in bold denote statistically significant correlations.

All of the analyzed sphericity factors were closely correlated. The above can be inferred by analyzing the coefficients of determination in regression equations of pairs of values (Tab. 4). In the combined population of seed batches representing five cereal species, the values of the coefficient of determination were very high, ranging from 0.772 for the relationship between K_1 and K_2 to 0.998 for the relationship between K_3 and K_4. The equations were applied to biological material, and they can be used to convert sphericity factors when only selected factors are given. This approach can be used to compare the shape of cereal seeds from various batches.

Table 4

Relationships between sphericity factors and other parameters of cereal seeds

Equation	Coefficient of determination R^2	Standard error of the estimate
$K_1 = 0.790\ K_2 + 0.018$	0.772	0.031
$K_1 = 1.011\ K_3 - 0.181$	0.942	0.016
$K_1 = 0.943\ K_4 - 0.012$	0.933	0.017
$K_1 = 1.286\ K_5 + 0.157$	0.938	0.016
$K_2 = 0.978\ K_1 + 0.074$	0.772	0.034
$K_2 = 1.121\ K_3 - 0.170$	0.935	0.018
$K_2 = 1.057\ K_4 + 0.012$	0.946	0.017
$K_2 = 1.418\ K_5 + 0.205$	0.921	0.020
$K_3 = 0.931\ K_1 + 0.198$	0.942	0.015
$K_3 = 0.834\ K_2 + 0.175$	0.935	0.016
$K_3 = 0.936\ K_4 - 0.165$	0.998	0.003
$K_3 = 1.262\ K_5 + 0.335$	0.981	0.008
$K_4 = 0.989\ K_1 + 0.037$	0.933	0.017
$K_4 = 0.895\ K_2 + 0.009$	0.946	0.015
$K_4 = 1.066\ K_3 - 0.176$	0.998	0.003
$K_4 = 1.352\ K_5 + 0.181$	0.988	0.007
$K_5 = 0.729\ K_1 - 0.106$	0.938	0.012
$K_5 = 0.649\ K_2 - 0.122$	0.921	0.014
$K_5 = 0.778\ K_3 - 0.258$	0.981	0.007
$K_5 = 0.731\ K_4 - 0.131$	0.988	0.005

Conclusions

1. Only minor similarities in the value of the sphericity factor, calculated based on two dimensions, were determined in rye and barley seeds and in barley and triticale seeds. The remaining comparisons revealed statistically significant differences. In the analyzed cereal seeds, the lowest values were noted for sphericity factor K_5 in the range of 0.046 to 0.275, and the highest values – for sphericity factor K_3 in the range of 0.359 to 0.650.

2. Sphericity factors were influenced mostly by variations in seed dimensions, whereas seed shape was most highly correlated with: thickness in barley seeds, width in wheat seeds, width and thickness in rye and triticale seeds, and length in oat seeds.

3. All of the presented sphericity factors can be used interchangeably to describe the shape of cereal seeds. Sphericity factors are closely correlated, therefore, they can be converted with the use of simple linear equations characterized by high values of the coefficient of determination. Sphericity factor K_3, which incorporates all three seed dimensions, delivers the most accurate results, and it is most frequently used in research papers.

References

AHMADI R., KALBASI-ASHTARI A., GHARIBZAHEDI S.M.T. 2012. *Physical properties of psyllium seed*. International Agrophysics, 26: 91–93.

BOAC J.M., CASADA M.E., MAGHIRANG R.G., HARNER III J.P. 2010. *Material and interaction properties of selected grains and oilseeds for modeling discrete particles*. Transactions of the ASABE, 53(4): 1201–1216.

CACAK-PIETRZAK G., SUŁEK A., GONDEK E., SUŁEK A. 2010. *Plonowanie oraz cechy jakościowe ziarna nowych odmian pszenicy jarej w zależności od poziomu nawożenia azotem*. Zeszyty Problemowe Postępów Nauk Rolniczych, 553: 11–19.

CHRZĄSTEK M., KRUK K., WÓJTOWICZ E. 2010. *Zmienność mieszańców międzygatunkowych owsa pod względem niektórych cech plonotwórczych wiechy głównej*. Zeszyty Problemowe Postępów Nauk Rolniczych, 556: 357–365.

FRĄCZEK J., WRÓBEL M. 2006. *Metodyczne aspekty oceny kształtu nasion*. Inżynieria Rolnicza, 12: 155–163.

GEODECKI M., GRUNDAS S. 2003. *Charakterystyka cech geometrycznych pojedynczych ziarniaków pszenicy ozimej i jarej*. Acta Agrophysica, 2(3): 531–538.

GREŃ J. 1984. *Statystyka matematyczna. Modele i zadania*. Wyd. PWN, Warszawa.

GROCHOWICZ J. 1994. *Maszyny do czyszczenia i sortowania nasion*. Wyd. AR, Lublin.

HEBDA T., MICEK P. 2005. *Zależności pomiędzy właściwościami geometrycznymi ziarna zbóż*. Inżynieria Rolnicza, 6: 233–241.

HEBDA T., MICEK P. 2007. *Cechy geometryczne ziarna wybranych odmian zbóż*. Inżynieria Rolnicza, 5(93): 187–193.

JAIN R.K., BAL S. 1997. *Properties of pearl millet*. Journal of Agricultural Engineering Research, 66: 85–91.

KALINIEWICZ Z., GRABOWSKI A., LISZEWSKI A., FURA S. 2011. *Analysis of correlations between selected physical attributes of Scots pine seeds*. Technical Sciences, 14(1): 13–22.

KALKAN F., KARA M. 2011. *Handling, frictional and technological properties of wheat as affected by moisture content and cultivar*. Powder Technology, 213: 116–122.

KOCIUBA W., KRAMEK A., DOLIŃSKI R. 2007. *Porównanie wartości cech użytkowych krajowych odmian pszenżyta ozimego zarejestrowanych w latach 1982-2003*. Zeszyty Problemowe Postępów Nauk Rolniczych, 517: 379–387.

KUSIŃSKA E., KOBUS Z., NADULSKI R. 2010. *Wpływ wilgotności na właściwości fizyczne i geometryczne ziarna żyta odmiany Słowiańskie*. Inżynieria Rolnicza, 4(122): 151–156.

MABILLE F., ABECASSIS J. 2003. *Parametric modelling of wheat grain morphology: a new perspective*. Journal of Cereal Science, 37: 43–53.

MARKOWSKI M., ŻUK-GOŁASZEWSKA K., KWIATKOWSKI D. 2013. *Influence of variety on selected physical and mechanical properties of wheat*. Industrial Crops and Product, 47: 113–117.

MIESZKALSKI L., SOŁODUCHA H.K. 2008. *Metody modelowania zbioru brył nasion*. Postępy Techniki Przetwórstwa Spożywczego, 1: 39–44.

MOHSENIN N.N. 1986. *Physical properties of plant and animal materials*. Gordon and Breach Science Public, New York.

OYELADE O.J., ODUGBENRO P.O., ABIOYE A.O., RAJIN.L. 2005. *Some physical properties of African star apple (Chrysophyllum alibidum) seeds*. Journal of Food Engineering, 67: 435–440.

PAKSOY M., AYDIN C. 2004. *Some physical properties of edible squash (Cucurbita pepo L.) seeds*. Journal of Food Engineering, 65: 225–231.

PRADHAN R.C., MEDA V., NAIK S.N., TABIL L. 2010. *Physical properties of Canadian grown flaxseed in relation to its processing*. International Journal of Food Properties, 13: 732–743.

RABIEJ M. 2012. *Statystyka z programem Statistica*. Wyd. Helion, Gliwice.

SADOWSKA U., ŻABIŃSKI A. 2009. *Niektóre właściwości fizyczne ziarniaków jęczmienia nagoziarnistego uprawianego w mieszance z soczewicą jadalną*. Inżynieria Rolnicza, 6(115): 229–236.

SEGIT Z., SZWED G., SZWED-URBAŚ K. 2003. *Uszkodzenia ziarniaków pszenicy twardej w wyniku obciążeń dynamicznych*. Acta Agrophysica, 2(4): 841–849.

SOLOGUBIK C.A., CAMPAÑONE L.A., PAGANO A.M., GELY M.C. 2013. *Effect of moisture content on some physical properties of barley*. Industrial Crops and Products, 43: 762–767.

TYLEK P. 2010. *Fizyczne i biologiczne aspekty mechanicznej separacji nasion buka zwyczajnego (Fagus sylvatica L.)*. Zeszyty Naukowe Uniwersytetu Rolniczego im. Hugona Kołłątaja w Krakowie, Rozprawy, 467(344).

ZDYBEL A., GAWŁOWSKI S., LASKOWSKI J. 2009. *Wpływ wilgotności na wybrane właściwości fizyczne ziarna żyta*. Acta Agrophysica, 14(1): 243–255.

Technical Sciences 18(4), 2015, 247–259

SELECTED PHYSICAL PARAMETERS OF COMMON HORNBEAM (*CARPINUS BETULUS* L.) NUTS

***Zdzisław Kaliniewicz*[1], *Paweł Tylek*[2], *Piotr Markowski*[1], *Andrzej Anders*[1], *Tadeusz Rawa*[1], *Michał Liedtke*[1]**

[1] Department of Heavy Duty Machines and Research Methodology
University of Warmia and Mazury in Olsztyn, Poland
[2] Department of Forest Work Mechanization
University of Agriculture in Kraków, Poland

Received 30 July 2015; accepted 10 October 2015; available on line 14 October 2015.

Key words: common hornbeam, seeds, physical parameters, range of variations, correlation, separation.

Abstract

Selected physical parameters of common hornbeam nuts were determined in five batches of nuts harvested from seed tree stands in northern Poland. The results were used to calculate the arithmetic and geometric mean diameters, aspect ratio, sphericity index, volume and density of each nut. The above parameters were compared by analysis of variance, correlation analysis and linear regression analysis. Habitat conditions had a greater influence on nut plumpness than the age of the tree stand. Nut width was highly correlated with nut mass, and the above observation can be used in the process of separating nuts into mass categories. When two mesh screens with 5 mm and 6 mm openings are used, nuts will be separated into a fine-sized fraction containing 71.4% of nuts with reduced plumpness, 24.1% of moderately plump nuts and 1.8% of plump nuts, and a coarse-sized fraction containing 2.0% of nuts with reduced plumpness, 43.6% of moderately plump nuts and 54.4% of plump nuts.

Symbols

D_a – arithmetic mean diameter of a nut, mm,
D_g – geometric mean diameter of a nut, mm,
k – volumetric coefficient of proportionality,
m – nut mass, mg,
R – aspect ratio, %,
SD – standard deviation of trait,
T, W, L – nut thickness, width and length, mm,
v – terminal velocity of a nut, m s^{-1},
V – nut volume, mm^3,
x – average value of trait,
γ – angle of static friction on steel, averaged for three nut positions on a steel friction plate, ^{o}

Correspondence: Zdzisław Kaliniewicz, Katedra Maszyn Roboczych i Metodologii Badań, Uniwersytet Warmińsko-Mazurski, ul. Oczapowskiego 11/B112, 10-719 Olsztyn, phone: +48 89 523 39 34, e-mail: zdzislaw.kaliniewicz@uwm.edu.pl

γ_1, γ_2, γ_3 – angle of static friction on a steel friction plate when the long axis of the nut is parallel to the direction of movement with the hilum down and up, and when the long axis is perpendicular to the direction of movement, °,

ρ – nut density, g cm^{-3},

Φ – sphericity index, %.

Introduction

The common hornbeam (*Carpinus betulus* L.) is a tree with a broad and irregular crown, and it grows to a height of 10–25 m. Its geographic range covers Central and Southern Europe, Caucasus, northern Turkey and Iran. It is a typical representative of lowland and highland tree species. The common hornbeam is rarely encountered at altitudes higher than 1000 m.a.s.l. It thrives on loamy, sandy and loamy, deep, fresh and fertile soils (SUSZKA et al. 2000, MURAT 2002, JAWORSKI 2011). It is a common admixture in stands of pines, oaks and beeches, and oak-linden-hornbeam forests are the optimal habitat for the analyzed species (MURAT 2002, BORATYŃSKI et al. 2007).

The common hornbeam is a monoecious species which produces individual male and female flowers on the same tree. It begins to produce fruit at the age of approximately 30 years, and abundant yields are reported every 2–3 years. Trees produce fruit even every year in locations with adequate sun exposure (SUSZKA et al. 2000, WESOŁOWSKI et al. 2015). Flowers appear in April or May, and inflorescences with a length of 5–15 cm mature between August and November, mostly in October. The fruit of the common hornbeam are nuts which are initially light green in color, but grow darker in successive stages of maturation to turn olive green and brown in fall (Fig. 1). Each nut is shielded by a 3-segmented seed coat which acts as a wing during dispersal. Mature nuts fall to the ground between fall and spring (SUSZKA et al. 2000, MURAT 2002, BORATYŃSKI et al. 2007, DRAGOMIR, SZEKELY 2011, JAWORSKI 2011).

Hornbeam nuts are harvested when maturing inflorescences turn olive green or brown. Nuts are harvested manually, they can be shaken off trees or collected from twigs that are cropped into sheets or nets spread under trees. The collected inflorescences are lightly dried, and nuts are mechanically separated from wings. Small amounts of seeds can be placed in a hard-wearing fabric bag and threshed by hitting with a flail or by stomping on top of the bag. Seed coats and crushed nut fragments are removed on a mesh screen, in a winnowing machine or a pneumatic sieve (SUSZKA et al. 2000, MURAT 2002).

Hornbeam nuts belong to the category of orthodox seeds which can withstand significant dehydration without losing their viability. Partially dried (8–10%) orthodox seeds can be stored at low temperatures (below 0°C) for many years. In hornbeam nuts, pre-sowing treatment is performed in deep

Fig. 1. View of common hornbeam nuts

dormancy, and it involves warm and cold stratification over a period of 18–20 weeks (SUSZKA et al. 2000, MURAT 2002, CZAPRACKI, HOLUBOWICZ 2010, ZHU et al. 2014).

According to the literature (KHAN 2004, PARKER et al. 2006, SHANKAR 2006, QUERO et al. 2007, BURACZYK 2010), seed mass is one of the key parameters that determine germination efficiency in most species. Plump seeds contain more reserve materials which are required for sprouting and contribute to the development of healthy germs. Despite the above, seeds are difficult to sort based only on their mass. Vibratory separators or pneumatic vibratory separators can be used, but in most processes, seeds are separated based on differences in their density. The separation process is effective when seeds have similar density but differ in size or when seeds have similar size but differ in density (GROCHOWICZ 1994). The separation process may be unsuccessful if seeds differ in both size and density, which is often the case in seed material. Thus, correlations between the physical parameters of seeds need to be identified to increase the efficiency of separation and support the selection of optimal parameters in separation equipment.

The objective of this study was to determine the variations in and correlations between the basic physical parameters of common hornbeam nuts so as to improve the efficiency of seed separation processes.

Materials and Methods

The experimental material comprised five batches of common hornbeam nuts supplied by a seed extraction plant in Jedwabno in 2012. Three batches were harvested from variously aged seed tree stands in one forest region, and two batches were obtained from similarly aged seed tree stands in the regions of Mazury and Podlasie in northern Poland. The analyzed batches were harvested from the following tree stands:

a) registration No. MP/1/45603/06, category of seed propagation material – from an identified source, region of origin – 205, municipality – Szczytno, geographic location – 53.32°N, 20.57°E, forest habitat – fresh forest, age – 77 years (symbol: CH-1a),

b) registration No. MP/1/44582/06, category of seed propagation material – from an identified source, region of origin – 206, municipality – Świętajno, geographic location – 53.35°N, 21.23°E, forest habitat – fresh forest, age – 71 years (symbol: CH-1b),

c) registration No. MP/1/9366/05, category of seed propagation material – from an identified source, region of origin – 251, municipality – Bartoszyce, geographic location – 54.12°N, 20.42°E, forest habitat – fresh forest, age – 74 years (symbol: CH-1c),

d) registration No. MP/1/42001/05, category of seed propagation material – from an identified source (removed from the list), region of origin – 251, municipality – Kolno, geographic location – 53.56°N, 21.03°E, forest habitat – fresh forest, age – 85 years (symbol: CH-2),

e) registration No. MP/1/43925/05, category of seed propagation material – from an identified source, region of origin – 251, municipality – Biskupiec, geographic location – 53.57°N, 20.53°E, forest habitat – fresh forest, age – 90 years (symbol: CH-3).

Analytical samples (initial samples had the weight of 1 kg) from every batch of nuts were divided by halving (*Nasiennictwo leśnych drzew*... 1995). Initial samples were halved, and one half was randomly selected for successive halving. The above procedure was repeated to produce samples of around 100 nuts each. The analyzed nut samples had the following size: CH-1a–109, CH-1b–118, CH-1c–111, CH-2–112, CH-3–122. The remaining nuts were sampled to determine their moisture content in the Radwag MAX 50/WH drying oven with a weighing scale. The analyzed nuts were characterized by similar moisture content in the range of 8.4% to 8.9%.

Terminal velocity of nuts was determined in the Petkus K-293 pneumatic classifier, seed dimensions were determined with the use of the MWM 2325 workshop microscope (length and width) and a thickness gauge, the angle of sliding friction was measured on a horizontal plane with an adjustable angle of inclination equipped with a steel friction plate (GPS – Ra = 0.45 μm), and seed mass was determined on the WAA 100/C/2 laboratory scale. All measurements were performed according to the methods previously described by KALINIEWICZ et al. (2011) and KALINIEWICZ and POZNAŃSKI (2013). The angle of static friction was measured in three positions: with the longitudinal axis parallel to the direction of movement with the hilum down (index 1) and the hilum up (index 2), and with the longitudinal axis perpendicular to the direction of movement (index 3).

The physical parameters of nuts were used to determine their arithmetic and geometric mean diameters, aspect ratio and sphericity index (MOHSENIN 1986):

$$D_a = \frac{T + W + L}{3} \tag{1}$$

$$D_g = (T \cdot W \cdot L)^{\frac{1}{3}} \tag{2}$$

$$R = \frac{W}{L} \times 100 \tag{3}$$

$$\Phi = \frac{(T \cdot W \cdot L)^{\frac{1}{3}}}{L} \times 100 \tag{4}$$

A 25 cm^3 liquid pycnometer with a thermometer and a capillary tube was used to determine volume V_p of all nuts in a given sample. The volume and density of each nut was calculated based on the below formula:

$$V = k \cdot T \cdot W \cdot L \tag{5}$$

$$\rho = \frac{m}{V} = \frac{m}{k \cdot T \cdot W \cdot L} \tag{6}$$

where:

$$k = \frac{V_p}{\Sigma T \cdot W \cdot L} \tag{7}$$

Nuts were divided into three plumpness categories based on their mass: seeds with reduced plumpness ($m < x$–SD), moderately plump seeds (x–SD $\leq m \leq x$+SD) and plump seeds ($m > x$+SD). The results were rounded off to the next multiple of 5.

The results were processed in the Statistica v. 10 application with the use of popular statistical procedures such as one-way ANOVA, correlation analysis and linear regression analysis (RABIEJ 2012). The results were regarded as significant at P-value of 0.05.

Results

The physical parameters of common hornbeam nuts are presented in Table 1. The volume and density of nuts were determined with the use of formulas (5) and (6) where the volumetric coefficient of proportionally was k = 0.475. The above value of k implies that a nut fills a rectangular cuboid, characterized by three basic parameters T, W and L, in 47.5%.

Table 1
Variations in the physical parameters of hornbeam nuts with an indication of significant differences

Property/ indicator	Nut batch				
	CH-1a x±SD	CH-1b x±SD	CH-1c x±SD	CH-2 x±SD	CH-3 x±SD
v [m s^{-1}]	10.00 ± 0.88^{a}	10.07 ± 1.11^{a}	9.63 ± 0.90^{bB}	10.01 ± 1.15^{A}	9.82 ± 0.93^{AB}
T [mm]	2.86 ± 0.27^{a}	2.85 ± 0.28^{a}	2.88 ± 0.29^{aA}	2.86 ± 0.29^{A}	2.85 ± 0.27^{A}
W [mm]	5.20 ± 0.48^{b}	5.92 ± 0.52^{a}	5.80 ± 0.54^{aA}	5.80 ± 0.58^{A}	5.87 ± 0.53^{A}
L [mm]	6.15 ± 0.71^{b}	6.67 ± 0.64^{a}	6.70 ± 0.61^{aA}	6.66 ± 0.59^{A}	6.75 ± 0.65^{A}
γ_1 [°]	23.99 ± 3.11^{a}	24.36 ± 2.88^{a}	24.26 ± 3.62^{aAB}	24.93 ± 2.43^{A}	23.70 ± 2.26^{B}
γ_2 [°]	23.96 ± 3.03^{a}	24.46 ± 2.65^{a}	24.02 ± 3.29^{aB}	25.05 ± 2.47^{A}	23.97 ± 2.20^{B}
γ_3 [°]	24.57 ± 3.15^{a}	24.36 ± 2.84^{a}	24.34 ± 2.94^{aA}	24.46 ± 2.19^{A}	23.54 ± 2.38^{B}
m [mg]	43.06 ± 8.10^{b}	49.97 ± 11.80^{a}	48.91 ± 10.48^{aA}	46.13 ± 11.01^{A}	47.57 ± 9.54^{A}
D_a [mm]	4.78 ± 0.38^{b}	5.15 ± 0.37^{a}	5.13 ± 0.38^{aA}	5.11 ± 0.40^{A}	5.16 ± 0.36^{A}
D_g [mm]	4.50 ± 0.34^{b}	4.82 ± 0.33^{a}	4.81 ± 0.35^{aA}	4.79 ± 0.37^{A}	4.82 ± 0.33^{A}
R [%]	85.20 ± 9.25^{b}	89.23 ± 8.54^{a}	86.94 ± 8.04^{abA}	87.41 ± 8.30^{A}	87.64 ± 9.49^{A}
Φ [%]	73.48 ± 4.69^{a}	72.56 ± 4.83^{ab}	71.96 ± 4.04^{bA}	72.13 ± 3.86^{A}	71.79 ± 4.69^{A}
V [mm^3]	43.87 ± 9.79^{b}	53.95 ± 11.39^{a}	53.72 ± 12.04^{aA}	53.22 ± 12.40^{A}	53.97 ± 10.79^{A}
ρ [g cm^{-3}]	0.99 ± 0.10^{a}	0.93 ± 0.13^{b}	0.92 ± 0.13^{bA}	0.88 ± 0.13^{B}	0.89 ± 0.15^{AB}

a, b – different letters indicate statistically significant differences in the value of a given parameter (indicator) between nuts harvested from similarly aged tree stands,
A, B – different letters indicate statistically significant differences in the value of a given parameter (indicator) between nuts harvested from the same forest region.

The errors in the estimated mean physical parameters of nuts did not exceed:
- for terminal velocity of a nut – 0.3 m s^{-1},
- for nut thickness – 0.1 mm,
- for nut width and length – 0.2 mm,
- for the angle of static friction – 0.7°,
- for nut mass – 2.2 mg.

The highest average terminal velocity was noted in batch CH-1b. Nuts from that batch were also characterized by the highest mean width, mass, geometric mean diameter and aspect ratio. In general, the lowest mean values of the measured parameters were observed in batch CH-1a in respect of the width, length, angle of static friction of nuts placed on a steel surface with the hilum up, mass, arithmetic and geometric mean diameters, aspect ratio and volume. Nuts from batch CH-1a were characterized by the highest mean values of the angle of static friction of nuts placed on a steel surface perpendicular to the direction of movement, sphericity index and density. Nuts harvested from similarly aged tree stands differed in all parameters and indicators, excluding thickness. It should be noted that none of the analyzed parameters was responsible for significant differences between the three examined batches. Nuts harvested from the same forest region differed locally only in their terminal velocity, angle of static friction and density. No significant differences were noted in the remaining parameters and indicators. Smaller differences in the measured parameters were observed between nuts harvested from the same forest region than between nuts harvested from different forest regions, which suggests that the characteristic attributes of common hornbeam nuts are influenced by the local climate.

The smallest angle of static friction was noted in CH-3 nuts positioned on a steel surface with the longitudinal axis perpendicular to the direction of movement, and the largest angle of static friction was observed in CH-2 nuts positioned on a steel surface with the longitudinal axis parallel to the direction of movement with the hilum down (Tab. 1). Despite statistically significant local differences in the angle of static friction between batches, the difference between the largest and smallest mean angle was estimated at only 6% (1.5°). An additional analysis of variance (the results are not given in Table 1) revealed an absence of significant differences between the angle of static friction of differently positioned nuts. For this reason, the mean angle of static friction from three positions was used in further analyses.

Despite the presence of statistically significant local differences, none of the analyzed batches differed considerably from the remaining batches, and the five analyzed batches of common hornbeam nuts were regarded as homogeneous. An analysis of linear correlations between the physical parameters of nuts (Tab. 2) revealed that nearly all evaluated traits were significantly correlated at 0.05. The only exceptions were terminal velocity, nut thickness and width. The correlations between the mass and basic dimensions of nuts, between nut density vs. terminal velocity and nut thickness, and between nut length and nut width were deemed as practically significant (coefficients of correlation higher than 0.4). The highest value of the correlation coefficient (0.727) was observed in a comparison of nut mass and nut width.

Table 2

Coefficients of linear correlation between selected physical parameters of hornbeam nuts

Property	T	W	L	γ	m	ρ
v	0.044	0.061	**-0.130**	**-0.275**	**0.332**	**0.501**
T	1	**0.262**	**0.289**	**-0.150**	**0.411**	**-0.420**
W	–	1	**0.528**	**-0.250**	**0.727**	**-0.165**
L	–	–	1	**-0.090**	**0.617**	**-0.356**
γ	–	–	–	1	**-0.320**	**-0.149**
m	–	–	–	–	1	**0.243**

Values in bold represent statistically significant correlations.

Regression equations where the coefficient of determination is higher than 0.2 are presented in Table 3. This condition was fulfilled by the relationships between the terminal velocity and density of nuts, between nut width and nut length, between nut length and nut mass, and between nut mass and nut width. The equation describing the relationship between nut width and nut mass was characterized by the highest value of the determination coefficient (0.529), and the highest percentage of explained variation. The above indicates that common hornbeam nuts should be divided into mass categories with the use of mesh screens with round openings.

Table 3

Regression equations for the physical parameters of hornbeam nuts

Equation	Coefficient of determination R^2	Standard error of the estimate
$v = 3.792\ \rho + 6.406$	0.251	0.875
$W = 0.461\ L + 2.687$	0.278	0.502
$W = 0.041\ m + 3.803$	0.529	0.405
$L = 0.603\ W + 3.137$	0.278	0.574
$L = 0.040\ m + 4.724$	0.381	0.531
$m = 12.968\ W - 27.098$	0.529	7.226
$m = 9.624\ L - 16.271$	0.381	8.283
$\rho = 0.066\ v + 0.266$	0.251	0.116

The average mass of common hornbeam nuts was determined at 47.18 ± 10.52 mg. Separation boundaries were rounded off to produce three nut plumpness categories: nuts with reduced plumpness (m<40 mg), moderately plump nuts (m = 40÷55 mg) and plump nuts (m>55 mg). The analyzed material contained 27.1% of nuts with reduced plumpness, 50.7% of moderately plump nuts and 22.2% of plump nuts. Figure 2 presents the distribution of nut width across three plumpness categories. Nuts representing all three plumpness categories are found in nearly every size fraction, excluding the two smallest (W≤4.5 mm) and the two largest (W>6.5 mm) fractions. When two mesh screens with 5 mm and 6 mm openings are used, nuts will be separated into three size fractions. The smallest fraction will contain approximately 28% of nuts with reduced plumpness, 5% of moderately plump nuts and only 1% of plump nuts. The material passed through the top mesh sieve will contain approximately 3% of nuts with reduced plumpness, 29% of moderately plump nuts and 84% plump nuts.

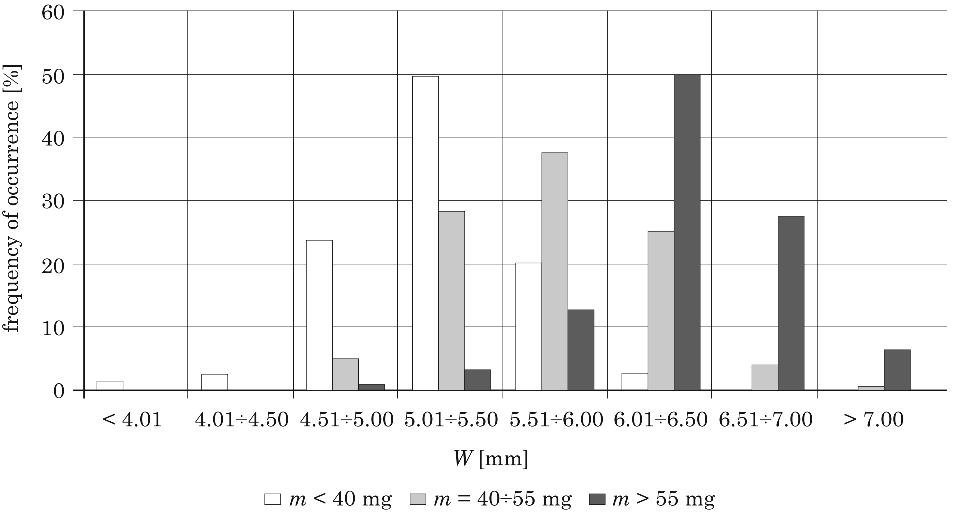

Fig. 2. Distribution of nut width across three mass categories

The separated size fractions will contain:

– fine-sized fraction ($W \leq 5$ mm) – 74.1% of nuts with reduced plumpness, 24.1% of moderately plump nuts and 1.8% of plump nuts,

– medium-sized fraction (W = 5–6 mm) – 33.9% of nuts with reduced plumpness, 59.9% of moderately plump nuts and 6.2% of plump nuts,

– coarse-sized fraction (W>6 mm) – 2.0% of nuts with reduced plumpness, 43.6% of moderately plump nuts and 54.4% of plump nuts.

Discussion

According to FRĄCZEK (1999) and HORABIK (2001), the frictional properties of seeds are determined by various factors, including seed orientation relative to the direction of movement. The above hypothesis was not confirmed by the results of our study where the position of common hornbeam nuts relative to the steel friction plate was not significantly correlated with the resulting angle of sliding friction. The above could be attributed to the fact that unlike most seeds, hornbeam nuts have a ribbed rather than a smooth surface. Due to relatively small contact area between nuts and the friction plate, the components of the friction force (deformation, adhesion and cohesion) do not undergo significant change, therefore, the angle of static friction remains similar when nuts are positioned differently on the steel surface. Our results indicate that when the angle of static friction is used as a separation trait, the position of common hornbeam nuts on the friction plate does not have to be precisely adjusted.

When the angle of static friction of hornbeam nutlets (approximately 24°) was converted into the coefficient of friction, our results were comparable with the values reported by BART-PLANGE and BARYEH (2003) in cocoa beans, by ALTUNTAŞ et al. (2005) in fenugreek seeds, by ÇALIŞIR et al. (2005) in Turkish okra seeds, and by MARKOWSKI et al. (2013) in wheat grain.

The mean terminal velocity of hornbeam nuts, which was determined in the range of 9.63 m s^{-1} to 10.07 m s^{-1}, was similar to that reported in filled beech nuts (TYLEK 2011). In terms of thickness, hornbeam nuts were similar to wheat seeds (GEODECKI, GRUNDAS 2003, KALKAN, KARA 2011, MARKOWSKI et al. 2013) and roselle seeds (SÁNCHEZ-MENDOZA et al. 2008), and in terms of width – to fir seeds (CZERNIK 1993), cowpeas (KABAS et al. 2007) and yellow lupine seeds (SADOWSKA, ŻABIŃSKI 2011). When both width and thickness were taken into account, hornbeam nuts were similar to lentils (RYBIŃSKI et al. 2009), and when width was combined with length, the analyzed nuts were similar to soybeans (DAVIES, EL-OKENE 2009). The sphericity index of hornbeam nuts was similar to that of ackee apple seeds (OMOBUWAJO et al. 2000). There are no published data on the range of variations in the physical parameters of hornbeam nuts. The only cited parameter is nut mass which, according to SUSZKA et al. (2000) and AGUINAGALDE et al. (2005), should range from 35 mg to 45 mg. In this study, nuts in four out of the five analyzed batches were heavier than 45 mg. The proportion of plump nuts in the evaluated material indicates that 2012 was a favorable year for the generative reproduction of hornbeams.

For a biological material, the regression equations presented in Table 3 effectively explain the relationships between the analyzed traits, and they can be used to model and perform separation processes.

Seed mass is one of the key parameters determining germination efficiency in most seed species, but the heaviest seeds are not always the first to sprout (KHAN 2004, PARKER et al. 2006, SHANKAR 2006, QUERO et al. 2007, UPADHAYA et al. 2007, NORDEN et al. 2009, BURACZYK 2010). Seeds can be separated into mass fractions to promote even germination, which is a very important production factor in tree nurseries. However, it is very difficult to separate seeds based on their mass only. For this reason, parameters that are significantly correlated with mass are identified and used in seed cleaning and separation process. In this study, the mass of common hornbeam nuts was most highly correlated with nut width. Our results indicate that hornbeam nuts should be separated with the use of mesh screens with round openings. The basic dimensions of hornbeam nuts were negatively correlated with nut density, which suggests that smaller nuts will germinate earlier than plump nuts. Further research is needed to verify this hypothesis.

Conclusions

1. An analysis of the physical parameters of common hornbeam nuts revealed greater differences between batches of nuts harvested from similarly aged trees in various forest regions than between batches harvested from differently aged trees in the same forest region. Our findings suggest that the plumpness of hornbeam nuts is more likely to be determined by local habitat conditions than the age of the tree stand.

2. In the group of the analyzed physical parameters of common hornbeam nuts, nut width was most highly correlated with nut mass (R = 0.727), whereas nut thickness was least correlated with terminal velocity (R = 0.044). A comparison of basic dimensions revealed the strongest correlations (R = 0.528) between nut width and length.

3. The results of this study indicate that hornbeam nuts should be separated with the use of mesh screens with round openings to obtain material characterized by similar mass. The most satisfactory results are obtained when hornbeam nuts are passed through screens with round openings with a diameter of 5 mm and 6 mm.

References

Aguinagalde I., Hampe A., Mohanty A., Martin J.P., Duminil J., Petit R.J. 2005. *Effects of life-history traits and species distribution on genetic structure at maternally inherited markers in European trees and shrubs*. Journal of Biogeography, 32: 329–339.

Altuntaş E., Özgöz E., Taşer Ö.F. 2005. *Some physical properties of fenugreek (Trigonella foenum-graceum L.) seeds*. Journal of Food Engineering, 71: 37–43.

Bart-Plange A., Baryeh E.A. 2003. *The physical properties of Category B cocoa beans*. Journal of Food Engineering, 60: 219–227.

Boratyński A., Boratyńska K., Mazur M., Marcysiak K. 2007. *Seed involucre variation in Carpinus betulus (Corylaceae) in Poland*. Acta Biologica Cracoviensia Sereies Botanica, 49(1): 103–111.

Buraczyk W. 2010. *Seed characteristics and morphological features of Scots pine (Pinus sylvestris L.) seedlings*. Leśne Prace Badawcze, 71(1): 13–20.

Çalişir S., Özcan M., Haciseferoğullari H., Yildiz M.U. 2005. *A study on some physico-chemical properties of Turkey okra (Hibiscus esculenta L.) seeds*. Journal of Food Engineering, 68: 73–78.

CZAPRACKI M., HOLUBOWICZ R. 2010. *Some factors influencing the germination of the common hornbeam (Carpinus betulus L.) seeds*. Bulletin UASVM Horticulture, 67(1): 422–429.

CZERNIK Z. 1993. *Studies of geometrical properties of silver fir seeds*. Sylwan, 8: 57–64.

DAVIES R.M., EL-OKENE A.M. 2009. *Moisture-dependent physical properties of soybeans*. International Agrophysics, 23: 299–303.

DRAGOMIR P., SZEKELY G. 2011. *Hornbeam trees in the parks of Timisoara*. Journal of Horticulture, Forestry and Biotechnology, 15(1): 47–49.

FRĄCZEK J. 1999. *Tarcie ziarnistych materiałów roślinnych*. Zeszyty Naukowe Akademii Rolniczej im. H. Kołłątaja w Krakowie, Rozprawy, 252.

GEODECKI M., GRUNDAS S. 2003. *Characterization of geometrical features of single winter and spring wheat kernels*. Acta Agrophysica, 2(3): 531–538.

GROCHOWICZ J. 1994. *Maszyny do czyszczenia i sortowania nasion*. Wydawnictwo Akademii Rolniczej, Lublin.

HORABIK J. 2001. *Physical attributes of loose plant material which are significant during storage*. Acta Agrophysica, 54.

JAWORSKI A. 2011. *Hodowla lasu.* Tom III. *Charakterystyka hodowlana drzew i krzewów leśnych*. PWRiL, Warszawa.

KABAS O., YILMAZ E., OZMERZI A., AKINCI İ. 2007. *Some physical and nutritional properties of cowpea seed (Vigna simensis L.)*. Journal of Food Engineering 79: 1405–1409.

KALINIEWICZ Z., GRABOWSKI A., LISZEWSKI A., FURA S. 2011. *Analysis of correlations between selected physical attributes of Scots pine seeds*. Technical Sciences, 14(1): 13–22.

KALINIEWICZ Z., POZNAŃSKI A. 2013. *Variability and correlation of selected physical attributes of small-leaved lime (Tilia cordata Mill.) seeds*. Sylwan, 157(1): 39–46.

KALKAN F., KARA M. 2011. *Handling, frictional and technological properties of wheat as affected by moisture content and cultivar*. Powder Technology, 213: 116–122.

KHAN M.L. 2004. *Effects of seed mass on seedling success in Artocarpus heterophyllus L., a tropical tree species of north-east India*. Acta Oecologica, 25: 103–110.

MARKOWSKI M., ŻUK-GOŁASZEWSKA K., KWIATKOWSKI D. 2013. *Influence of variety on selected physical and mechanical properties of wheat*. Industrial Crops Products, 47: 113–117.

MOHSENIN N.N. 1986. *Physical properties of plant and animal materials*. Gordon and Breach Science Public, New York.

MURAT E. 2002. *Szczegółowa hodowla lasu*. Oficyna Edytorska „Wydawnictwo Świat”, Warszawa.

Nasiennictwo leśnych drzew i krzewów iglastych. 1995. Ed. A. Załęski. Oficyna Edytorska „Wydawnictwo Świat”, Warszawa.

NORDEN N., DAWS M.I., ANTOINE C., GONZALEZ M.A., GARWOOD N.C., CHAVE J. 2009. *The relationship between seed mass and mean time to germination for 1037 tree species across five tropical forests*. Functional Ecology, 23(1): 203–210.

OMOBUWAJO T.O., SANNI L.A., OLAJIDE J.O. 2000. *Physical properties of ackee apple (Blighia sapida) seeds*. Journal of Food Engineering, 45: 43–48.

PARKER W.C., NOLAND T.L., MORNEAULT A.E. 2006. *The effects of seed mass on germination, seedling emergence, and early seedling growth of eastern white pine (Pinus strobus L.)*. New Forests, 32: 33–49.

QUERO J.L., VILLAR R., MARAÑÓN T., ZAMORA R., POORTER L. 2007. *Seed-mass effects in four Mediterranean Quercus species (Fagaceae) growing in contrasting light environments*. American Journal of Botany, 94(11): 1795–1803.

RABIEJ M. 2012. *Statystyka z programem Statistica*. Helion, Gliwice.

RYBIŃSKI W., SZOT B., RUSINEK R., BOCIANOWSKI J. 2009. *Estimation of geometric and mechanical properties of seeds of Polish cultivars and lines representing selected species of pulse crops*. International Agrophysics, 23: 257–267.

SADOWSKA U., ŻABIŃSKI A. 2011. *Influence of mixed sowing of yellow lupine with gymnosperm barley on the selected physical properties of seeds*. Inżynieria Rolnicza, 6(131): 187–195.

SÁNCHEZ-MENDOZA J., DOMÍNGUEZ-LÓPEZ A., NAVARRO-GALINDO S., LÓPEZ-SANDOVAL J.A. 2008. *Some physical properties of Roselle (Hibiscus sabdariffa L.) seed as a function of moisture content*. Journal of Food Engineering, 87: 391–397.

SHANKAR U. 2006. *Seed size as a predictor of germination success and early seedling growth in 'hollong' (Dipterocarpus macrocarpus Vesque)*. New Forests, 31: 305–320.

SUSZKA B., MULLER C., BONNET-MASIMBER M. 2000. *Nasiona leśnych drzew liściastych od zbioru do siewu*. Wydawnictwo Naukowe PWN, Warszawa-Poznań.

TYLEK P. 2011. *Analysis of aerodynamic properties of common fir and common beech*. Inżynieria Rolnicza, 6(131): 247–253.

UPADHAYA K., PANDEY H.N., LAW P.S. 2007. *The Effect of Seed Mass on Germination, Seedling Survival and Growth in Prunus jenkinsii Hook.f. & Thoms*. Turkish Journal of Botany, 31: 31–36.

WESOŁOWSKI T., ROWIŃSKI P., MAZIARZ M. 2015. *Interannual variation in tree seed production in a primeval temperature forest: does masting prevail?* European Journal of Forest Research, 134: 99–112.

ZHU Z., XU Y., WANG S. 2014. *The causes of European hornbeam seed dormancy and methods of breaking dormancy*. Journal of Food, Agriculture & Environment, 12(2): 1149–1152.

Technical Sciences 18(4), 2015, 261–270

ANALYSES OF SOIL-STRUCTURE INTERACTION BASED ON VERTICAL LOAD TESTS OF DISPLACEMENT PILES

Vaidas Martinkus, Arnoldas Norkus

Department of Geotechnical engineering
Vilnius Gediminas Technical University

Received 16 September 2015; accepted 23 November 2015; available on line 24 November 2015.

Key words: soil structure interaction, displacement pile group, frame, support, cohesionless soil.

Abstract

The current paper presents a research based on experimental and numerical analysis of three different frame supported by displacement pile groups embedded in sand. The vertical load tests performed under lab conditions have shown different responses of single piles installed at the same pile group, and a densification effect was named as a key player taking the main roll in explaining this phenomenon. A numerical analysis based on experimental data revealed unfavourable changes on deformation and internal forces of three different frame types caused by densification phenomenon. Performed research has emphasised the significance of soil structure interaction analysis, especially when displacement pile groups embedded in sands are used.

Symbols:
E_d – deformation modulus determined using dynamic load plate test, MPa,
ρ – soil density, g/cm^3,
w – soil moisture content, %,
ρ_s – particle density, g/cm^3,
e – void ratio, p.u.,
q_c – cone resistance, MPa,
f_s – sleeve resistance, kPa,
$k_{z,i}$ – vertical stiffness, kN/m',
$k_{h,i}$ – horizontal stiffness, kN/m'.

Correspondence: Vaidas Martinkus, Department of Geotechnical Engineering, Vilnius Gediminas Technical University, Saulėtekis av. 11, LT-10-223 Vilnius, phone: +37 061 672 542, e-mail: vaidas.martinkus@vgtu.lt

Introduction

Displacement pile groups are often used in engineering practice as an effective and reliable foundation type, especially in cohesion less soil. Despite an often and long term usage of this foundation type the researchers still perform the experimental and numerical investigations on this field. Some of the most recent works analyse the soil structure interaction (SSI) problems.

A broad numerical analysis of multi-storey 3D frame supported by pile groups embedded in cohesive soil was presented by CHORE et al. (2010). The author concluded that frame's deformation and internal forces have increased significantly when SSI was taken into account. RASAL et al. (2010) performed a similar numerical analysis and reported considerable increase in horizontal displacement of super structure's top floor. KHARE and CHORE (2013) also investigated the same problem and the determined results were in line with the previous author's reports. The results of numerical analyses of single storey multi-span frame, resting on pile groups consisting of different number of piles, was presented by DODE et al. (2014). The researcher highlighted that soil-structure interaction effect was found to be increasing the horizontal displacements and absolute positive and negative moments at the column, and that the effect of the soil-structure interaction is observed to be significant for the configuration of the pile groups. PULIKANTI and RAMANCHARLA (2014) have made an attempt to understand the SSI behaviour of framed buildings supported by the pile groups under transient loading taking into account the pile-soil interface effects. The results have shown that if the contact between piles and soil is modelled, under transient loading the acceleration response of top floor is reduced twice. MOHD et al. (2014) performed a broad parametric analysis of combined piled raft, and finally concluded that the interaction of building foundation-soil field and superstructure has remarkable effect on the structure. Very recent research papers presented by REDDY and RAO (2011, 2012), KRASINSKI and KUSIO (2014), also LANG et al. (2014) are based on experimental investigations of pile groups. Those investigations, in conjunction with the numerical analyses discussed above, have thoroughly exanimated the total response of different parameter displacement pile groups under vertical loading, but none of them has investigated the behaviour of an isolated pile placed in a pile group. Consequently, the first aim of this paper is to show that an isolated displacement pile response differs from that of the same pile in a group embedded in sand and the second one is to emphasize the negative effects on a super structure induced by this phenomenon.

Experimental background

Static vertical load tests of single piles placed in a pile group were carried out in a 5.0 m width, 7.0 m length and 4.5 m height soil box (Fig. 1). First of all, a preparation of the box's soil deposit was carried out, filling it with compacted sand up to the necessary level. The compaction was carried out using 65 kg weight single direction plate compactor (0.61 × 0.9 m) (Fig. 1b). A watering was used in order to improve compaction properties of the soil deposit. According to the primary prove compaction tests, the average thickness of each soil layer of 0.15 m was chosen. The control of the compaction was carried out using a

a

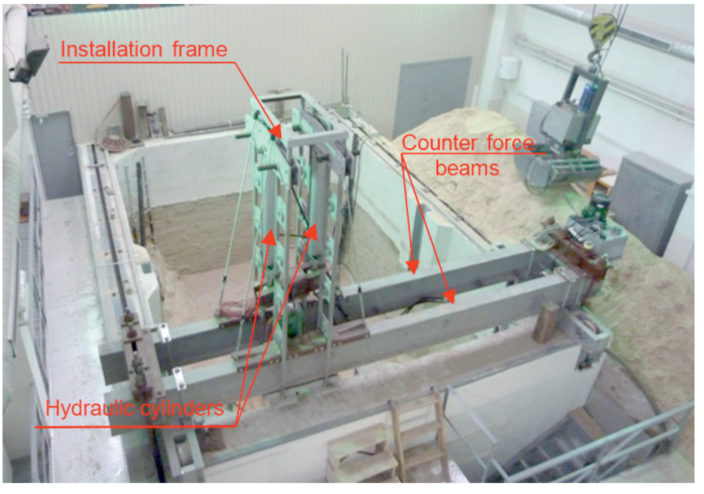

b

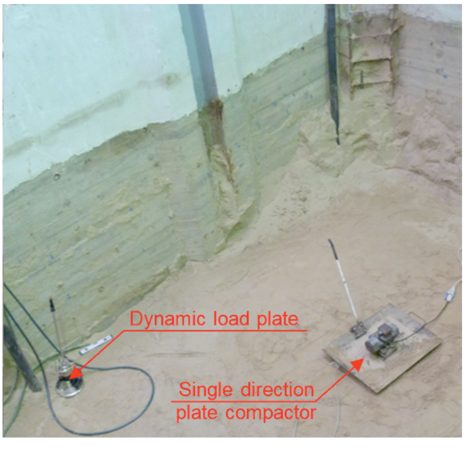

Fig. 1. Soil box: *a* – equipment of installation and loading; *b* – equipment used for soil compaction and compaction's monitoring

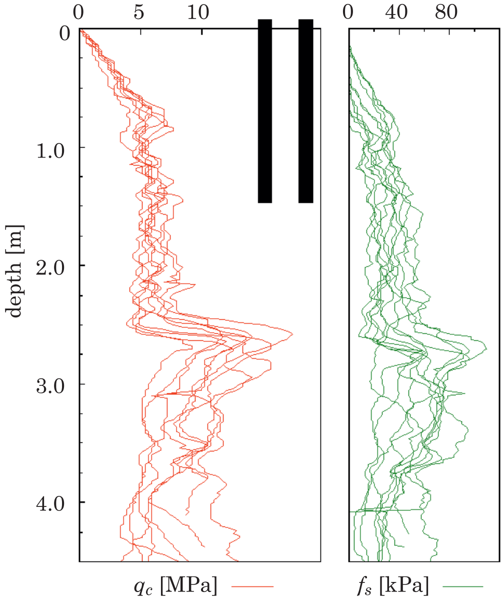

Fig. 2. Cone penetration test data

Dynamic plate load test (DPL). The compaction criterion of each soil layer deformation modulus E_d higher than 19 MPa was adopted. For each layer 12 DPL tests were performed at the same place as for each above soil layers.

From three different levels, 9 soil samples (3 samples for each level) were collected for determination of the soil physical properties (soil density ρ = 1.64 g/cm^3, soil particle density ρ_s= 2.65 g/cm^3, soil moisture content w = 4.38%, void ratio e = 0.69 and mean particle size 0.33 mm). It should be noted that specimen were taken after the watering and compaction of a particular layer, before filling the next one. Sieving test showed that compacted soil is even graded medium coarse sand. According to known geological investigation report of quarry, from which the soil was brought, sand mainly consists of silica particles. All soil's physical properties were determined using standardised procedures.

In total 12 Cone Penetration Tests (CPT) were performed at the same places as DPL tests using the standard probe with 10 cm^2 area and 60° peak angle cone. All CPT curves are presented at the same graph in order to demonstrate the scatter of cone resistance q_c and sleeve resistance f_s (Fig. 2).

For this research study 0.22 m width and 1.45 m length piles made of regular steel (without any additional surface treatment) were used, which were installed in 0.66 m spacing group, by means of the installation frame consisted of two hydraulic cylinders (Fig. 1a). Maximum pushing velocity of hydraulic

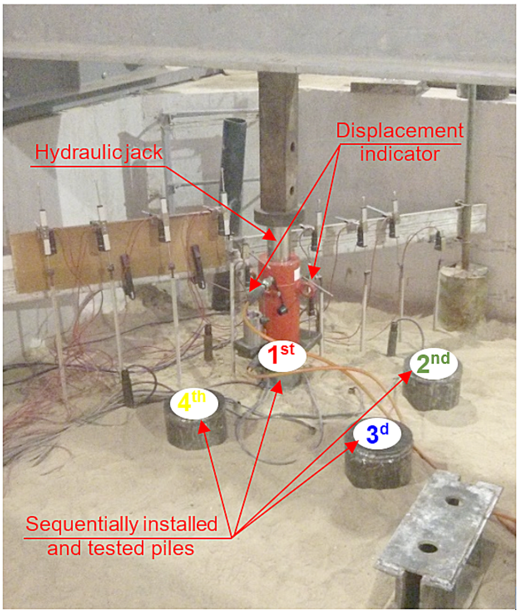

Fig. 3. Vertical load test

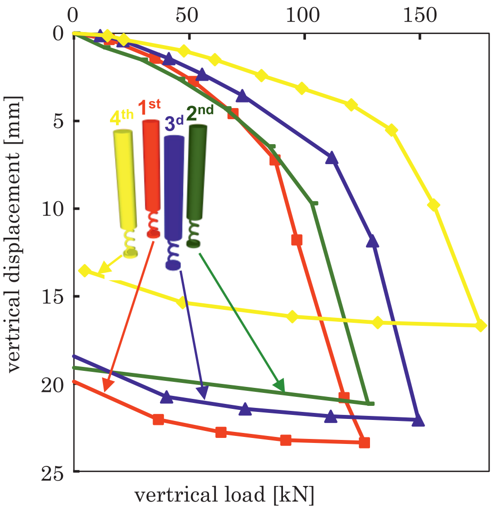

Fig. 4. Load-settlement curves of tested piles

cylinders 5 mm/s was applied. During the installations piles were released for a few times due to lengthening necessity of hydraulic jacks' arms. Piles were installed clockwise starting from 1^{st} to 4^{th} pile as shown in Figure 3. After the installation the piles were tested in the same order as they were installed. The tier loading procedure with 10 loading and 4 unloading steps were used for the static vertical load tests. The duration of loading step was adopted equal to 60 min and for the unloading steps 15 min. The vertical displacement of pile's head was measured by means of two linear pot indicators, and the total load was measured by means of vibrating wire load cell. The ultimate settlement equal to 10 percent of a single pile diameter was adopted as a failure criterion. Experimental load settlement curves are presented in Figure 4.

Numerical analyses

For three different types of frame, which discretization is presented in Figure 5, a static FEM (Finite element method) analysis was performed using SCIA Engineer software. The constitutive model of linear elastic isotropic materials was adopted for the analysis. Considering that relatively small deformation was expected, the solver with linear relation between the deformations and displacements was used for the analysis, it means that none of global or local imperfections, as well as secondary effects were taken in to account. The load combination consisting of self-weight (assigned automatically), dead weight and snow load were applied for all cases. Using the same load combination three different types of support with symmetric and asymmetric orientation were used for each frame (Fig. 6). Using the support type named „Fixed" soil's deformation was eliminated in order to demonstrate the pure deformations of considering frames (Fig. 6). For other two support types named „Springs (pile-cap fixed)" and „Springs (pile-cap hinged)" the linear vertical and horizontal springs were used in order to get the general deformations of frame-support-soil system (Fig. 6).The stiffness of vertical springs were determined from the curves presented in Figure 4, assuming allowable serviceability limit state settlement equal to 5% (5 mm) of pile diameter. The applied ratio of settlement and pile diameter is acceptable in most cases according to codes regulation. The determined secant stiffness are as follows: $k_{z,1}{}^{st}$ = 9.89 MN/m', $k_{z,2}{}^{nd}$ = 10.11 MN/m', $k_{z,3}{}^{d}$ = 12.61 MN/m' and $k_{z,4}{}^{th}$ = 16.48 MN/m'. The stiffness of horizontal springs defined for each pile was calculated according to code CSN 73 1004 increasing by depth and was equal to $k_{h,1}{}^{st} = k_{h,2}{}^{nd} = k_{h,3}{}^{d} = k_{h,4}{}^{th} = 0 \rightarrow 120$ MN/m^3. It must be noted that in order to get a point stiffness with dimensions MN/m', the value shown above should be integrated at particular area of pile side surface.

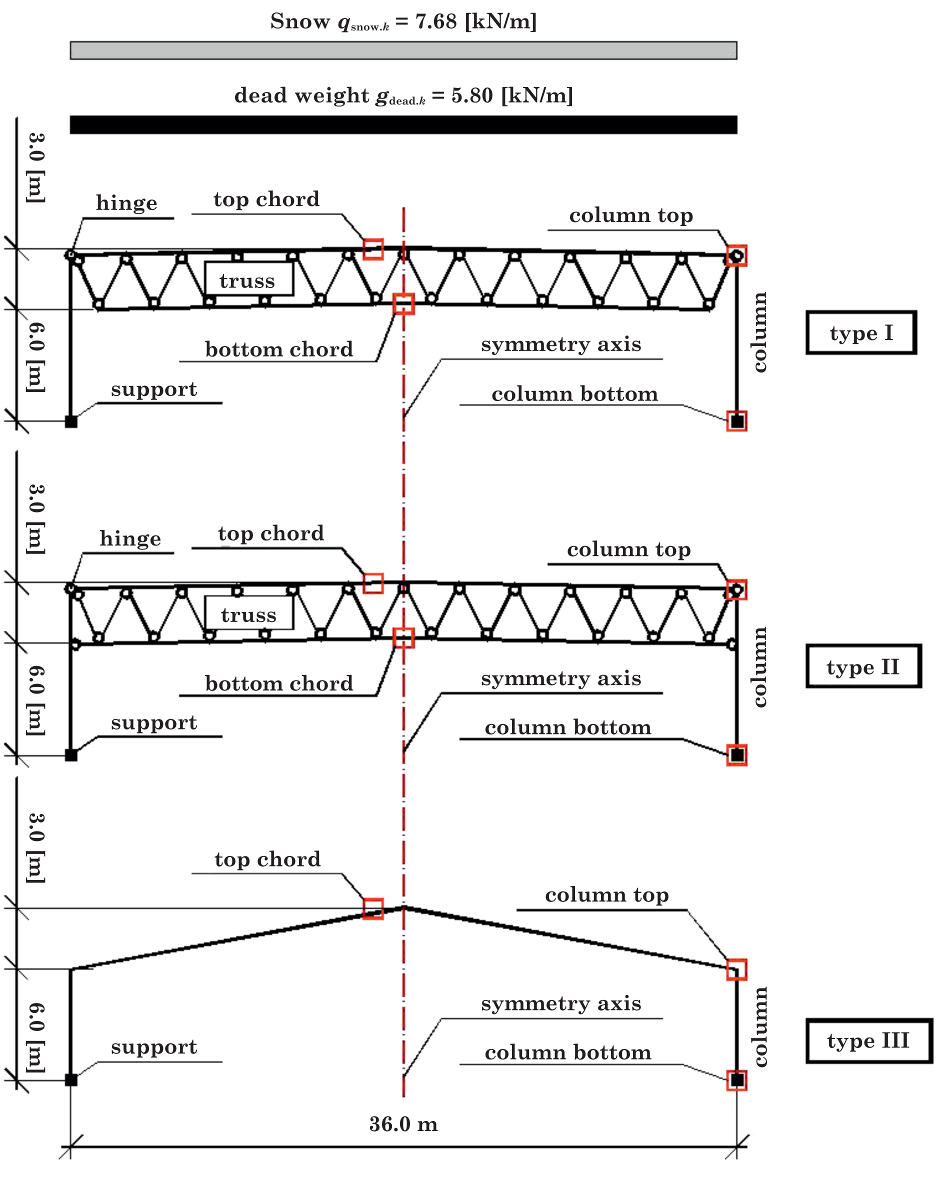

Fig. 5. Computational schemes of analysed frames

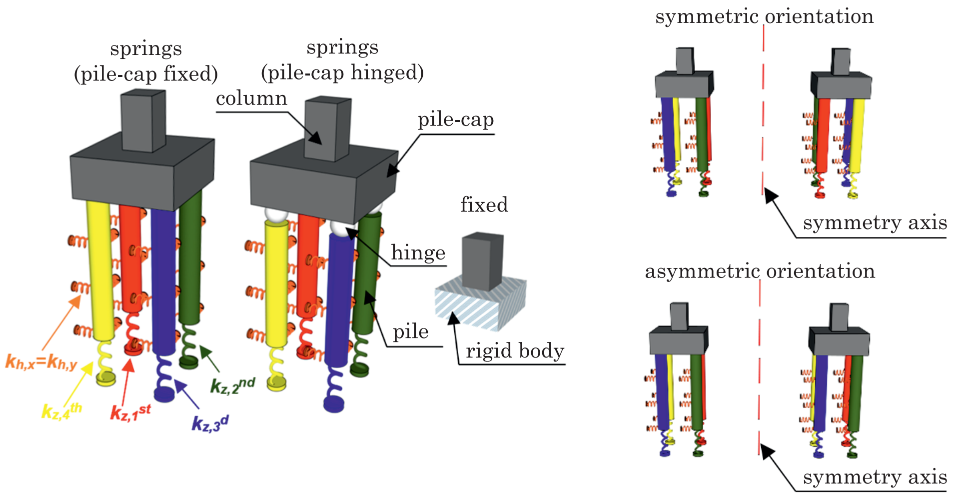

Fig. 6. Types of support defined for each type of frame (springs $k_{z,1}{}^{st}$ to $k_{z,4}{}^{th}$ represent experimental response (stiffness) of each pile; $k_{h,x}$ and $k_{h,y}$ represent horizontal soil stiffness)

Results and Discussion

Closer look to experimental load-settlement curves presented in Figure 4 revealed that displacement pile response (placed in a pile group) under static vertical loading differs according to installation sequence. The performance of the 1st pile has been determined to be the poorest whereas the 4th pile showed the best performance in terms of stiffness. Mean while intervening piles 2nd and 3^{d} have performed respectively ($k_{z,1}{}^{st}<k_{z,2}{}^{nd}<k_{z,3}{}^{d}<k_{z,4}{}^{th}$). It is worth mentioning that the additional settlements induced by adjacent piles' stress fields overlapping was not taken into account, because neighbouring piles were not being loaded, while one of them was tested.

The numerical analysis, which data are presented in Table 1, showed that vertical displacements of column bottom and horizontal translations of column top may be larger respectively up to 830 and 802%, when the soil structure interaction is being considered. It can be concluded that the pile groups' orientation and the type of pile-cap connection depending on frame type had the key influence.

Tension force at truss' bottom chord and compression force at truss' top chord mostly increased (up to 13%) on frame type II. Significant increase (up to 21%) in bending moment appeared at column of frame type III. It should also be mentioned that this amount of internal force increase exceeds the reliability level required in most of the construction design codes.

Table 1

Results of numerical analysis

Frame type	Support type	Support orientation	Vertical displacement of column bottom [mm]	Horizontal displacement of column top [mm]	Tension force at truss' bottom chord [kN]	Compression force at truss' (or frame) top chord [kN]	Maximal bending moment at column [kNm]	Vertical reaction of support (vertical spring) [kN] 1st	2nd	3d	4th	total
I	fixed	–	0	5.0	1029.5	1025.6	24.5	–	–	–	–	425
I	springs (pile–cap hinged)	symmetric	7.7	5.1 (↑2%)	1028.9 (↓0.1%)	1029.9 (↑0.4%)	19.5 (↓20%)	97	101	116	146	460
I	springs (pile–cap hinged)	asymmetric	7.9	45.1 (↑802%)	1029.2 (↓0.0%)	1027.7 (↑0.2%)	2.8 (↓89%)	115	120	99	126	460
I	springs (pile–cap fixed)	symmetric	7.7	5.1 (↑2%)	1029.0 (↑0.0%)	1029.4 (↑0.4%)	14.6 (↓40%)	96	99	116	149	460
I	springs (pile–cap fixed)	asymmetric	7.8	26.7 (↑434%)	1029.2 (↑0.0%)	1027.6 (↑0.2%)	4.4 (↓82%)	105	108	108	139	460
II	fixed	–	0	4.2	803.9	904.3	346.3	–	–	–	–	425
II	springs (pile–cap hinged)	symmetric	7.5	4.4 (↑5%)	903.5 (↑12%)	943.6 (↑4%)	244.3 (↓29%)	82	85	128	165	460
II	springs (pile–cap hinged)	asymmetric	7.9	9.3 (↑121%)	908.9 (↑13%)	945.5 (↑5%)	221.2 (↓36%)	85	89	126	160	460
II	springs (pile–cap fixed)	symmetric	7.5	4.4 (↑5%)	901.4 (↑12%)	940.8 (↑4%)	253.2 (↓27%)	79	81	131	169	460
II	springs (pile–cap fixed)	asymmetric	7.9	9.0 (↑114%)	907.4 (↑13%)	943.3 (↑4%)	232.1 (↓33%)	82	85	128	165	460
III	fixed	–	0	24.5	–	575.3	1591.8	–	–	–	–	425
III	springs (pile–cap hinged)	symmetric	7.2	62.3 (↑154%)	–	353.1 (↓39%)	1870.8 (↑18%)	60	65	149	186	460
III	springs (pile–cap hinged)	asymmetric	8.0	65.6 (↑168%)	–	349.9 (↓39%)	1853.9 (↑16%)	62	68	147	183	460
III	springs (pile–cap fixed)	symmetric	7.0	54.1 (↑121%)	–	340.3 (↓41%)	1931.0 (↑21%)	40	45	166	209	460
III	springs (pile–cap fixed)	asymmetric	8.3	58.0 (↑137%)	–	337.4 (↓41%)	1916.6 (↑20%)	43	47	164	206	460

Vertical reactions of supports were obtained to be different (up to 45% above the average of frame type III and up to 23% of frame type I) due to different spring stiffness.

Conclusions

When displacement pile groups are used as a support for different type buildings, an analysis of soil-structure interaction must be performed in order to determine more reliable values of structures internal forces and deformation.

While design of pile caps is being performed, the likely increase on internal forces due to uneven pile reaction distribution must be taken into account.

In order to reduce the negative effects (additional deformation and internal forces) on super structures, the correct installation sequence of displacement pile at pile groups in sand must be chosen. Furthermore, the rigid non-rotational connection between piles and cap must be ensured, which decreases the horizontal displacements of super structure.

Concerning the future targets, the results of numerical analysis should be examined experimentally. Furthermore the additional experimental study should be carried out in order to determine the horizontal stiffness of isolated piles, and likely effects caused by installation procedure of neighbouring piles.

References

CHORE H.S., INGLE R.K., SAWANT V.A. 2010. *Building Frame – Pile Foundation – Soil Interaction Analysis: A Parametric Study*. Interaction and Multi Scale Mechanics, 3(1): 5–79.

DODE P.A., CHORE H.S., AGRAWAL D.K. 2014. *Interaction analysis of a building frame supported on pile groups*. Coupled Systems Mechanics, 3(3): 305–318.

KHARE R.J., CHORE H.S. 2013. *Interaction of building frame with pile*. International Journal of Electrical, Electronics and Computer Systems (IJEECS), 1(1): 2347–2820.

KRASINSKI A., KUSIO T. 2014. *Comparative model tests of SDP and CFA pile groups in non-cohesive soil*. Studia Geotechnica et Mechanica, 4(36).

LANG R., LIU R., LIAN J., DING H. 2014. *Study on Load-Bearing Characteristics of a New Pile Group Foundation for an Offshore Wind Turbine*. The Scientific World Journal, 2014(2014), article ID 394104. On line: http://dx.doi.org/10.1155/2014/394104.

MOHD A., MAHMOUD H.M., JAVED M., MOHD A.H. 2014. *3D Analysis of Soil – Foundation – Structure Interaction in Layered Soil. Open Journal of Civil Engineering,* 4: 373–385.

PULIKANTI S., RAMANCHARLA P.K. 2014. *SSI Analysis of Framed Structure Supported on Pile Foundations – With and Without Interface Elements*. Frontiers in Geotechnical Engineering (FGE), 1(3).

RASAL S.A., CHORE H.S, DODE P.A. 2010. *Interaction of frame with pile foundation*. IOSR Journal of Mechanical and Civil Engineering, 1: 59–62.

REDDY C.R.K, RAO T.D.G. 2011. *Experimental study of a modelled building frame supported by pile groups embedded in cohesion less soil*. Interaction and Multi scale Mechanics, 4(4): 321–336.

REDDY C.R.K, RAO T.D.G. 2012. *Study of soil interaction in a model building frame with plinth beam supported by pile group*. International Journal of Advanced Structural Engineering, 4(11).

Technical Sciences 18(4), 2015, 271–282

POINT CLOUD UNIFICATION WITH OPTIMIZATION ALGORITHM

***Wioleta Błaszczak-Bąk*[1], *Anna Sobieraj*[2]**

[1] Institute of Geodesy
University of Warmia and Mazury in Olsztyn
[2] Chair of Geodesy
Gdansk University of Technology

Received 24 February 2015; accepted 25 June 2015; available on line 4 July 2015.

Key word: laser scanning, unification, optimization.

Abstract

Terrestrial laser scanning is a technology that enables to obtain three-dimensional data – an accurate representation of reality. During scanning not only desired objects are measured, but also a lot of additional elements. Therefore, unnecessary data is being removed, what has an impact on efficiency of point cloud processing. It can happen while single point clouds are displayed – user decides what he wants to deleted and does it manually, or by using tools provided in dedicated for point cloud processing softwares. In Leica Geosystems Cyclone – software used here in tests, user can apply tools e.g. for merging or unification of point clouds. Both of them change the separate points clouds into one points cloud, however unification can be executed with reduction – low, medium, high, highest or no reduction at all. It should be noted, that the modeled objects may have complex structure and unification with selected type of reduction can have a very big impact on the result of modeling. In such situation it is desirable to apply different types of reduction.

In this article authors propose to apply an optimization algorithm on unified point clouds. Unification conducted by means of Cyclone Leica Geosystems (v.7.3.3) enables to merge point clouds and reduced the number of points. The point elimination is determined mainly by spacing between points. It may leads to loose of important points – representing some essential elements of scanned objects or area. Applying optimization algorithm, especially for complex objects, may help to reduce the number of points without losing the information necessary for proper modeling.

Introduction

Currently, terrestrial laser scanning is used in many fields, for example, to create 3D models of buildings, cities, in research on displacements (ASPERSKI et al. 2010, PILECKI 2013), planning applications (FIDERA et al. 2004), documenting cultural heritage (VOZIKIS et al. 2004, ARMESTO-GONZALEZ et al. 2010,

Correspondence: Wioleta Błaszczak-Bąk, Instytut Geodezji, Wydział Geodezji, Inżynierii Przestrzennej i Budownictwa, Uniwersytet Warmińsko-Mazurski w Olsztynie, ul. Oczapowskiego 1 (bl. 22), pok. 25, 10-719 Olsztyn, phone: 89 523 48 70, e-mail: wioleta.blaszczak@uwm.edu.pl

BERNAT et al. 2014) and many others. It is a fast and accurate way to acquire reliable data about measured objects. Precise determination of the shape and geometric relationships between objects is strictly related to the measurement of distances and angles between scanner and points from which laser beam bounced off. Measured values are a basic for calculation of *XYZ* coordinates (VOZIKIS et al, 2004, FRYŚKOWSKA, KEDZIERSKI 2010). Modern scanners can measure up to 1,000,000 points per second (Leica Geosystems Brochure Leica ScanStation P20). Acquired a huge number of data points distributed across the observed surface is called a point cloud. It is a final product of scanning. Next to coordinates of points, it also consists of their corresponding intensities. A single point cloud usually does not cover the whole object of interest, therefore a few measurement positions are needed. Obtained point clouds are then registered in order to have all data in single coordinate system. Aspects related to the point cloud registration are presented by BARNEA and FILIN (2008), BRENNER et al. (2008), YANG and ZANG (2014), RABBANI et al. (2007). During scanning not only desired objects are measured, but also a lot of additional elements. Therefore, removing unnecessary data has an impact on efficiency of point cloud processing. User can clear the point cloud(s) manually or can apply tools provided in dedicated for point cloud processing softwares which enable the reduction of point cloud.

Proposal of unification with optimization algorithm

Point clouds become a subject to various types of processing. Essential one is registration – a process of transformation of point clouds into single coordinate system. Registration based on targets, clouds or modeled objects is conducted by means of software dedicated for point cloud processing (e.g. Trimble RealWorks, Faro SCENE, Leica Geosystems Cyclone). Oriented point clouds are then the basics for 3D modeling, creating 2D drawings (plans, sections, profiles), and other purposes. To realize them, a various workflows are proposed, determined by used software and desired goal. In Leica Cyclone, for 3D modeling a solution based on merging point clouds is suggested (VOZIKIS et al. 2004). There are two tools available: merge and unify. Both of them change the separate points clouds into one, however unification can be executed with reduction – low, medium, high, highest or no reduction at all. Point elimination is determined mainly by spacing between them. When object has a complex structure such approach may lead to loosing of significant points. In such situation it is desirable to apply algorithm which adjust reduction to the complexity of the measured object.

Authors propose to use the optimization algorithm presented in the papers BŁASZCZAK 2006, BŁASZCZAK, KAMINSKI 2007, BŁASZCZAK-BAK et al. 2011, BŁASZCZAK-BAK, SOBIERAJ 2013. Optimization algorithm was adopted for reduction of TLS datasets and consists of the following steps:

– Defining belts in the *XY* plane parallel to the axis of measurement *Y*.

– Results of laser scanning are arranged in measurement belts in projection onto a plane. On the basis of the calculated azimuth of the belt, the point cloud is fitted in coordinate system. In this system belts in the *XY* plane are defined.

– The choice of cartographic generalization method used to reduce the size of the set of measurement such as Douglas-Peucker (DOUGLAS PEUCKER 1973), Visvalingham-Whyatt (VISVALINGAM, WHYATT 1992). The choice of the method is made by user. In this article authors used Visvalingham-Whyatt method.

A general scheme of the generalization is presented in Figure 1.

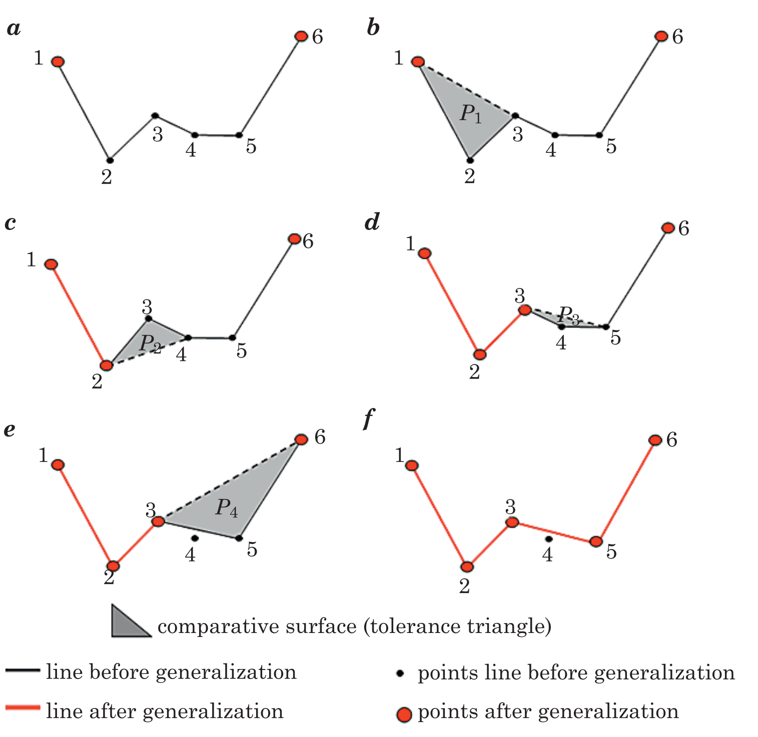

Fig. 1. Stages in line generalization based on comparative surface
Source: VISVALINGHAM, WHYATT (1992).

In each belt (in the *YZ* plane) chosen method of generalization is used. Applying generalization algorithm in *YZ* plane allows to preserve third dimension of the data.

An important step is to choose a belt measurement, as well as the selection of appropriate tolerances in the method. The choice of the tolerances determines the degree of reduction of dataset (number of deleted points).

Material and methods

The optimization algorithm used in this paper was developed and presented in articles by BŁASZCZAK 2006, BŁASZCZAK, KAMINSKI 2007, BŁASZCZAK-BĄK et al. 2011, BŁASZCZAK-BĄK, SOBIERAJ 2013. In mentioned papers algorithm was tested only on ALS dataset. In this paper, authors decided to test it on TLS dataset and compare its efficiency with results obtained by using tools provided in software dedicated for point cloud processing.

In this study laser scanner Leica C10 was used. Its characteristics are presented below:

– speed measurement: up to 50,000 points/s,
– field of view: 360 degrees Vertical, 270 degrees Horizontal
– range <300 m,
– accuracy of the modeled area of >2 mm,
– positional accuracy of >6 mm, distance >50 m 4 mm,
– dual axis compensator ensures the accuracy of measurement,
– built-in camera allows you to take pictures of the scanned object,
– power supply: internal batteries – operating time up to 3.5 hours on one set – allows measurements independent of an external power source,
– memory: built-in 80GB hard disk drive – allows recording data from the whole measurement.

As a research facility building located within the University of Gdansk was used. On the front elevation (north wall) there is a relief. It shows the image of a dragon and a man coal-stoker with a shovel. Points covering this wall became the subject for detailed tests.

Measurement was made on the four positions. Layout of positions is presented in Figure 2.

The unification was carried out for three options:

1) point clouds encompasses simple area/object, here: fragment of relief,
2) point clouds encompasses one object, here: whole relief,
3) point clouds encompasses given/complex area, here: fragment of wall with relief.

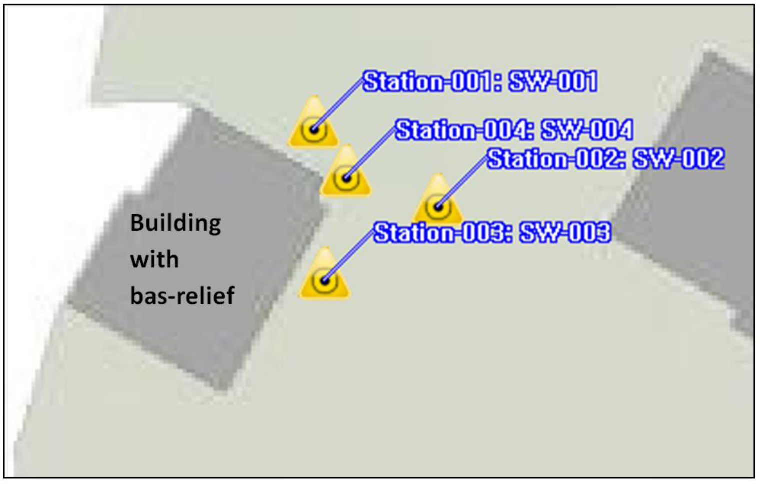

Fig. 2. Layout of scanned positions
Source: own research in Cyclone.

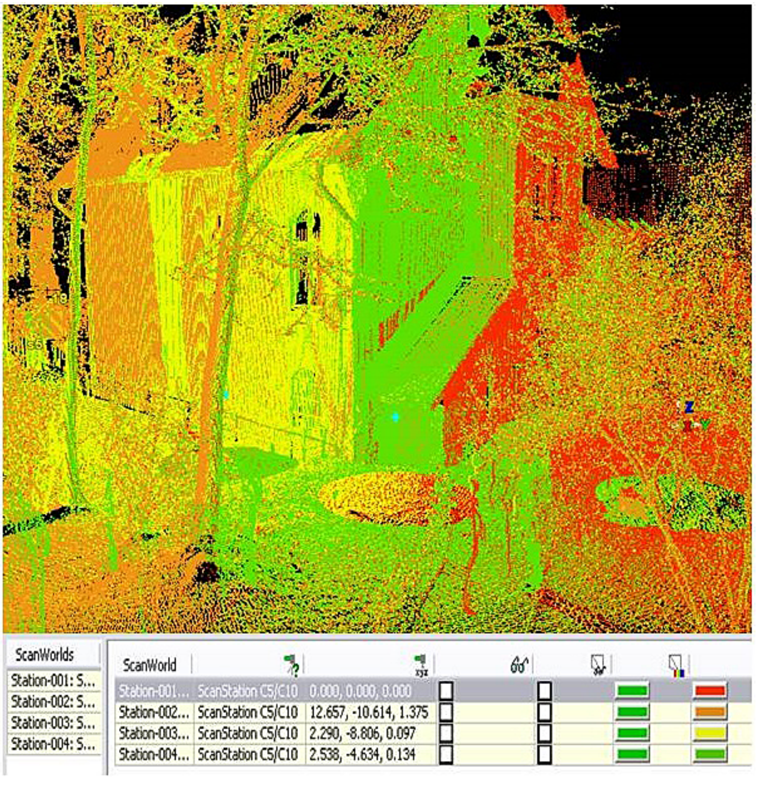

Fig. 3. Obtained point clouds
Source: own research in Cyclone.

Point clouds and the adopted color scheme for each of the sets of measurement are presented in Figure 3.

For each option unification was conducted for two cases: 1) unification based on optimization algorithm, 2) unification with high reduction in Leica Cyclone software.

The influence of optimization algorithm was tested by visual inspection of points distribution for mentioned two cases. Additionally statistical parameter – coefficient of determination (D) was calculated. Coefficient of determination is the measure of model adjustment (the closer to 1, the better the match of the model to another model). It illustrates the degree of match of reduced datasets to a set of original data. To calculate the parameter D in both cases on the basis of reduced sets DTM was generated. The size of the GRID was equal to 2 cm. The coefficient of determination was calculated:

$$D^2 = \frac{\sum_{i=1}^{k}(Z_{\mathrm{DTM_{ORG}}} - Z_{\mathrm{mean}})^2}{\sum_{i=1}^{k}(Z_{\mathrm{DTM_{OA}}} - Z_{\mathrm{mean}})^2},\ D^2 = \frac{\sum_{i=1}^{k}(Z_{\mathrm{DTM_{ORG}}} - Z_{\mathrm{mean}})^2}{\sum_{i=1}^{k}(Z_{\mathrm{DTM_{URC}}} - Z_{\mathrm{mean}})^2} \tag{1}$$

where:

Z_{mean} – is a mean height calculated from heights of both DTMs, z_i ($i=1, 2..., k$) are heights of the point assumed for creating DTM, k is the size of the subset used for DTM construction,

$Z_{\mathrm{DTM_{ORG}}}$ – are height of DTM points generated from **ORG**inal data.

$Z_{\mathrm{DTM_{OA}}}$ – are height of DTM points generated from data obtained after unification with **O**ptimization **A**lgorithm,

$Z_{\mathrm{DTM_{URC}}}$ – are height of DTM points generated from data obtained after **U**nification with **R**eduction conducted in **C**yclone.

Result and discussion

For each option a different fragments of measuring dataset were chosen. They were visible from all 4 positions. Chosen fragments encompass selected part of relief, the whole relief and part of it with the wall. They are presented in Figures 4, 6 and 8. Next, a unifications were performed. The first one was a unification with optimization algorithm and the second was a unification with high reduction available in Leica Geosystems Cyclone. The results of unifications for each options are presented in Figures 5, 7 and 9.

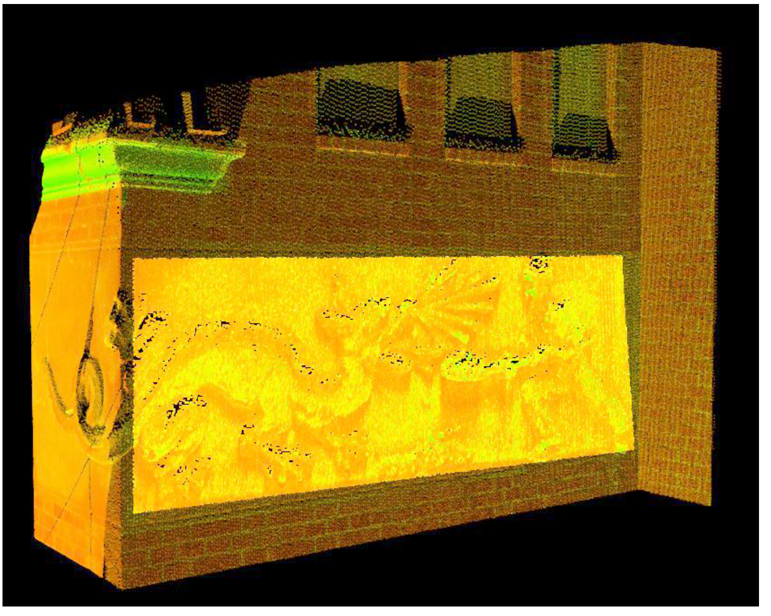

Fig. 4. Option 1 – area chosen for unification
Source: own research in Cyclone.

a ***b***

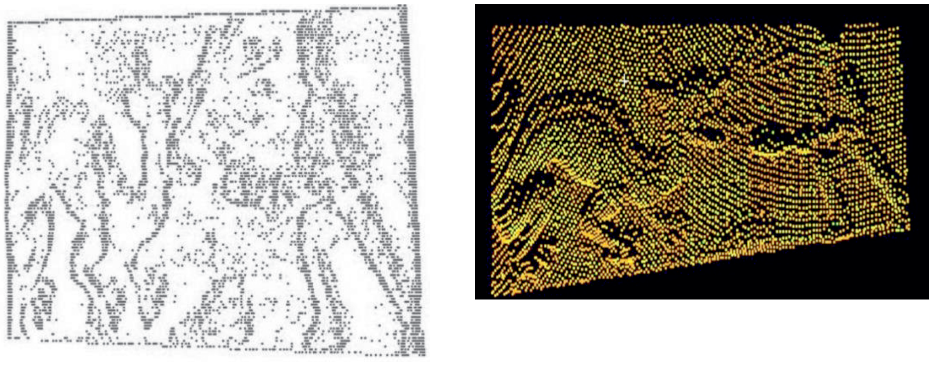

Fig. 5. Option 1 – unification: a – own algorithm, b – in Cyclone
Source: own research.

To reproduce fragment of relief (e.g. for 3D modeling purpose) distinctive points like outline of man, are essential. During unification relief points were obtained, but some of outline points was lost due to high reduction. Applying optimization algorithm, also with high reduction, but investigating the suitability of each point, the degree of reduction was maintained. Only points from flat surfaces was removed.

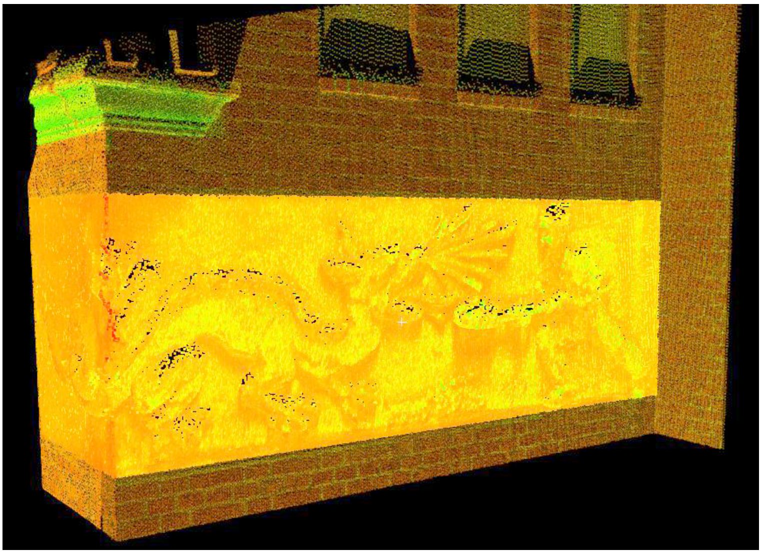

Fig. 6. Option 2 – selected object for unification
Source: own research in Cyclone.

a

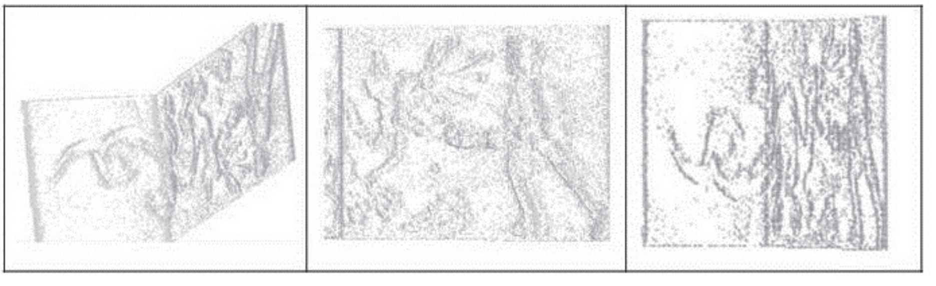

b

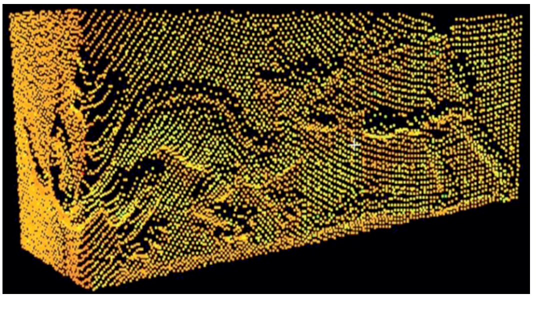

Fig. 7. Option 2 – unification: a – own algorithm, b – in Cyclone
Source: own research.

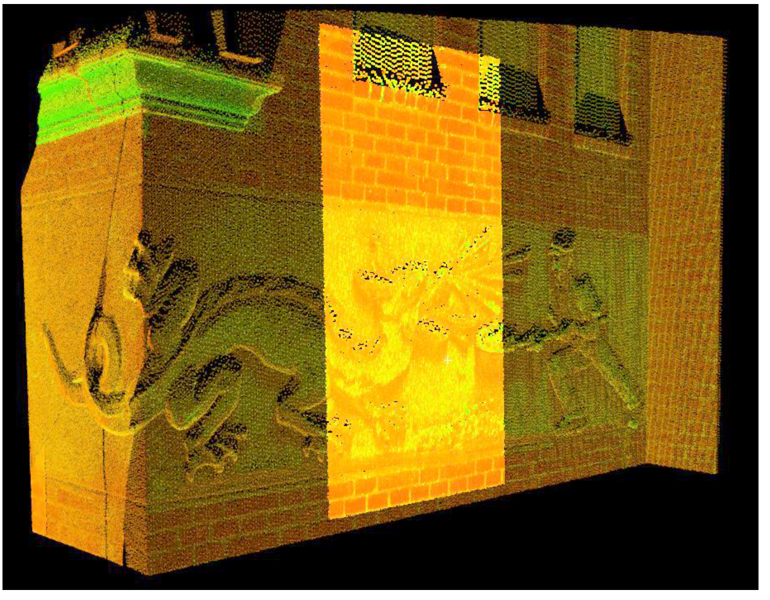

Fig. 8. Option 3 – the selected fragment to unification
Source: own research in Cyclone.

a ***b***

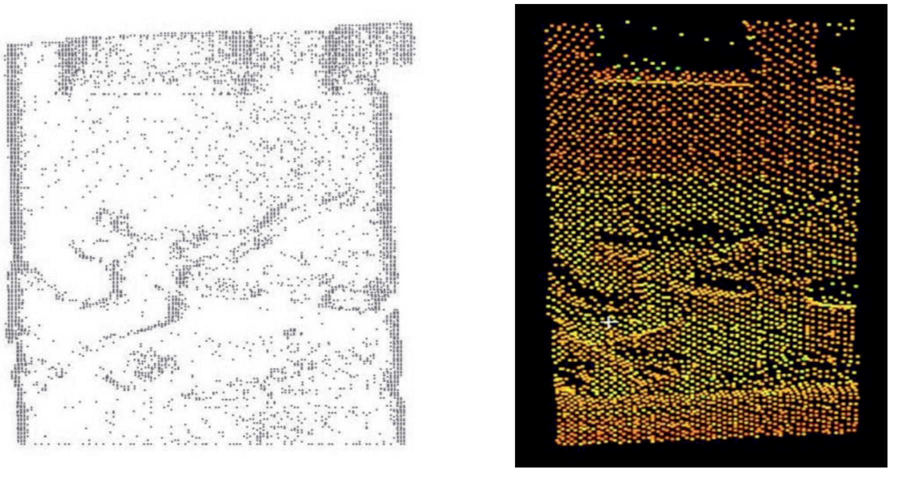

Fig. 9. Option 3 – unification: a – own algorithm, b – in Cyclone
Source: own research.

The effects of the conducted unifications are presented in Figure 7*a* and 7*b*. Figure 7*a* shows the object from different perspectives. The distribution of points has changed because of applied unification with optimization algorithm.

Unification algorithm with varying degrees of reduction performed the computations in the *YZ* plane. Therefore, in order to compare the bas-relief, it is presented in several versions view.

In Table 1 the results of unifications are presented – the number of datasets after applying unification based on optimization algorithm and unification with high reduction available in Cyclone. There are also values of calculated coefficient of determination (*D*).

Table 1

Results of unifications

Specification	Option 1		Option 2		Option 3	
	number of points	*D*	number of points	*D*	number of points	*D*
Original dataset (points from 4 points clouds)	454,818	–	753,853	–	302,727	–
Unification with optimization algorithm	176,590	0.98	476,325	0.97	179,892	0.98
Unification with a high reduction	198,522	0.94	489,600	0.94	156,600	0.97

For option 1, after conducting unification with high reduction, dataset consisted of 44% of original TLS measuring data. After unification with reduction based on optimization algorithm, obtained dataset comprised of 37% of original data. Coefficient of determination is closer to 1 in the latter case. In option 2, unification with high reduction decreased the dataset and it consisted of 65% of original TLS measuring data. After unification with reduction based on optimization algorithm, obtained dataset comprised of 63% of original data. Coefficient of determination is closer to 1 for dataset obtained after unification with optimization algorithm. For option 3 the number of dataset after unifications with high reduction was less reduced than with unification with optimization algorithm, however the value of *D* indicated that in both cases the match to original is similar.

Conclusions

The article presents a new approach to the problem of point clouds unification. Unification provided in software like Leica Geosystems Cyclone enables reduction of number of points while merging points clouds into one. User can decided is there will be reduction (low, medium, high, highest) or not. As a final result of such unification user obtains one point cloud with various number of points. However, using such unification with reduction may lead to the lost of important data. If the points clouds will be used further, e.g. for 3D modeling, there should be all significant points in dataset. In this paper authors propose to apply optimization algorithm based on cartographic generalization method in unification with reduction. The use of this algorithm enables to reduce the number of points in the point cloud with varying degrees of reduction in different areas. Thus, points, which are not essential in the generation process (e.g. modeling) will be removed from the measurement dataset. The reduction is not random, and each point is tested prior to removal because of its usefulness. Optimization algorithm is designed to leave a larger number of points in the places where there is such a need, such as refraction, embossed edges etc. During tests it was seen as a higher density of points in areas with more details like the outline of figures in relief. Within regular surfaces it leaves smaller, but a sufficient for modeling number of points. Unification with optimization algorithm has no negative influence on information content of dataset, what was confirmed by calculating D. It also should be noted that the user can determines the degree of reduction by identifying relevant parameters of optimization. Proposed solution can be a good and effective alternative for unifications provided by commercial software.

References

ALKAN R.H., KARSIDAG G. 2012. *Analysis of The Accuracy of Terrestrial Laser Scanning Measurements*. FIG Working Week 2012, Rome, Italy, 6–10 May.

ARMESTO-GONZÁLEZ J., RIVEIRO-RODRÍGUEZ B., GONZÁLEZ-AGUILERA D., TERESA RIVAS-BREA M. 2010. Journal of Archeological Science, 37: 3037–3047.

ASPERSKI J., DELACOURT C., ALLEMAND P., POTHERAT P., J.M., VARREL E. 2010. *Application of a Terrestrial Laser Scanner (TLS) to the Study of the Sechilienne Landslide (Ismre, France)*. Remote Sens., 2(12): 2785–2802.

DEMIR N., BAYRAM B., ALKIS Z., HELVACI C., ÇETIN I., VÖGTLE T., RINGLE K., STEINLE E. 2004. *Laser Scanning for Terrestrial Photogrammetry, Alternative system Or Combined With Traditional System?* ISPRS Archives, XXXV(B5): 193–197. On line: http://www.isprs.org/proceedings/XXXV/congress/comm5/papers/548.pdf.

BERNAT M., JANOWSKI A., RZEPA S., SOBIERAJ A., SZULWIC J. 2014. *Studies on the Use of Terrestrial Laser Scanning in the Maintenance of Buildings Belonging to the Cultural Heritage*. 14th SGEM GeoConference on Informatics, Geoinformatics and Remote Sensing, SGEM2014, June 19–25 Conference Proceedings, 3: 307-318, http://dx.doi.org/10.5593/SGEM2014/B23/S10.039.

BARNEA S., FILIN S. 2008. *Keypoint based autonomous registration of terrestrial laser point-cloud*. ISPRS Journal of Photogrammetry Remote Sensing, 63: 19–35.

BŁASZCZAK W. 2006. *Optymalizacja dużych zbiorów wyników pomiaru zasilający bazy danych systemów informacji przestrzennej*. Praca doktorska. Uniwersytet warmińsko-Mazurski w Olsztynie.

BŁASZCZAK W., KAMIŃSKI W. 2007. *Optymalizacja dużych zbiorów wyników pomiaru zasilających bazy danych systemów informacji przestrzennej*. Przegląd Geodezyjny, 6: 7–9.

BŁASZCZAK-BĄK W., SOBIERAJ A. 2013. *Impact of optimization of ALS point cloud on classification*. Technical Sciences, 16(2): 147–164.

Błaszczak-Bąk W., Janowski A., Kamiński W., Rapiński J. 2011. *Optimization algorithm and filtration using the adaptive TIN model at the stage of initial processing of the ALS point cloud*. Canadian Journal of Remote Sensing, 37(6): 583–589.

Brenner C., Dold C., Ripperda N. 2008. *Coarse orientation of terrestrial laser scans in urban environments*. ISPRS Journal of Photogrammetry & Remote Sensing, 63: 4–18.

Fryśkowska A., Kędzierski M. 2010. *Wybrane aspekty integracji danych naziemnego i lotniczego skaningu laserowego*. Archiwum Fotogrametrii, Kartografii i Teledetekcji, 21: 97–107.

Fidera A., Chapman M.A., Hong J. 2004. *Terrestrial Lidar for Industrial Metrology Applications: Modelling, Enhancement and Reconstruction*. International Archives of Photogrammetry and Remote Sensing, XXXV(B5): 880–883.

Pilecki R. 2012. *Zastosowanie naziemnego skanera laserowego*. Czasopismo Techniczne Politechniki Krakowskiej, 109(9-M): 223–233.

Rabbani T., Dijkman S., Heuvel F., Vosselman G. 2007. *An integrated approach for modelling and global registration of point clouds*. ISPRS Journal of Photogrammetry & Remote Sensing, 61: 355–370.

Vozikis G., Haring A., Vozikis E., Kraus K. 2004. *Laser Scanning: A New Method for Recording and Documentation in Archeology*, In Proceeding of FIG Working Week 2004, Athens, Greece, May 22–27, On line: http://fig.net/pub/athens/papers/wsa1/WSA1_4_Vozikis_et_al.pdf.

Yang B., Zang Y. 2014. *Automated registration of dense terrestrial laser-scanning point clouds using curves*. ISPRS Journal of Photogrammetry & Remote Sensing, 95: 109–121.

Technical Sciences 18(4), 2015, 283–298

USE OF SATELLITE AND ALS DATA FOR CLASSIFICATION OF ROOFING MATERIALS ON THE EXAMPLE OF ASBESTOS ROOF TILE IDENTIFICATION

Katarzyna Osińska-Skotak, Wojciech Ostrowski

Department of Photogrammetry,
Remote Sensing and Spatial Information Systems
Warsaw University of Technology

Received 19 October 2014; accepted 19 October 2015; available on line 24 November 2015.

Key words: roofing materials detection, multispectral classification, topographic correction, WorldView-2.

Abstract

Classification of roofing materials with the use of high resolution satellite imagery is a difficult issue, especially due to the fact that roofs are characterised by large diversity of shapes and textures, mainly caused by different roof surfaces illumination. To automate the process of roofing material types classification the influence of diversified illumination of individual roof surfaces should be eliminated. Topographic correction of satellite imagery may decrease influence of such effects and therefore leads to more accurate classification results. This paper presents classification results of roofing materials based on an 8-channel WorldView-2 satellite image. The digital terrain model and the digital surface model created with the use of aerial laser scanning data provided by the ISOK project were used for the topographic correction. The accuracy of the supervised classification of WorldView-2 image achieved for asbestos-cement roofing materials was at the level of 76–92%, (depending on the variant of classification). After grouping roofing materials by similar materials (e.g. painted sheet metal and metal tiles) it is possible to achieve classification results with the accuracy of ca. 70–80%.

Introduction

Classification of very high resolution (VHR) satellite imagery is a challenging issue, especially in case of the pixel-oriented approach. This is due to the high diversity of image texture of various objects, additionally increased by different illumination of individual objects. This effect is visible in multispec-

Correspondence: Katarzyna Osińska-Skotak, Zakład Fotogrametrii, Teledetekcji i Systemów Informacji Przestrzennej, Politechnika Warszawska, pl. Politechniki 1, 00-661 Warszawa, e-mail: k.osinska-skotak@gik.pw.edu.pl

tral images, as well as in pansharpened images. In conventional image classification of roofing material types the diversity of illumination of individual roof surfaces causes the necessity to define multiple training fields for each type of a roofing material. Application of topographic corrections might solve this problem as it limits the illumination variability caused by roof shapes and by the roof position with respect to the Sun at the moment of image acquisition. In order to apply the topographic image correction, data acquired by aerial laser scanning (ALS), available for the majority of Poland, can be utilized to generate a 3D representation of roof surfaces. The topographic correction of satellite imagery can be performed in an automated way. This should potentially contribute to more accurate classification results and to reduction of the workload related to collection of training fields.

The automatic detection of roofing materials has recently become a significant task due to the requirement of removal of all asbestos containing products in Europe by the end of 2032. The restriction on asbestos mining and production, as well as on processing of asbestos containing products in the EU-countries was introduced by the European Parliament and Council Directive 2003/18/WE of March 27, 2003 and the total ban on asbestos use has been introduced by the Directive 1999/77/WE of January 1, 2005. Although asbestos has been mined for several thousand years, its harmfulness for human health has been documented only in the first half of the twentieth century and further classified as a pathogenic and carcinogenic substance. Health problems can occur when asbestos fibres are released into the atmosphere, i.e. during asbestos products deterioration. Due to their small size, when inhaled into respiratory system they are not removed through the usual body purification mechanisms (DYCZEK 2007). Currently deterioration of asbestos-cement products causes the biggest problem for the air pollution additionally accelerated by acid rain and other chemical atmospheric pollutants (SZESZENIA-DĄBROWSKA, SOBALA 2010).

Poland the total marketing suppression on asbestos products has been in force since 1999. According to the Polish asbestos reduction program estimates, in 2008 about 14.5 million tons of asbestos containing products existed („Programme for Asbestos Abatement in Poland 2009–2032”), with majority consisting of flat asbestos-cement plates and corrugated asbestos-cement plates commonly used as roofing materials in sixties and seventies of the 20th century, known under local trade name as Eternit. In accordance with the provisions of „Programme for Asbestos Abatement in Poland 2009–2032” the local government prepares and updates the plan for removal of asbestos and asbestos containing products, based on local asbestos products inventories. According to the information available on the 31st of August 2014 about 80% of municipalities have already completed their inventories (bazaazbestowa.gov.pl). About

4.15 million tons of asbestos containing products were recorded, including 3.97 million tons of asbestos-cement roofing materials. However, only a small fraction (about 205,000 tons) of asbestos containing products has been neutralized till now.

A field inventory is a time consuming process, therefore orthophotomaps from governmental resources are commonly used for asbestos-cement roofing materials inventory. Other image-based materials i.e. VHR satellite images are not used probably due to limited availability, relatively high costs of data acquisition, and in some cases limited spectral resolution.

Remote sensing of roofing materials – literature review

Only a few attempts to utilise aerial or satellite image data for detecting roofing materials have been discussed in literature (HEROLD et al. 2003, ROBERTS, HEROLD 2004, BASSANI et al. 2007). The majority of work consists of urban areas with focus on issues related to automation of classification or building extraction based on object-oriented classification OBIA (e.g. HEROLD et al. 2002, ALMEIDA et al. 2007, CHEN et al. 2009, DINIS et al. 2010). Another direction supplementing urban research is determination of geometric properties of roofs (i.e. BELGIU et al. 2012) and further using such information to determine the function of buildings (VALERO et al. 2008).

A few papers reporting research on remote sensing of roofing materials exist. All of them discuss mostly use of airborne hyperspectral data. HEROLD et al. (2003) dealt with classification of urban areas using data acquired by the AVIRIS hyperspectral scanner recording 224 spectral bands (0.37–2.51 μm), as well as satellite IKONOS and LANDSAT TM data. As reported the classification accuracy based on AVIRIS' 14 spectral channels was dependent on roofing material type (13 material types) and ranged from 40 to 70%. In the case of IKONOS data, the classification accuracy was even lower, mainly due to low spectral resolution. One of the roofing materials, wooden shingle, was classified with a higher accuracy. This result was also confirmed by other work (ROBERTS, HEROLD 2004). The high producer's accuracy was also achieved for ceramic roof tiles, however this class was significantly over-estimated as can be argued from the respective low user's accuracy.

BASSANI et al. (2007) aimed at the detection of asbestos-cement roofing materials by MIVIS hyperspectral scanner (102 spectral channels), ranging from the visible to the far infrared part of the spectrum (0.43 to 2.47 μm and 8 to 14 μm). A detection rate between 80% and 90% could be achieved. MOREOVER, BASSANI et al. (2007) performed detailed spectrometric analyses of asbestos minerals; as a result they confirmed that chrysotile may be detected in the channel of 2.327 μm. This mineral was mostly used for production of asbestos-cement roofing materials. According to them, another spectral channel, which is interesting for detection of asbestos, is radiation of 9.44 μm wavelength (thermal channel).

Another interesting information on classification of asbestos-cement roofing materials or its properties can be found in the context of inventory and monitoring of urban areas (FONSECA et al. 2011), development and estimation of population in cities (ALMEIDA et al. 2007) as well as, climatic analyses in cities (ATTURO, FIUMI 2005). Overall, the accuracy of asbestos-cement roofing materials classification described in the above mentioned publications was reported as lower than the values achieved by BASSANI et al. (2007).

Methodology

Test field

The test field is the Powsin housing estate, located in the southern part of the capital city of Warsaw (Poland), in Wilanów district. Powsin has been mentioned for the first time in 1259 as the settlement owned by Bogusza Miecławic of the Doliwów family – the voivode of Łęczyca. Since 1951 Powsin has been located inside the administrative boundaries of the capital city of Warsaw. The long history of this area and its rural traditions have had an impact on its current shape. Until now it has preserved a lot of its old character, among others a well preserved street pattern. The majority of buildings in Powsin are single-family houses – detached, semidetached and terraced. The typical for this part of Warsaw farmstead compounds, residential houses with farm buildings, can be found along the main streets. During recent years several estates of single-family houses have been built, mainly as semidetached or terraced houses. Besides single-family houses, a school complex with modern sport fields, the St. Elisabeth of Hungary church and the headquarters of several companies are located in Powsin.

Due to different times of building development various roofing materials can be found at Powsin's area: ceramic tiles, cement tiles, bituminous tiles, metal tiles, different sheet metal, corrugated sheet metal, roofing felt, shingle and asbestos-cement in the form of flat and corrugated plates. The asbestos-cement and the roofing felt are dominant on farm buildings and older houses, the metal tiles on buildings after renovation and the ceramic tiles is the basic roofing material of new, single-family houses (Fig. 1). The metal sheets can be found on farm buildings (painted sheet metal) or on storage sheds and also (the copper sheet) on roofs of several houses and church. As for the shape of roofs, in the case of the farm buildings mainly flat or gabled roofs can be found while in the case of residential buildings the hip, pyramid hip or multisurface roofs dominate (new single-family detached or semidetached houses). The hip or pyramid hip roofs have slopes between 10° and 15°; most multisurface roofs have slopes between 20° and 35°.

Data source and pre-processing

Threefold data have been used in the study: airborne laser scanning (ALS), the WorldView-2 multispectral satellite image (Fig. 1a) and the roof coverings database (RCDB) (Fig. 1*b*).

The ALS data were acquired for the ISOK Project (IT System of the Country's Protection against Extreme Hazards for Poland, http://www.isok.gov.pl/en/press-releases,press-information-about-isok-project). For the Powsin study area the flight was performed in April 2012 with average point density 12 points/m^2 (standard II of ISOK Project) obtained from two perpendicular flight paths. Considering the points height accuracy (<0.10 m) of the ISOK standard II data the accuracy of models obtained from these data can be estimated as 15–30 cm (KURCZYŃSKI, BAKUŁA 2013). The ALS data in standard II of ISOK Project were sufficient for modelling the roof planes. Three height models in 0.5 m GRID format were generated with use of the classified point clouds.

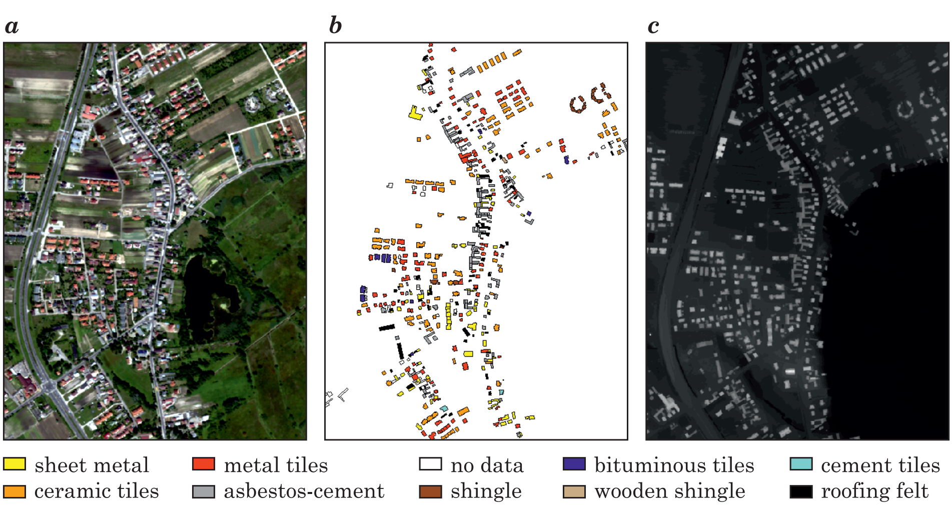

Fig. 1. Sample of WorldView-2 satellite image (*a*), visualization of the roof coverings database for the study area (*b*) and Digital Surface Model generated based on ALS data (*c*)

The Digital Terrain Model (DTM) was generated based on triangulation of points classified as ground points. During the Digital Surface Model (DSM) generation modelling of the classified point clouds dependent on land cover type according to the rules proposed by HOLLAUS et al. (2010) was applied. To determine the object height in flat (smooth) areas such as ground or roofs the IDW (Inverse Distance Weighting) interpolation was used. For areas covered with medium and high vegetation, considered as rough surfaces, the maximum point height in particular cells of resulting DSM was used (Fig. 1c).

The WorldView-2 image was acquired on August 4, 2011. Multispectral image bands are captured in the following wavelengths: 0.400–0.450 μm, 0.450–0.510 μm, 0.510–0.580 μm, 0.585–0.625 μm, 0.630–0.690 μm, 0.705–0.745 μm, 0.770–0.895 μm, 0.860–1.040 μm. The WorldView-2 satellite does not register middle infrared bands which according to BASSANI et al. (2007) are the most useful spectral range for chrysotile asbestos detection. However, at the start of this study WorldView-2 was the only very high resolution satellite system capturing such a large number of spectral bands, therefore it offered the best possibilities of remote detection of roofing materials. Available satellite systems capturing spectral data at the wavelength of ca. 2.3 μm, that is according to BASSANI et al. (2007) the best wavelength for chrysotile detection, have too large ground sampling distance for detection of roof materials (e.g. OLI on LANDSAT 8, HYPERION on EO-1, ASTER on TERRA). The characteristics of WorldView-2 satellite data used in the study are presented in Table 1.

Table 1

Characteristics of WorldView-2 multispectral image

Acquisition date	2011–08-04
Acquisition time	09:52:16.8
GSD	1.98 m
Global incidence	17.9°
Viewing angle across the track/ viewing angle along the track	17.8°/–1.7°
Sun azimuth	159.7°
Sun elevation	54.0°

The Worldview-2 image orthorectification was performed in the Photomod software (www.racurs.ru) using the Rational Polynomial Coefficients (RPC) model. 21 control points evenly distributed over the test area were used in order to register the scene. Accuracy of the registration was checked with the use of check points (Table 2). The orthorectification was performed in two ways. Firstly, a standard orthophoto with 2 m spatial resolution and a positioning accuracy of 2 to 3 pixels was created using the DTM. However, since objects above the terrain appeared displaced and the building roofs included many artefacts, it was decided to use the surface model (including additional information about heights of buildings) in the second orthorectification process. As results improved roofs localization in the corrected image was obtained.

Table 2
Accuracy assessment of orthorectification process of WorldView-2 image (MS DTM orthophoto)

Parameter	dX [px]	dY [px]	ds [m]
Control Points			
	dX [px]	dY[px]	ds [m]
RMS	0.36	0.38	0.28
Mean	0.30	0.30	0.26
Max.	0.57	0.85	0.43
Check Points			
RMS	0.31	0.54	0.31
Mean	0.27	0.48	0.28
Max.	0.42	0.71	0.40

Vector data from the roof covering database (RCDB) were used as the reference data for the classification accuracy assessment. This database was created based on visual interpretation of aerial orthophotomaps (with ground resolution of 0.25 m, building boundaries at ground level) and on the field observations. There are 636 residential houses and farm buildings in the roof covering database of Powsin housing estate.

Experiments description

In order to evaluate the possibilities of automatic extraction of information on roofing material types several experiments were performed which included the supervised classification. All operations were performed with the use of ERDAS Imagine 2014 software, made available by the Intergraph Polska. The flowchart of the procedure used in the study is shown in Figure 2, where MS stands for multispectral image, MS DTM for standard orthophoto based on the DTM, MS DSM for true-orthophoto based on the DSM and MS TOPO for true-orthophoto based on the DSM and with topographically corrected roof reflectance's. The superscript „f" indicates results after majority filtering.

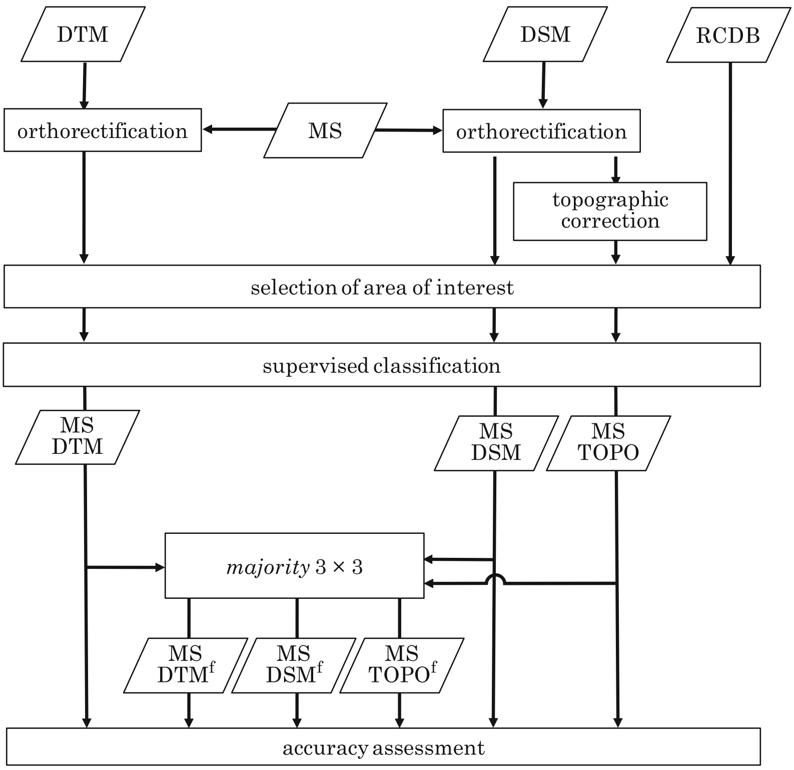

Fig. 2. Methodology scheme

The supervised classification was performed for the building roofs only, obtained by masking areas outside of the roof coverings vectors (RCDB). Building outlines could also be obtained from laser scanning data by applying an appropriate filtering algorithm. In many cases the ALS-based roofs and those from the RCDB overlap and in deliver comparatively satisfying results, but especially in regions with tall vegetation hanging OVER roofs problems occur. Therefore the decision has been made to further use the RCDB only.

The supervised classification was performed using the maximum likelihood algorithm for set of orthophotos: the MS DTM, the MS DSM, and the MS TOPO. Topographic effect is caused by differences in illumination due to the incidence angle of sun radiation onto the object surface, thus a significant variation in the pixel values of the same object occurs. One way to reduce topographic effect in imagery is by applying transformations based on the Lambertian reflectance models. The topographic corrections were performed with the cosine method described, among others, in RICHTER et al. (2009). This method assumes that the surface reflects incident solar energy uniformly in all directions, and that variations in reflectance are due to the amount of incident radiation which in turn depends on the incidence angle of the illumination (COLBY 1991). But for low illumination, i.e., large incidence angles and thus small values of cosine, the corrected reflectance is too large and the corresponding parts of an image are overcorrected (RICHTER et al. 2009). In the study area in most cases the local solar illumination angles vary in the range of 15–58°. The largest angles of incidence are on the north-west facing roof planes because of the south-east sun azimuth at the time of image acquisition.

For every variant a set of training fields was prepared, representing all types of roofing materials present within the study area, namely: sheet metal, metal tiles, bituminous tiles, cement tiles, ceramic tiles, asbestos cement, shingle, wooden shingle (only one roof) and roofing felt. In the case of the sheet metal roofings three training fields (zinc coated sheet metal, copper sheet and painted sheet – only red painted sheet in the study area) and for metal tiles two training fields (red metal tiles and dark red metal tiles) were defined. Prepared training fields contain ca. 300–500 pixels. Examples of spectral characteristics of class patterns obtained for multispectral image (MS DSM orthophoto) are presented in Figure 3.

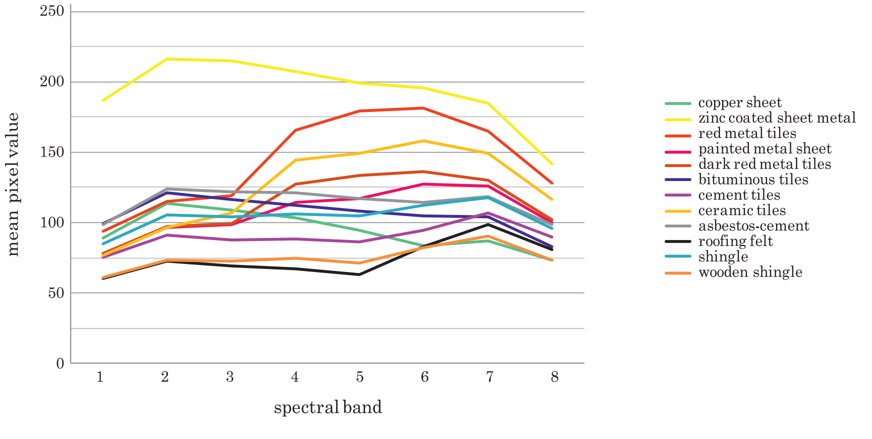

Fig. 3. Mean spectral characteristics of class patterns obtained for MS DSM orthophoto

Due to the spatial resolution of 2 m the stripe texture of roofing materials for corrugated metal plates and asbestos-cement plates, often used as roofing material of farm buildings, was not visible. This limited the necessity to define more samples and simplified the process of representative sample selection. All training fields fulfilled the criteria for this type of patterns. The evaluation of class separability with the transformed divergence and Jeffries-Mattusita's distance yielded good results, except for the following pairs: dark red metal tiles and ceramic tiles, asbestos-cement and cement tiles, asbestos-cement and shingle (cement shingle), shingle and copper sheet as well as dark red metal tiles and red painted sheet. The latter pair showed the highest radiometric similarity and therefore it was decided not to include the red painted sheet in the classification process. When analysing the separability of training fields derived from the three variants of input data (i.e. MS DTM, MS DSM, MS TOPO), MS TOPO showed a slightly better separability than MS DSM.

Results analysis and discussion

The obtained classification results show that roofs made of one material are usually classified as several types of roofing materials (Fig. 4). That effect is mainly caused by the differences in illumination of individual roof shapes caused by additional roof elements such as skylights, roof windows, chimneys, and so-called the mixels on roof edges.

The variable influence of illumination is clearly visible in the case of classification of the multispectral image after orthorectification with the use of DTM (MS DTM, Fig. 4*a*) as well as after orthorectification with the use of DSM (MS DSM, Fig. 4*b*). The satellite image was acquired at 9:52 AM and with the south-east Sun position the north-west roof shapes were half-shaded. After detailed analysis of obtained results it can be noticed that after orthorectification with the use of DSM the number of mixels on roof edges decreased, but it has no significant influence on evaluation of classification results. Unfortunately, the topographic correction performed with the cosine method did not result in expected significant improvement of the classification results. An improvement is only visible in the case of roofs with not complicated shapes with a relatively low slope angle value. In the case of multi-shaped roofs of diverse slopes the topographic correction resulted in deterioration of the classification results. The main problem concerning topographic correction is that the cosine method results are overcorrected for low illumination (RICHTER et al. 2009). In the case of areas with diversified relief or roofing shapes this type of situations occurs quite often (in the analysed image it may be visible only on the northern-west side of roofs).

Due to the fact that several classes can be found in an individual roof, including single-pixel classes, a *majority* 3×3 filter was used to filter the classification results. This filter selects the most common pixel value within the filter window. In result more homogeneous classification results were obtained for individual roofs and the influence of edge-pixels and pixels of different roof elements (such as roof windows, roof hatches, chimneys) was limited. The result after filtering is presented in Figure 4*d, e, f*.

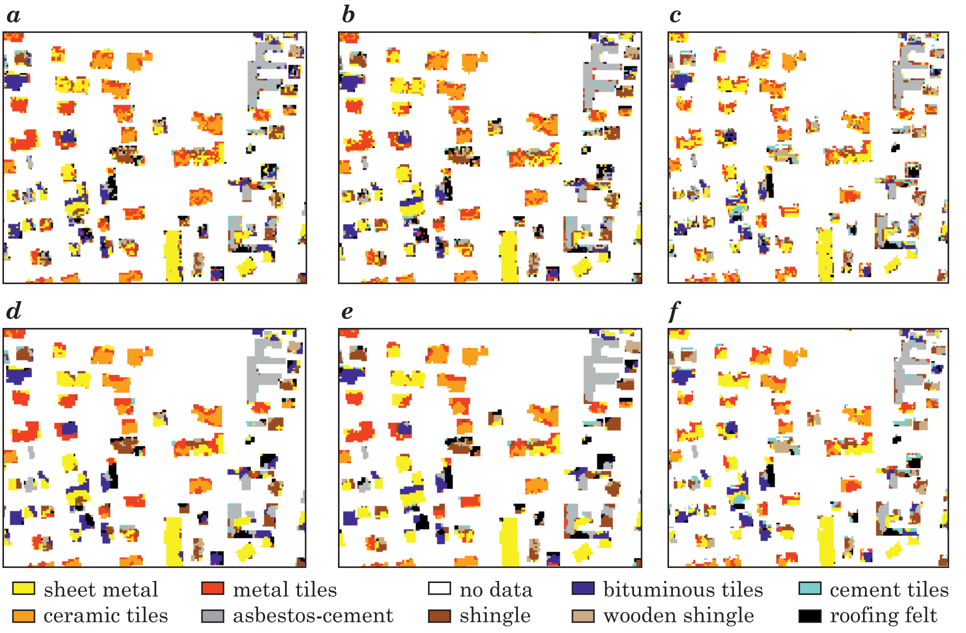

Fig. 4. Comparison of the supervised classification results of the multispectral image orthorectified using the DTM (*a*), the multispectral image orthorectified using the DSM (*b*), the multispectral image orthorectified using the DSM after topographic correction (*c*) and results of classification after majority filter 3×3 (*d*, *e*, *f*)

Evaluation of the classification results was done by comparison with the roofing materials coverings database. It was performed according to two approaches: a conventional pixel-oriented and the object-oriented approach[1], with respect to the roofing materials vector database. In the per object analysis for individual roof (polygon/object in vector database) major roofing material type is considered because during the field survey it was not noticed that the mixed type of roofing material for individual building existed. Additionally it eliminates the problem of different class values in the case of edge pixels or pixels of roof windows or pixels of different elements of roofs which results in incorrect values of roofing material classes.

Comparison of the classification results of different input data given per object with the reference database is presented in Figure 5. Results obtained from classification of three orthophotos (MS DTM, MS DSM, MS TOPO) seem to be similar when compared visually however some differences rise in the accuracy assessment statistic. Table 3 presents results of the accuracy assessment of several classification variants, according to the pixel and per object approaches, for: MS DTM, MS DSM, MS TOPO.

[1] Not to be confused with of object oriented classification (OBIA).

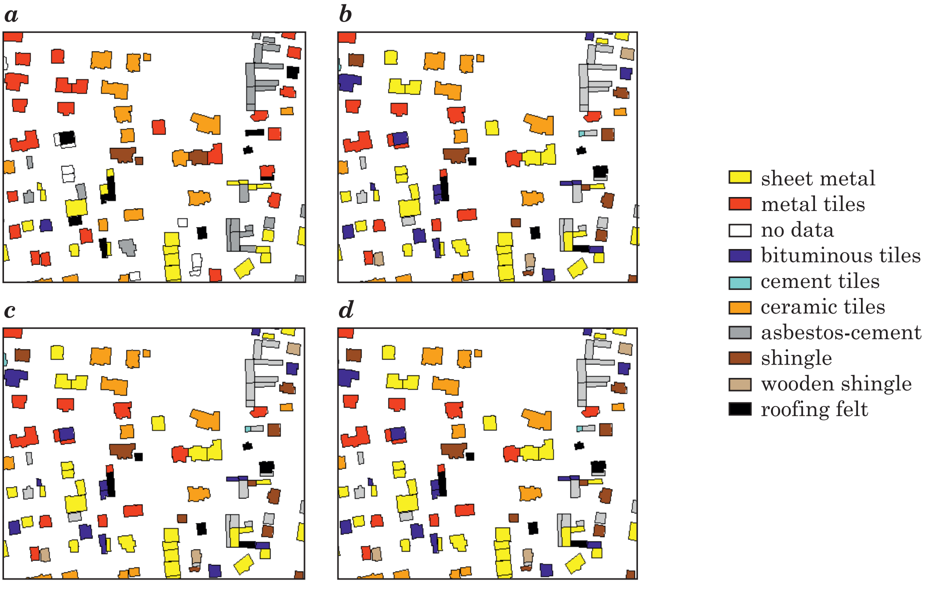

Fig. 5. Comparison of supervised classification results in object-oriented approach of the multispectral image orthorectified using the DTM (*b*), the multispectral image orthorectified using the DSM (*c*), the multispectral image orthorectified using the DSM after topographic correction (*b*), and the roofing materials database (*a*)

Based on results analysis it may be stated that asbestos-cement roofing, as well as ceramic roofing plates are classified with the highest accuracy. In the case of other roofing materials both, much lower producer's and user's accuracy may be noticed. For the asbestos-cement roofing and ceramic roofing plates slightly higher values of the user's accuracy may be noticed for the image orthorectified based on the DSM than with the use of the DTM. This results from the fact that in an image rectified based on the DSM the roof position is correct (no building layover effect) and after masking of the area of interest we deal with the lower number of edge pixels.

In the case of information extraction concerning asbestos-cement roofing the producer's accuracy reaches the level of 81–85%, depending on the type of classified data. The user's accuracy reaches 57–66% in this case. Asbestos-cement roofings are quite often classified as (damaged) roofing felt or cement roof tiles or cement shingle. In the case of ceramic roof tiles the producer's accuracy reaches as much as 95%, but the user's accuracy varies between 41 and 53%. This is due to the fact that roofs with red metal roof tiles are mainly classified as ceramic roof tiles. Similar accuracy was obtained by HEROLD et al. (2003) for classification of ceramic roof tiles. However, using the principle component analysis method (made only for roofs image), at the stage

Table 3

Summary of the accuracy* of different variants of the classification – the pixel-oriented approach (P) and pre object (O). MS DTM – multispectral image orthorectified using the digital terrain model, MS DSM – multispectral image, orthorectified using the digital surface model, MS TOPO – multispectral image after orthorectification using the digital surface model after topographic correction

Specyfication			Sheet metal	Metal tiles	Bituminous tiles	Cement tiles	Ceramic tiles	**Asbestos-cement**	Shingle	Roofing felt
Validation samples	No. of pixels		54715	87852	11112	2324	99546	**77968**	13673	42935
	No. of roofs		83	120	11	4	101	**143**	26	82
MS DTM	user's accuracy	P	54.4	29.3	45.3	40.7	50.0	**65.7**	33.4	28.6
		O	63.9	34.2	45.5	50.0	57.4	**79.7**	42.3	39.0
	producer's accuracy	P	43.9	36.0	11.7	6.4	94.5	**81.5**	11.0	52.8
		O	53.0	47.1	8.1	5.9	100	**86.4**	20.4	71.1
MS DSM	user's accuracy	P	56.8	26.6	41.5	42.8	52.6	**65.8**	35.2	30.5
		O	65.1	26.7	27.3	50.0	59.4	**84.2**	46.2	40.2
	producer's accuracy	P	46.2	35.9	13.0	6.0	93.7	**81.3**	10.3	48.4
		O	58.1	42.1	6.3	5.0	98.4	**88.1**	16.4	64.7
MS TOPO	user's accuracy	P	51.9	21.6	40.4	41.7	41.1	**57.1**	26.7	25.5
		O	59.0	20.8	45.5	50.0	47.5	**76.9**	23.1	20.7
	producer's accuracy	P	34.5	29.8	11.7	4.0	89.0	**84.6**	9.4	58.9
		O	44.5	37.3	7.4	2.9	98.0	**91.7**	10.9	58.6
MS DTM**	user's accuracy	P	57.8	32.0	51.0	53.1	52.4	**74.1**	41.2	31.9
		O	61.4	33.3	45.5	50.0	56.4	**79.7**	42.3	36.6
	producer's accuracy	P	49.6	37.0	13.1	10.1	97.3	**85.1**	15.1	56.5
		O	53.7	46.5	8.3	6.3	100	**86.4**	17.5	71.4
MS DSM**	user's accuracy	P	60.5	27.9	46.7	56.3	56.2	**73.9**	40.9	35.7
		O	66.3	26.7	27.3	50.0	59.4	**83.9**	46.2	42.7
	producer's accuracy	P	52.1	36.6	14.6	9.3	96.3	**84.9**	13.2	51.7
		O	60.4	41.6	6.7	5.3	98.4	**88.2**	16.7	66.0
MS TOPO**	user's accuracy	P	56.4	22.1	48.3	47.2	45.5	**65.6**	28.7	26.4
		O	57.8	20.8	45.5	50.0	47.5	**76.2**	26.9	23.2
	producer's accuracy	P	39.4	30.9	13.4	4.6	94.4	**87.4**	11.2	62.5
		O	46.2	35.2	7.7	2.4	96.0	**91.6**	13.2	67.9

* – because in the test area there is only one building with wooden shingle, it was omitted in the accuracy assessment.
** – image after filtering using *majority* 3×3 filter.

prior to the image classification, it is possible to improve the classification accuracy of those roofing materials (the user's accuracy may be improved to 70%). This was proved by (OSIŃSKA-SKOTAK 2014).

For the assessment per object higher accuracy was achieved for all types of roofing materials, both, with respect to the user's and the producer's accuracy. The highest accuracy was obtained for asbestos-cement roofing materials. In the case of classification of an image after topographic rectification accuracy of almost 92% was obtained, and the user's accuracy reached 77%. Image filtering using the *majority* 3×3 filter did not lead to considerable improvements in obtained accuracy.

When analysing the list of results presented above, it may be noticed, that the applied topographic correction did not considerably improve the classification results. Only improvements of the classification results may be seen in the case of uncomplicated, gable or hip pyramid roofs or in the case of hip roofs. In the case of more complicated roof constructions of high inclination angles, too high „saturation" value of pixels is noticeable. This might be partly explained by differences in spatial information content between satellite multispectral data (2 meters) and ALS data used.

Conclusions

Results of experiments performed in the study prove that automatic detection of roofing materials is a challenging issue. The highest accuracy of the supervised classification of the WorldView-2 image was achieved for asbestos-cement roofing materials (76–92%, depending on the variant of classification). Another type of roofing materials which is characterised by the very high producer's accuracy are ceramic roof tiles. Much lower accuracy values were achieved for other types of roofing materials. This results from the high similarity of some roofing materials (metal tiles, painted steel plates, bituminous tiles and roofing felt). However, after grouping roofs made of similar materials it is possible to achieve classification results with the accuracy of ca. 70–80%.

As presented, the accuracy of classification of a multispectral image orthorectified with the use of the digital surface model is slightly higher comparing to the accuracy of classification of a multispectral image orthorectified using the digital terrain model. Unfortunately, topographic correction of a multispectral image performed using the cosine method did not result in expected improvements of roofing materials classification results. Some positive effects may be seen only in the case of uncomplicated roof construction, such as gable and hip pyramid roofs, as well as hip roofs.

Acknowledgements

The authors are grateful to MGGP Aero company for making the aerial orthophotomap of Capital City Warsaw available for the purpose of presented analyses. The authors also wish to thank Intergraph Poland for access to the latest version of the ERDAS Imagine software.

References

ALMEIDA C.M., SOUZA I.M.E., ALVES C.D., PINHO C.M.D., PEREIRA M.N., FEITOSA R.Q. 2007. *Multilevel Object-Oriented Classification of QuickBird Images for Urban Population Estimates*. 15th ACM International Symposium on Advances in Geographic Information Systems (ACM GIS 2007), Seattle.

ATTURO C., FIUMI L. 2005. *Thermographic analyses for monitoring urban areas in Rome to study Heat Islands*. International Conference „Passive and Low Energy Cooling 145 for the Built Environment", May' 2005, Santorini, Greece, p. 145–150.

BASSANI C., CAVALLI R.M., CAVALCANTE F., CUOMO V., PALOMBO A., PASCUCCI S., PIGNATTI S. 2007. *Deterioration status of asbestos-cement roofing sheets assessed by analyzing hyperspectral data*. Remote Sensing of Environment, 109(2007): 361–378.

BELGIU M., TOMLJENOVIC I., LAMPOLTSHAMMER T.J., BLASCHKE T., HÖFLE B. 2012. *Ontology-Based Classification of Building Types Detected from Airborne Laser Scanning Data*. Remote Sensing, 6: 1347–1366, DOI:10.3390/RS6021347.

CHEN Y., SU W., LI J., SUN Z. 2009. *Hierarchical object-oriented classification using very high resolution imagery and LIDAR data over urban areas*. Advances in Space Research, 43: 1101–1110.

COLBY J.D. 1991. *Topographic Normalization in Rugged Terrain*. Photogrammetric Engineering & Remote Sensing, 57(5): 531–537.

DINIS J., NAVARRO A., SOARES F., SANTOS T., FREIRE S., FONSECA A., AFONSO N., TENEDÓRIO J. 2010. *Hierarchical object-based classification of dense urban areas by integrating high spatial resolution satellite images and LIDAR elevation data*. The International Archives of the Photogrammetry, Remote Sensing and Spatial Information Sciences, XXXVIII(4/C7): 6.

DYCZEK J. 2007. *Azbest i materiały zawierające azbest. Ocena ryzyka emisji włókien azbestu*. In: *Bezpieczne postępowanie z azbestem i materiałami zawierającymi azbest*. Ed. J. Dyczek. Wydawnictwo Naukowe „Akapit", Kraków, p. 7–26.

FONSECA L., NAMIKAWA L., CASTEJON E., CARVALHO L., PINHO C., PAGAMISSE A. 2011. *Image Fusion for Remote Sensing Applications*. In: *Image Fusion*. Ed. O. Ukimura. Publisher: InTech, p. 153–178.

HEROLD M., SCEPAN J., MÜLLER A., GÜNTHER S. 2002. *Object-Oriented Mapping and Analysis of Urban Land Use/Cover Using IKONOS Data*. Proceedings of 22nd EARSeL Symposium Geoinformation for European-Wide Integration, Prague, Czech Republic, 4–6 June 2002.

HEROLD M., GARDNER M., ROBERTS D. 2003. *Spectral resolution requirements for mapping urban areas*. IEEE Trans. Geoscience Remote Sensing, 419): 1907–1919.

HOLLAUS M., MANDLBURGER G., PFEIFER N., MÜCKE W. 2010. *Land cover dependent derivation of digital surface models from airborne laser scanning data*. The International Archives of the Photogrammetry, Remote Sensing and Spatial Information Sciences, 38: 1–3.

KURCZYŃSKI Z., BAKUŁA K. 2013. *The selection of aerial laser scanning parameters for country wide digital elevation model creation*. 13th SGEM GeoConference on Informatics, Geoinformatics and Remote Sensing. SGEM2013 Conference Proceedings, 2: 695–702, DOI:10.5593/SGEM2013/BB2.V2/S10.020.

OSIŃSKA-SKOTAK K. 2014. *Zastosowanie technik teledetekcyjnych do inwentaryzacji cementowo-azbestowych pokryć dachowych*. Teledetekcja Środowiska, 51(2): 73–83.

Richter R., Kellenberger T., Kaufmann H. 2009. *Comparison of topographic correction methods.* Remote Sensing, 1: 184–196, DOI:10.3390/RS1030184.

Roberts D.A., Herold M. 2004. *Imaging spectrometry of urban materials.* In: *Infrared Spectroscopy in Geochemistry, Exploration and Remote Sensing*. Eds. P. King,, M.S. Ramsey, G. Swayze. The Mineralogical Association of Canada, Short Course Series, 33: 155–181.

Story M., Congalton R. G. 1986. *Accuracy assessment: A user;s perspective*. Photogrammetric Engineering and Remote Sensing, 52: 397–399.

Szeszenia-Dąbrowska N., Sobala W. 2010. *Zanieczyszczenie środowiska azbestem. Skutki zdrowotne*. Raport z badań, Instytut Medycyny Pracy im. prof. J. Nofera, Oficyna Wydawnicza MA, Łódź.

Valero S., Chanussot C., Gueguen P. 2008. *Classification of basic roof types based on VHR optical data and digital elevation model*. IGARSS' 2008, Commission IV, p. 149–152.

Technical Sciences 18(4), 2015, 299–311

EVALUATION OF STATIC GNSS POSITIONING ACCURACY DURING SELECTED NORMAL AND HIGH IONOSPHERIC ACTIVITY PERIODS

Stepan Savchuk, Iryna Hiryak

Department of Higher Geodesy and Astronomy
Lviv National Polytechnic University, Lviv, Ukraine

Received 25 June 2015; accepted 24 August 2015; available on line 27 August 2015.

Key words: ionosphere, index I95, magnetic activity, single frequency GNSS observations, dual frequency GNSS observations.

Abstract

This article presents the results of the experimental research into the ionospheric influences on the accuracy of the GNSS measurements by comparing single and dual frequency GNSS observations. In the research, GNSS data from three reference stations in central Poland were used. The selection of the observation period depended on the calm and disturbed ionospheric conditions. The purpose of the research was to determine the differences between the control coordinates of the stations and the coordinates of these stations received after processing the results of single and dual frequency GNSS observations. For a better visibility, these differences were presented as horizontal and vertical components. The values of these components are compared with the global magnetic activity and regional ionospheric index I95. The results obtained show that the ionosphere has a considerable impact on single frequency GNSS measurements according to the geodetic requirements, although this impact depends more on the state of ionosphere rather than on its space-time changes.

Introduction

The main principle of the GNSS measurements is based on the determination of the amount of time it takes for an electromagnetic signal to travel from the satellite to the receiver. Because the signal travels through the heterogeneous atmosphere (ionosphere and troposphere), it will be distorted under its influence. One of the major errors in this case is the ionospheric delay.

The ionospheric impact on the distribution of the GNSS signals causes phase and group delays. The signal delay in the ionosphere depends on the

Correspondence: Stepan Savchuk, Department of Higher Geodesy and Astronomy, Lviv National Polytechnic University, 6 Karpinski St., 79013 Lviv, Ukraine, e-mail: imsavchuk@ukr.net

solar activity, seasonal and daily variations, zenith distance and azimuth satellites, location of an observer. The measurement error of the pseudorange can be more than 50 m due to the delay of the GNSS signals in the ionosphere (SEEBER 2003).

Unlike the troposphere, that is not a dispersive medium and does not affect the propagation of the GNSS signals, the ionosphere is a dispersive medium and its impact depends on the satellite signal frequency. This factor helps minimize the measurement error in the computation of the ionospheric delay for the satellite signal.

The overall ionospheric impact on the satellite signal can be hypothetically divided into three components:

– 1st order impact (≈ 99%);
– 2nd order impact (≈ 0.8%);
– 3d order impact (≈ 0.2%).

The first order refractive index only accounts for the electron density within the ionosphere, while the effect of the Earth's magnetic field and its interactions with the ionosphere are considered in the higher order terms; i.e. the second and third terms.

The 1st order impact of the ionosphere can be fully compensated due to the dispersion, namely 99% of its total impact if to use dual frequency (multifrequent) equipment (receiver and antenna). The detection and estimation of ionospheric impact during single frequency GNSS observation poses a special problem.

The main source of errors in single frequency equipment when measuring pseudorange is the signal propagation delay in the ionosphere that is caused by the total electron content (TEC) along the pass of the signal. This type of equipment does not allow to use the signals at the two coherent frequencies to avoid the ionospheric measurement error.

There are two methods to compute the ionospheric delay for single frequency equipment (SEEBER 2003). The first one is the correction of pseudoranges using ionospheric model parameters (KLOBUCHAR 1991) received in a GPS navigation message. The application of ionospheric model that is used in GPS allows to reduce ionospheric impact on the standard deviation when determining coordinates. It is experimentally proven that the real deviation reduction is possible only on approximately 50% (KAZANTSEV, FATEEV 2002). The second and the most promising method is the usage of properties of the received signals. According to this method, the calculation of the ionospheric signal delay is based on the fact that the phase and group ionospheric delays of the GNSS signals are equal in values but opposite in signs (GUOCHANG 2007).However, existing methods based on this approach have one common limitation – the additional identification of initial ambiguities in phase measurements (KRANKOWSKI et al. 2007). This problem complicates the implementation and reduces the efficiency of such method, which explains its limited use in practice.

Lately, the scientists actively work on the study of phase fluctuations and failures in GNSS phase and code measurements under conditions of geomagnetic disturbances (AFRAYMOVICH, USHAKOV 2003). Magnetospheric storms and substorms cause geomagnetic disturbances that result in a wide range of irregularities and processes in the Earth's ionosphere (HUNSUCKERET et al. 1996). Classic picture of ionospheric disturbances is proven by numerous observations (CHERNOGOR et al. 2014, BURMAKA, CHERNOGOR 2012). However, the physical nature of numerous mechanisms is not yet clear enough. The effects of a storm/substorm in the ionosphere depend on a great number of parameters such as local time, latitude, season, solar activity phase, storm/substorm intensity, and others. Thus, it is necessary to study the impact of signal propagation delay in the ionosphere on the measurement errors of defining coordinates, as this issue remains unexplored throughout the whole period of GNSS usage.

Experiment description

For the study of the ionospheric impact, three stations with accurate coordinates (determined from long-term GNSS observations and adopted as control coordinates) are chosen. One station is used as a base station and two other are used as test stations to form 2 baselines for the computations. The distance between the stations depended on the possibility to determine the significant ionospheric impact. Thus, for short distances it would be more difficult to analyze the research results. That is why the approximate distances from the vector stations to the basic have to be 35–40 km and 85–90 km correspondingly. Based on hourly observations, the coordinate change had to be determined during the processing of single and dual frequency observations. For practical implementation of this research, we processed GNSS data from three reference stations in central Poland: BOGO (Borowa Gora), JOZE (Jozefoslaw), and LODZ (Lodz).The basic station in the research was JOZE. The distance between the BOGO and JOZE stations was approximately 40 km and between the JOZE and LODZ stations – 90 km. The observation period depended on the calm (2–6/12/2014, 9–15/02/2015, 16/03/2015) and disturbed (1, 7/12/2014, 17–22/03/2015) ionospheric conditions.

GNSS observation data was processed in Trimble Business Center.

Figure 1 shows the location of the stations on the map and Table 1 provides the control coordinate values (EPN 2015).

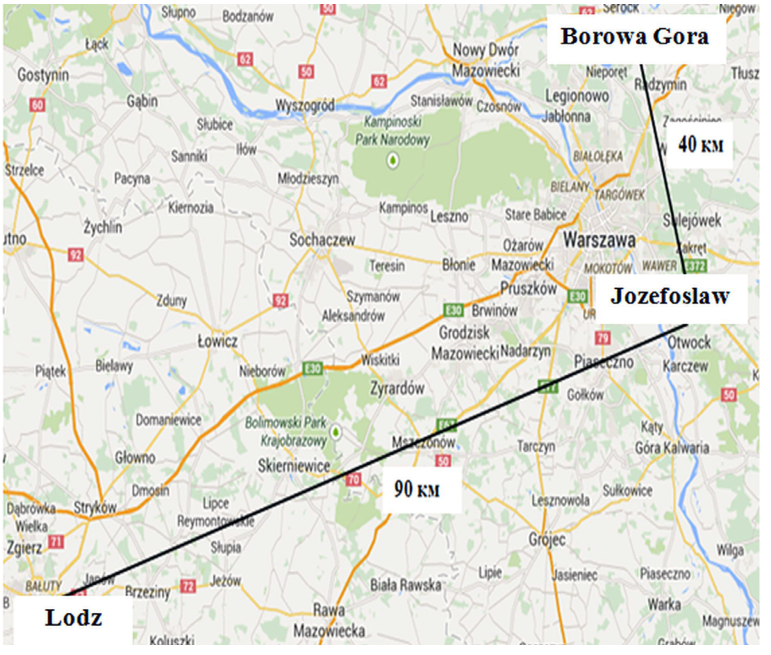

Fig. 1. Location scheme of the reference stations BOGO, JOZE, LODZ

Table 1

Control coordinates of the stations BOGO, JOZE, LODZ

Station name	Coordinates [m]		
	X	*Y*	*Z*
BOGO	3633738.798	1397434.280	5035353.563
JOZE	3664939.989	1409154.013	5009571.472
LODZ	3728601.378	1317402.626	4987811.422

The purpose of the research is to compare station coordinates obtained after processing of single and dual frequency GNSS observations with the control coordinates provided in Table 1.

For a better clarity and visibility, the differences between the processed and control coordinates are converted into topocentric coordinates dN, dE, and dU, which are further represented as horizontal $H = \sqrt{N^2 + E^2}$ and vertical $V = U$ components. These components are the object of the analysis and are compared with the regional ionospheric index (I95) and global magnetic activity (MAG).

Using ionospheric index I95, the impact of the ionosphere on the determination of coordinates with the help of GNSS can be calculated with the accuracy up to 95% (WANNINGER 2004). Therefore, I95 is a statistic index that provides information about the value of differential ionospheric errors. Index is calculated using the GNSS observations results. One value of I95 includes differential ionospheric errors of all accessible satellite signals from at least three reference stations. The I95 value depends not only on the ionospheric conditions but also on other factors such as distance between the reference stations and elevation (SAPOS 2015).

Index values range between:

0–2 – normal level of ionospheric activity;

2–4 – moderate level ionospheric activity;

4–8 – high level of ionospheric activity.

Magnetic activity is a disturbance in Earth's magnetic field that is connected with the changes in magnetosphere-ionosphere current system. It is a part of the Sun-Earth connection physics and, correspondingly, the space weather. The main manifestations of the magnetic activity are strong disturbances – magnetic storms and substorms, and light disturbances – different kinds of magnetic pulsations (GFZ-Potsdam 2015).The condition of the magnetic field can be described using the Kp index:

$K \leq 2$ calm storm conditions;

$K = 2, 3$ minor disturbances;

$K = 4$ disturbances;

$K = 5, 6$ magnetic storm;

$K \geq 7$ strong magnetic storm.

The information about ionospheric conditions and the change in magnetic activity parameters can be obtained on the Internet (TESIS 2015).

Calculation results

Figures 2, 3, 4, and 5 show the variations of *H* and *V* components for the BOGO station. Analysis of Figures 2 and 3 shows that there are considerable jumps in values of horizontal and vertical components for single frequency observations. These values are mostly positive and reach up to 40 cm. Figures 4 and 5 show that the values of horizontal and vertical components are smaller and do not exceed 5 and 10 cm, correspondingly.

Figures 6, 7, 8, and 9 illustrate variations of *H* and *V* components for the LODZ station. Figures 6 and 7 show that single frequency observations at a bigger distance have considerable influence on the way the vertical component changes. The values of these changes are both positive and negative and

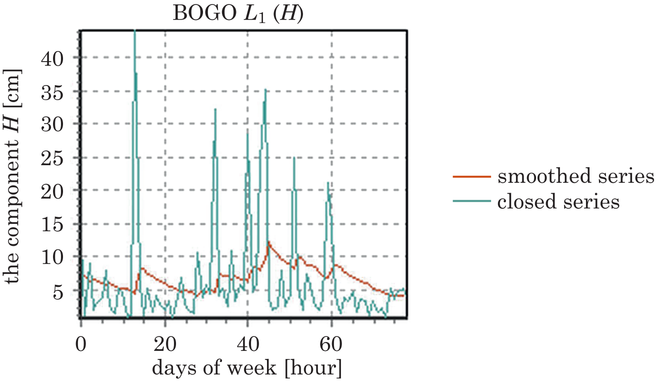

Fig. 2. H variations for single frequency observations

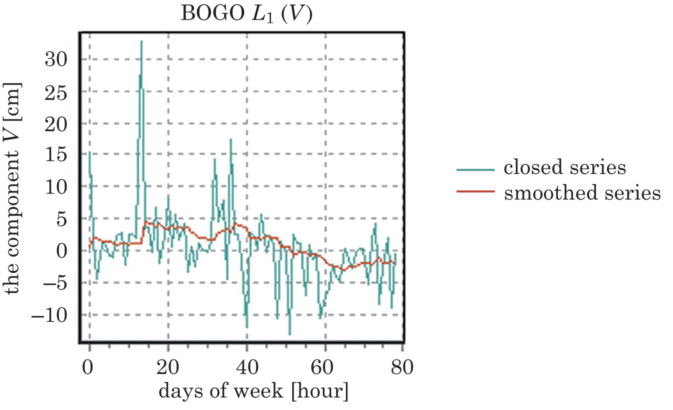

Fig. 3. V variations for single frequency observations

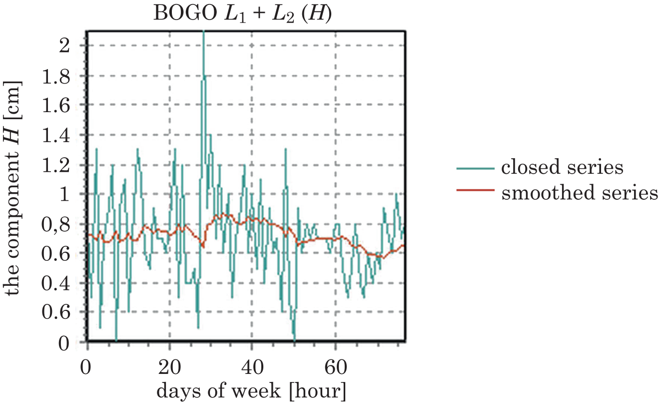

Fig. 4. H variations for dual frequency observations

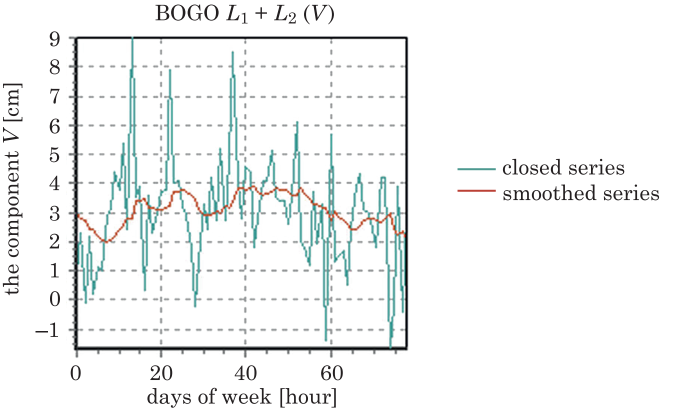

Fig. 5. V variations for dual frequency observations

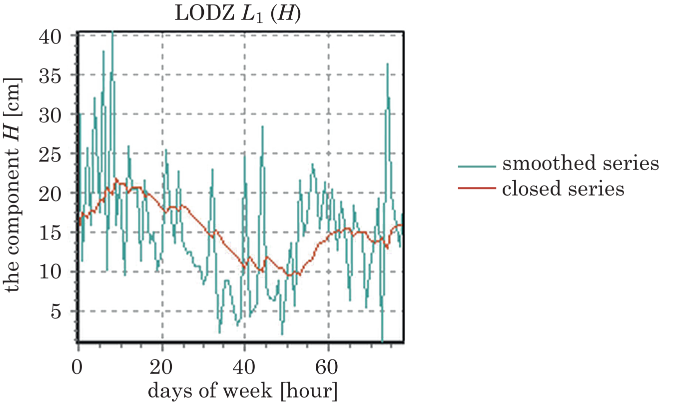

Fig. 6. H variations for single frequency observations

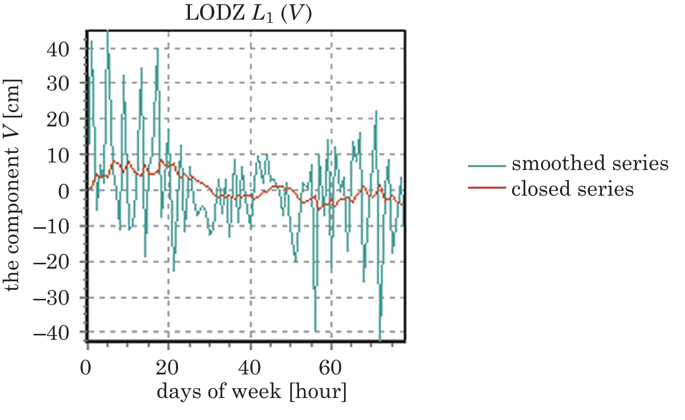

Fig. 7. V variations for single frequency observations

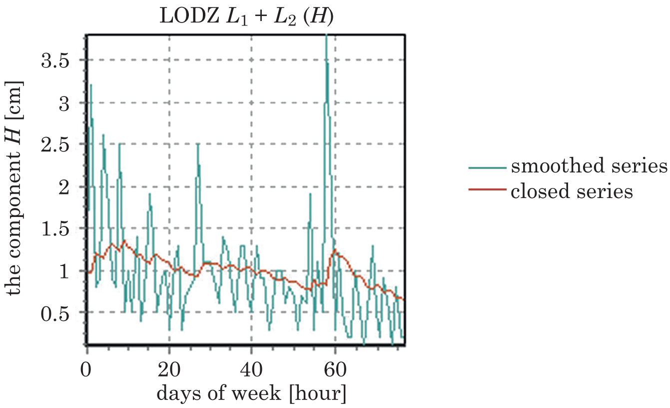

Fig. 8. N variations for dual frequency observations

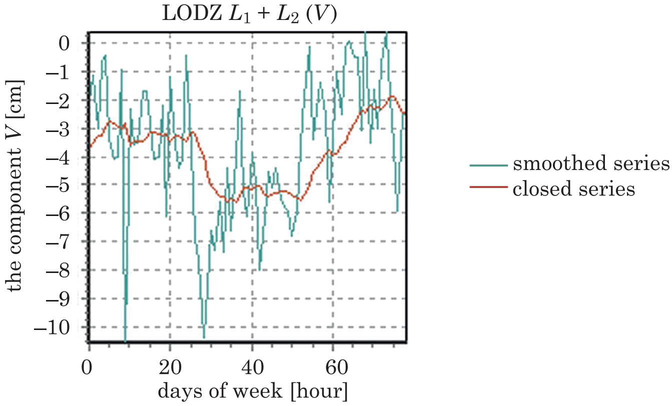

Fig. 9. V variations for dual frequency observations

range between -40 and 40 cm. Such fluctuations can be caused by the shift in ionosphere heterogeneity changes in space and time. Figures 8 and 9 show that bigger distance between the stations does not influence the results of dual frequency observations as the values of horizontal and vertical components do not exceed 5 and 10 cm correspondingly.

To our opinion, only the ionosphere can cause considerable deviations of single frequency observations discovered during the analysis of the obtained results.

Similar studies were conducted for three other reference stations in western Ukraine: MYKO (Mykolaiv), STRY (Stryi), and SKOL (Skole). The distances between these stations are similar to those in Poland. MYKO is used as a base station. The distance between the MYKO and STRY stations is approximately 35 km and between the MYKO and SKOL – 70 km. The observation period is 03/12/14. Figure 10 shows locations of the stations, and Table 2 provides their control coordinates.

Table 2

Control coordinates of the MYKO, STRY, and SKOL stations

Station name	Coordinates [m]		
	X	*Y*	*Z*
MYKO	3790465.481	1685988.196	4828829.875
STRY	3812850.835	1687385.931	4810814.627
SKOL	3841562.710	1671363.028	4793846.225

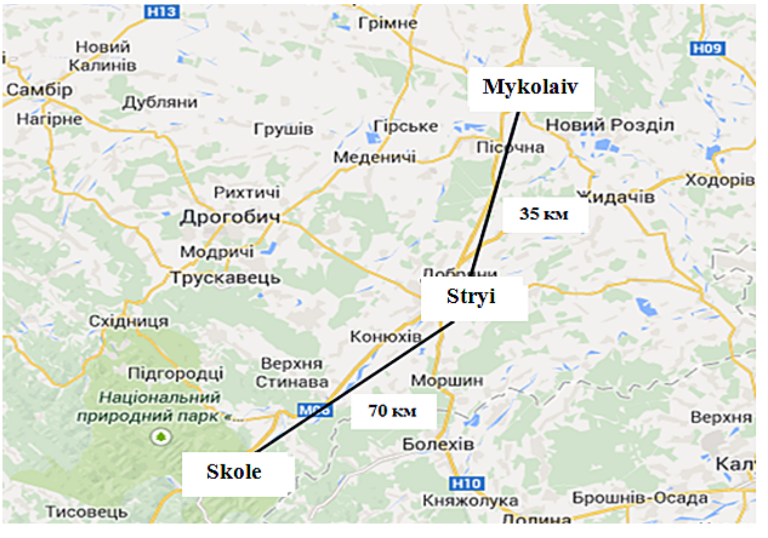

Fig. 10. Location scheme from MYKO, STRY, and SKOL reference stations

Considerable coordinate changes can be observed after the analysis of the obtained results from the reference stations in both Poland and Ukraine. Graphically the results are represented in Figures 11 and 12. The distance between the stations is 35–40 km. The similar results are obtained for the stations at the distance 70–90 km between each other (Fig. 13 and 14).

In general, 168 hourly observing sessions are processed. Approximately 5% of them did not result in a fixed solution. Most likely, this can be caused by the impact of the ionosphere.

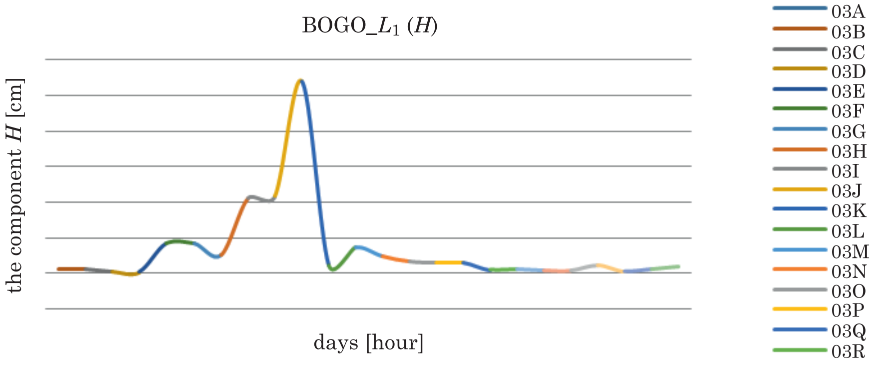

Fig. 11. H variations for single frequency observations at the BOGO station

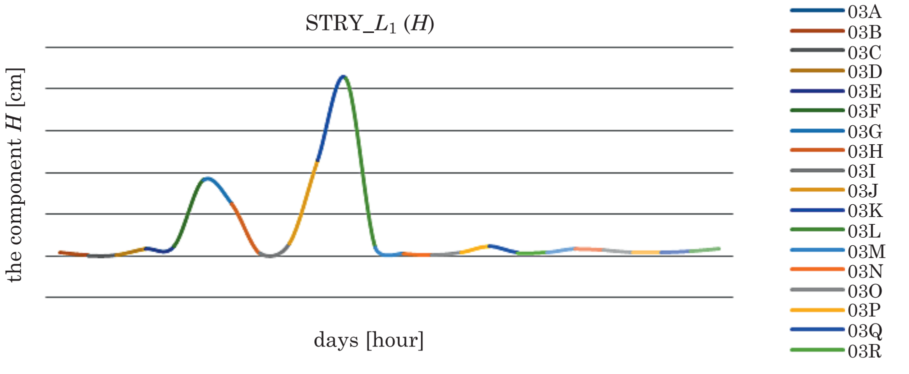

Fig. 12. H variations for single frequency observations at the STRY station

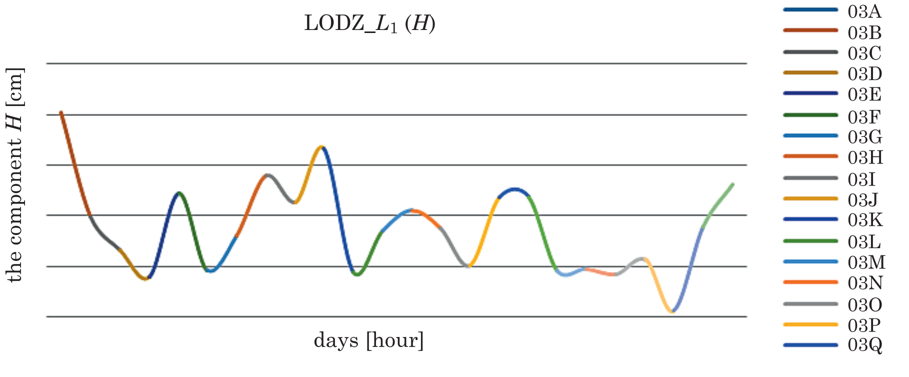

Fig. 13. V variations for single frequency observations at the LODZ station

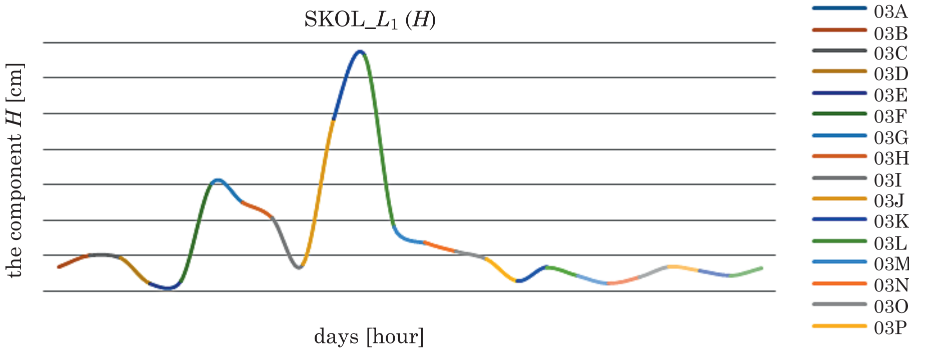

Fig. 14. *V* variations for single frequency observations at the SKOL station

The figures above show that the connection of the vertical and horizontal components with regional ionospheric impact is evident and with global magnetic activity is practically missing. This is due to the processing technology of the satellite observation results according to the relative method and the fact that the important factor is ionospheric space-time change and not its absolute indicators.

Table 3 includes the value percentage of the horizontal and vertical components obtained from the GNSS observations processing.

Thus, the ionospheric impact on the relative single frequency GNSS observations is essential to understand the geodetic practice requirements, especially with the distance between the stations of 40 km and more. The condition of the ionosphere (either calm or disturbed) is not as important as the space-time change.

Table 3

H and *V* percentage for single and dual frequency observations

Value	Percentage [%]			
	L_1		$L_1 + L_2$	
	H	*V*	*H*	*V*
≈ 100 cm	0	0	0	0
≈ 50 cm	1	1	0	0
≈ 20 cm	14	20	0	0
≈ 10 cm	30	29	1	5
≈ 5 cm	55	50	99	95

Conclusions

The conducted research resulted in the following:

1. The accuracy of defining coordinates according to the single frequency observations is much worse. It ranges between 2 and 40 cm. The accuracy of the dual frequency observations is approximately 1–2 cm.

2. The distance between the research stations also influences the computation results. The ionospheric impact increases when the distance from the basic station gets bigger. For example, the errors for the BOGO station range between 1 and 50 cm for single frequency and between 0-3 cm for dual frequency observations. For the LODZ station, they range from 0 to 60 cm and 0–11 cm correspondingly.

3. Ionospheric disturbances slightly influenced the accuracy of the GNSS coordinates.

The errors are bigger for the calm condition of the ionosphere rather than for the disturbed. This indicates that the impact of the ionosphere is not driven by the absolute TEC level, but rather depends on its space-time dynamics, e.g., gradients in the TEC level, and the orientation of the processed baselines.

References

AFRAYMOVICH E.L., USHAKOV I.I. 2003. *Statistika sboev kodovyih izmereniy dalnosti v navigatsionnoy sisteme GPS pri geomagnitnyih vozmuscheniyah*. Sbornik dokladov IX mezhdunarodnoy konferentsii „Radiolokatsiya, navigatsiya, svyaz”, Voronezh, T. 3, p. 1680–1690.

BURMAKA V.P., CHERNOGOR L.F. 2012. *Volnovyie vozmuscheniya v ionosfere v techenie prodolzhitelnogo minimuma solnechnoy aktivnosti*. Geomagnetizm i aeronomiya, 52(2): 197–210.

EPN. 2015. On line: http://www.epncb.oma.be/

GFZ-Potsdam. 2015. On line: http://www.gfz-potsdam.de/kp-index/

GUOCHANG XU. 2007. *GPS Theory, Algorithms and Applications*. Springer Berlin Heidelberg New York.

HUNSUCKER R.D., ROSE R.B., ADLER R.W., LOTT G.K. 1996. *Auroral-E mode oblique HF propagation and its dependence on auroral oval position*. IEEE Transactions on Antennas and Propagation, 44: 383–388.

HUNSUCKER R.D., ROSE R.B., ADLER R.W., LOTT G.K. 1996. *Auroral-E mode oblique HF propagation and its dependence on auroral oval position*. IEEE Transactions on Antennas and Propagation, 44: 383–388.

KAZANTSEV M.YU., FATEEV YA.L. 2002. *Opredelenie ionosfernoy pogreshnosti izmereniya psevdodalnostey v odnochastotnoy apparature sistem GLONASS i GPS*. Zhurnal radioelektroniki, 12.

KLOBUCHAR J.A. 1991. *Ionospheric effects on GPS*. GPS World, 2(4): 48–51.

KRANKOWSKI A., SHAGIMURATOV I.I., BARAN L.W., YAKIMOVA G. 2007.*The structure of the mid- and high-latitude ionosphere during the November 2004 storm event obtained from GPS observations*. Acta Geophys., 55(4): 490–508.

SAPOS. 2015.On line: http://www.sapos.de/

SEEBER G. 2003. *Satellite Geodesy*. Walter de Gruyter, Berlin, New York, p. 586.

TESIS. 2015. On line: http://www.tesis.lebedev.en/

CHERNOGOR L.F., DOMNIN I.F., EMELYANOV L.YA., KATSKO S.V., KOTOV D.V., LYASHENKO M.V., PANASENKO S.V. 2014. *Rezultatyi nablyudeniy ionosfernyih protsessov nad Ukrainoy v 2012–2014 g.g*. Kosmichni doslidzhennya v Ukraini, 2012–2014: 21–28.

WANNINGER L. 2004. *Ionospheric Disturbance Indices for RTK and Network RTK Positioning. Proc. ION GNSS*. Long Beach, CA, 2849–2854.

Technical Sciences 18(4), 2015, 313–321

MATHEMATICAL PROBLEM OF STRAIGHTENING TEXT LINES

***Oleksandr Tymchenko*[1], *Irena Kulczycka*[2], *Karolina Szturo*[1]**

[1] Department of Safety Engineering
University of Warmia and Mazury
[2] Ukrainian Academy of Printing, Lviv

Received 19 February 2015; accepted 31 July 2015; available on line 17 August 2015.

Key words: recognition, optical recognition system, text document image, image distortion.

Abstract

The rapid distribution of digital cameras has caused several new problems related to text recognition. Based on experimental studies, was revealed that existing OCR systems cannot cope with complex perspective and geometric distortions that arise when photographing text document. Therefore it is necessary to apply text documents pre-processing so that the text lines were straight and horizontal. This article briefly consider existing methods pre-processing documents and found that it depend on the type of distortion and not universal. Proposed new method involving the mathematical raising of straightened text lines on the image and heterogeneous distortion correction based on a page surface transformation model. This method is better than others because it is universal and corrects any type of distortion, including a combination of several types of distortion.

Introduction

Very often there is a need to convert a paper text document or book into an electronic form (ARMS 2000). The process of translating paper documents into a digital form is carried out by a scan or photography. Because it is difficult to work with text document images (it is sometimes necessary to edit some part of the text), it is more convenient to present this image in a text editor. Optical recognition systems are often sufficient to deal with this task (such as FineReader, Omnipage, Readlris). The optical text recognition system acquires digital representation of the scanned or pictured document and has to form a text which is contained in this image, in a form suitable for saving in an electronic text document format.

Correspondence: Oleksandr Tymchenko, Katedra Inżynierii Bezpieczeństwa, Uniwersytet Warmińsko-Mazurski w Olsztynie, ul. Oczapowskiego 11, 10-719 Olsztyn, phone: 89 524 61 25

Optical recognition systems can generally recognize high quality images with high enough precision. However, if an image has some distortions (this problem is very often found in photographed text documents), the quality of recognition is considerably worsened and, sometimes, the process of recognition becomes generally impossible. Such images need previous geometrical correction of existing distortions to ensure that the lines of text on the image are direct and horizontal.

The existing methods (MASALOVICH 2007, FU et al. 2007, YIN et al. 2007) are based on certain models distortion document and depend on the type of distortion (distortion types discussed below). First out some text lines and text lines distortion function is constructed on the image. Then, based on this information, there is straightening the image. If only geometric distortions present in the document (when scanning thick books), then the total distortion function documents are taking from information of distortions of two text lines and build a linear approximation between them (FU et al. 2007). If there are only perspective distortions on the image, then it is enough to find the point of intersection of the lines on the image (YIN et al. 2007). To find the point of intersection is possible to construct a linear approximation for each word in the image and find the point at which intersect the continuation of all received segments. All of analyzes methods have their drawbacks, are not universal and can be used in the case when only one of all the types of distortion are on the image. Therefore, recognition of distorted test documents remains an actual problem.

Types of distortions. Maximal possibilities of the optical character recognition systems

To allow this recognition system to recognize a text document image without errors, all text lines must be straight and horizontal. However, after scanning or photographing there are often problems which can result in a worsening of image quality and the recognition will become impossible. Several algorithm is a result of recognition:

1) A skewed page which is characterized by the turning of all of the text lines towards a corner. Such curvature can appear as a result of unequal position of a document in a scanner.

2) Geometrical distortions can appear during the scanning of thick books in the area of the bend of a book.

If an image is acquired by a digital photocamera, except for previous problems, there can be perspective distortions and more difficult geometrical distortions, related to inequality of the initial document (incurving, concavity, etc.) which is hard to predict.

As shown in Figure 1*a*, an image defect usually takes a place when the image plane of a digital camera (R) is parallel with the document (plane D). If the image plane of camera R is not parallel to plane (D), perspective distortions appear, as shown in Figure 1*a*. Geometrical distortions appear when scanning or photographing thick books (in the area of the bend), when a text is placed on a smoothly curved and not flat surface (Fig 1*b*).

Note that there are not only damaged documents considered in this paper; distortion in scanning documents related with damage of a document eg. crease or tear are not analyzed.

From OCR Software rating (OCR Software Review, on line) for test we selected such OCR programs as OmniPage, ABBY FineReader and Rediris. Based on experimental studies, the maximal recognition possibilities of the disfigured texts in this system are:

1) Distortion of image. ABBY FineReader and Rediris recognizes images, where the angle between the horizontal line of image and the line of text is less than 25 degrees. If this angle is more than 25 degrees, the system does not recognize an image and reports an error (it did not find text characters in the image); pretreatment of the image is needed. OmniPage corrects documents with any angle of text strings and recognizes characters with almost no mistakes.

2) Perspective and geometrical deformation. All systems recognizes an image with a great amount of errors. The quality of recognition is poor.

None of this programs cannot correct non-linear distortion. So, it is obvious that for high-quality character recognition of a text document, pretreatment of such images is necessary.

Definition of the mathematical problem of straightening text lines

The task of straightening text lines in the picture is formulated as follows (MASALOVICH 2007):

If an image I is given on rectangular area $m \times n$, the image can belong to the plural of images with the distorted lines $£_{\text{damaged}}$ or to the plural of images without distortions of lines $£_{\text{normal}}$. It is necessary to build a reflection ϕ of source image I, to get such an image $\bar{I}$, that will satisfy the following terms:

1) if the initial image lines were distorted, on a regenerated image, where lines are practically level, the quality of recognition must be better by far, than on the initial;

2) if there were direct lines on an initial image, the regenerated image quality of recognition must be not worse than on the initial image.

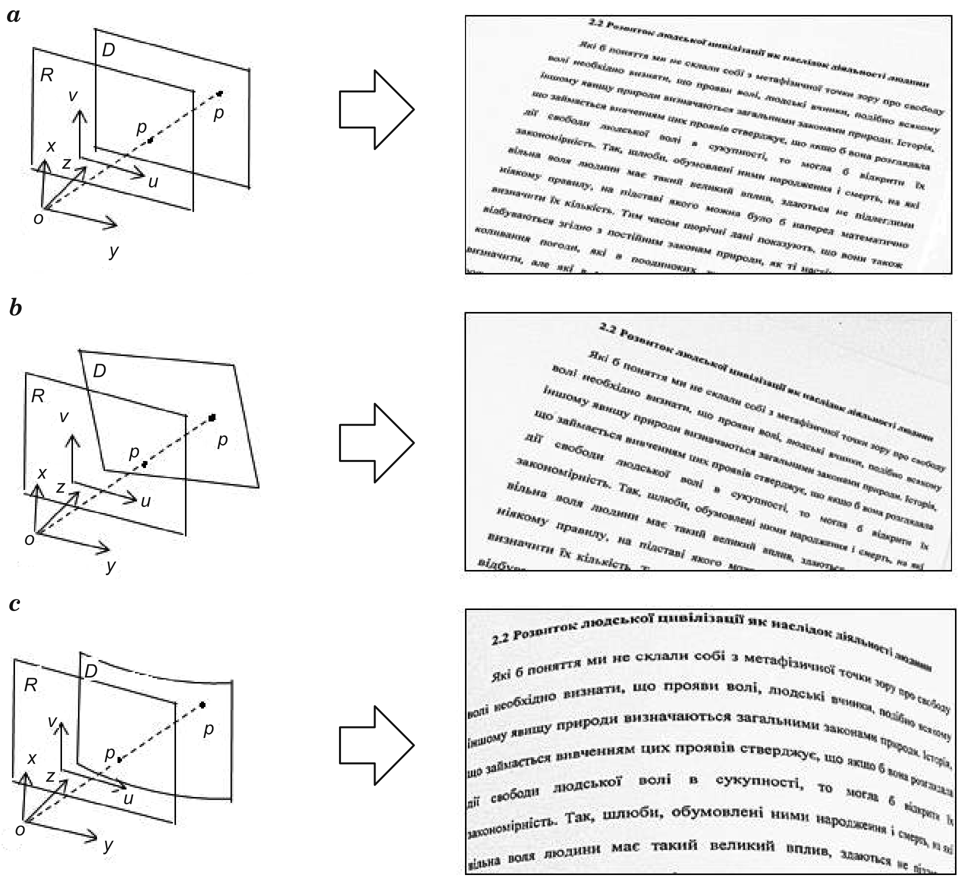

Fig. 1. Issues of the image projections

The digital image can be represented as a rectangular matrix of size $m \times n$. Each element of the matrix (pixel) a_{ij}, $i = \{1, ..., m\}$, $j = \{1, ..., n\}$ is a color in the corresponding image point. If the image is binary, then $a_{ij} = \{1,0\}$ [6,7].

The task of straightening the text lines can be described by the following mathematical formula:

$$\bar{I} = \Phi^{-1}\,(I) = \{\bar{C}(x,y) = C(\Phi_x(x,y),\ \Phi_y(x,y))\} \tag{1}$$

$C{:}R^2 \rightarrow \{0;\ 1\}$ – presentation of binary image I is as a two – dimensional function of color

$$C(x,y) = \begin{cases} 1, & if\, x < 0 \wedge x > m \wedge y < 0 \wedge y > n \\ 0, & if a_{ij} = \text{white};\ i = [x], j = [y] \\ 1, & if a_{ij} = \text{black};\ i = [x], j = [y] \end{cases} \tag{2}$$

$\Phi(t, u)$: $R^2 \rightarrow R^2$ – function of image transformation:

$$\Phi(t, u) = \begin{cases} \Phi_x\ (t, u) \\ \Phi_y\ (t, u) \end{cases};\ \Phi_x\ (t, u): R^2 \rightarrow R,\ \Phi_y\ (t, u): R^2 \rightarrow R \tag{3}$$

The ultimate goal of every text document image distortion correction algorithm is improvement of the results of recognition of the corrected image. As it is impossible to create an ideal initial document, the efficiency of the straightening limits are estimated with segments, by algorithm will accept a value which equals the difference between a value which determines the quality of text recognition before the straightening of text lines and a value which determines the quality of text recognition after straightening text lines.

Correction method by the construction of a page surface transformation model

It is necessary to build a model of transformation to represent the projection of an extended surface in a two-dimensional rectangular area. To find the projection of an extended surface it is necessary to estimate the text limits of the document. The left and right text limits are estimated using segments by the least-squares method, which base on of all of the discovered most left/right points, except for those points of text lines which do not begin from the beginning of document (titles, cross-headings). For the estimation of the highest and lowest bound of text, the polynomial of the third degree least-squares method is also utilized.

Thus, we will have two segments-off: AD, which relies on the left text bound

$$y = a_l x + b_l \tag{4}$$

and BC, that relies on the right limit of text

$$y = a_r x + b_r \tag{5}$$

the equation of the curved highest bound of text AB will look like:

$$y = a_{u1}x^3 + a_{u2}x^2 + a_{u3}x + a_{u4} \tag{6}$$

the same for curve BC:

$$y = a_{l1}x^3 + a_{l2}x^2 + a_{l3}x + a_{l4} \tag{7}$$

It is necessary to perform a transformation to represent the projection of the curved surface, limited by curves AB, DC and by lines AD, BC in a two-dimensional rectangular area. Let the $A'(x'_1,y'_1)$, $B'(x'_2,y'_2)$, $C'(x'_3,y'_3)$, $D'(x'_4,y'_4)$ – angular points of rectangular area (Fig. 2). Let $|\widehat{AB}|$ be length of arc between points A and B, $|AB|$ – Euclidean distance [8] between points A and B.
Width W of the rectangular area determined as:

$$W = \min\left(|\widehat{AB}|,\ |\widehat{DC}|\right) \tag{8}$$

Height H of the rectangular area equals:

$$H = \min\left(|AD|,\ |BC|\right) \tag{9}$$

In our example, (Fig. 2) $W = |\widehat{AB}|$, $H = |AD|$.

The angular points of the rectangular area are calculated as follows:

$$\left.\begin{array}{ll} x'_1 = x_1, & y'_1 = y_1 \\ x'_2 = x'_1, + W, & y'_2 = y'_1 \\ x'_3 = x'_2, & y'_3 = y'_2 + H \\ x'_4 = x'_1, & y'_4 = y'_3 \end{array}\right\} \tag{10}$$

The function Φ now creates the accordance between curves AB and DC.

$$\Phi(E(x_u,y_u)) = G(x_l,y_l), \text{ if } \frac{|\widehat{AE}|}{|\widehat{AB}|} = \frac{|\widehat{DG}|}{|\widehat{DC}|} \tag{11}$$

Where $E(x_u,y_u)$ – is a point-on curve AB, $G(x_l,y_l)$ – is a point-on-curve DC

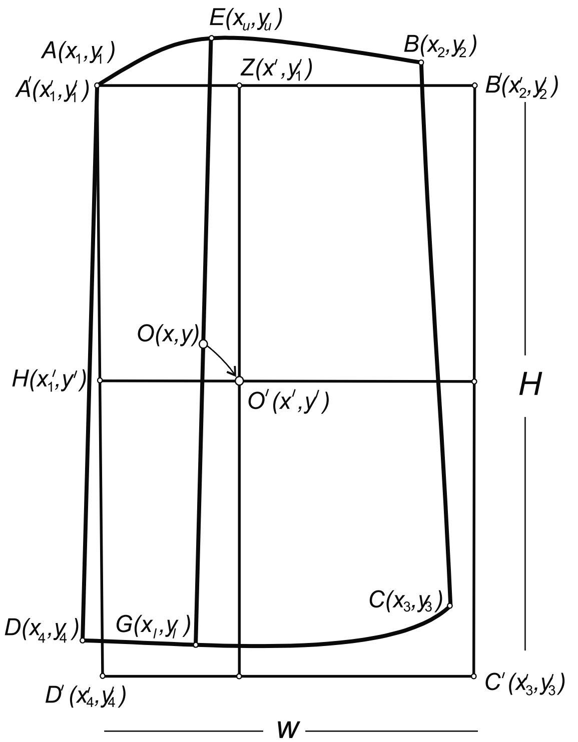

Fig. 2. Projection of curved surface

All points from the projection of curved surface determine the new position. Let $O(x,y)$ be a point on the projection of a curved surface. Our task is to define the new position $O'(x',y')$ of point $O(x,y)$ (Fig. 2).

First, we will define a line EG, which satisfies the next terms:

1. It crosses points $E(x_u,y_u)$, $G(x_l,y_l)$ that lie on curves AB and DC, accordingly.
2. $\Phi\ (E(x_u,y_u)) = G(x_l,y_l)$
3. Point $O(x,y)$ belongs to the line EG.

Farther calculate position $O'(x',y')$:

$$x' = x'_1 + |A'Z| \tag{12}$$

$$y' = y'_1 + |A'H| \tag{13}$$

where H – is a point $H(x'_1,y')$ Z – is a point $Z(x',y'_1)$. The lengths of segments $|A'Z|$, $|A'H|$ are calculated as follows:

$$\frac{|\widehat{AB}|}{|\widehat{AE}|} = \frac{W}{|A'Z|} \Rightarrow |A'Z| = \frac{W}{|\widehat{AB}|}\,|\widehat{AE}| \tag{14}$$

$$\frac{|EG|}{|EO|} = \frac{H}{|A'H|} \Rightarrow |A'H| = \frac{H}{|EG|}\,|EO| \tag{15}$$

Repeat this sequence of executions for all points from the projection of a curved surface. If a point is out of an area, it accepts transformation of the nearest point.

Figure 3 shows the experimental application of this method to images taken with a digital camera (with geometric distortion).

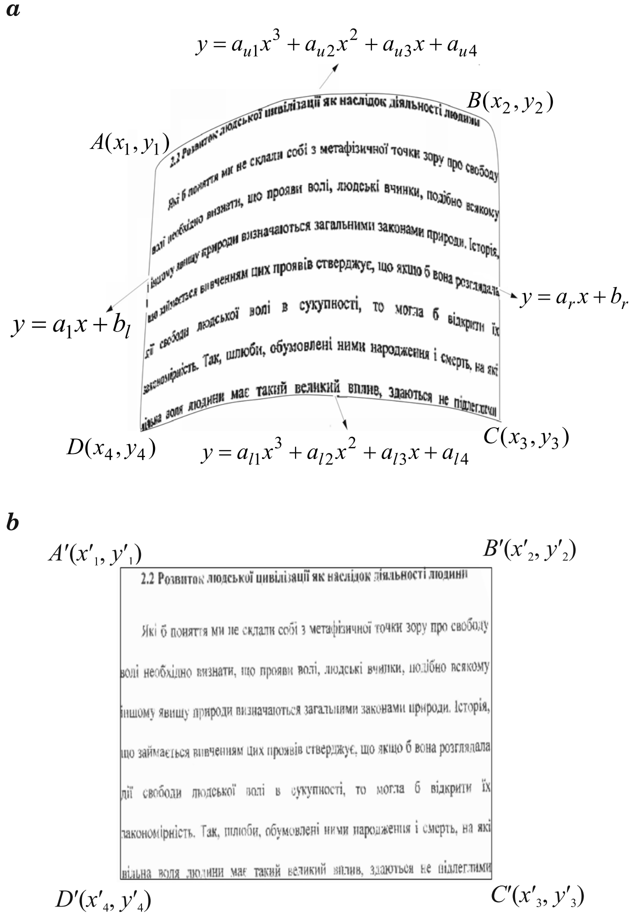

Fig. 3. Example of dewarping image: *a* – extraction of curved surface projection, *b* – corrected image

Conclusion

All of types of distortions which can arise on a text document image are analyzed in this article. If there are only perspective distortions or the problem of a page defect on the image, after a prognostication model of the curvature of all of lines of phototypography it is possible to align text strings (YIN et al. 2007). However, various heterogeneous distortions can appear in the photography of a text image. They can carry an arbitrary form and differ within the bounds of one page, or one line. For example, a page can be curved from one side, and curved inwards from other, with the different angles of slope and yet, despite this, there can be perspective distortions. Thus, it is hard to predict the model of distortion. The described method is universal and does not depend on the type of distortion. It is necessary to develop software on the basis of the described algorithm to define the efficiency of its application to the images with arbitrary heterogeneous line curvatures.

References

ARMS W. 2000. *Digital Libraries*. M.I.T. Press. On line: http://www.cs.cornell.edu/wya/diglib/ (access: October 2014).

FU B., WU M., LI R., LI W., XU Z., YANG CH., 2007. *A model based book dewarping method using text line detection*. Proceedings of the Second International Workshop on Camera-Based Document Analysis and Recognition (CBDAR-2007), Curitiba, pp. 63–70. On line: http://imlab.jp/cbdar2007/proceedings/papers/P1.pdf (access: October 2014).

JÄHNE B. *Digital image processing*. 2002. Springer, Berlin, p. 29. On line: http://cgrava.webhost.uoradea.ro/teaching/PAI/documentatie/Jahne_Digital_Image-Processing.pdf (access: October 2014).

MARTI U.V. 2001. *Using a statistical language model to improve the performance of an HMM-based cursive handwriting recognition system*. Int. Journal of Pattern Recognition and Artifical Intelligence, 15(1): 65–90.

MASALOVICH A.A. 2007. *Use of patch Bez;e for approximation of distortion of text documents*. In: // Labours 17 International Conference on Computer Graphics and Sight. Ed. A.A.Masalovich, L.M. Mesteckiy. Grafikon, Moscow. On line: http://www.machinelearning.ru/wiki/images/a/a2/Gr–2007-Masalovich.pdf (access: October 2014).

OCR Software Review. On line: http://ocr-software-review.toptenreviews.com (access: October 2014).

PRATT W. 2007. *Digital image processing*. Fourth edition. PixelSoft, Inc. Los Altos, California. A Wiley-Interscience Publication, pp. 91–99. On line: https://docs.google.com/file/d/0B30qTepNcnnAOGhlOUQ4Z1o1Sm8/edit (access: October 2014).

YIN X.-C., SUN J., NAOI S. 2007. *Perspective rectification for mobile phone camera-based documents using a hybrid approach to vanishing point detection*. Proceedings of the Second International Workshop on Camera-Based Document Analysis and Recognition (CBDAR-2007), Curitiba, pp. 37–44.

Reviewers of Years – book 2015

Aivars Aboltins
Petar Agatonović
Viorel Badescu
Alaa El-Din A. Bekhit
Mariana Belgiu
Ireneusz Białobrzewski
Lukasz K. Bonenberg
Shyam S. Chandel
Andrzej Chochowski
Armands Celms
Davide Ciucci
Neringa Dirgllienl
Tomas Dolansky
Jerzy Domański
Ch'ng Pei Eng
Adriana Estokova
Adam Figiel
Jarosław Frączek
Urszula Gałązka
Stig Geving
Pierre Grussenmeyer
Raquel P.F. Guiné
Klaus Hanke
Christopher Henry
Józef Horabik
Josef Jansa
Agnieszka Kaleta
Yevhen Kharchenko
Hakan Kibar
Jan Krzysztoforski
Krystyna Kurowska
Thomas Lampoltshammer
Cosmin Marculescu
Kaisa Matschoss
Fan Min
Krzysztof Nalepa
Bartosz Nowak
Krzysztof Pancerz
Józef Pelc
Zbigniew Popek
Rama Chandra Pradham
Ekateryna K. Pushkarova
Krystian Pyka
Elżbieta Radziszewska
Ahmet Sivacioğlu
Adnan Sözen
Czesław Suchocki
Dominik Ślęzak
Juha Vinha
Vinita Vishwakarma
Paweł Wielgosz
Agnieszka Wierzbicka
Jing Tao Yao
Agnieszka Zalejska-Jonsson
Xianyong Zhang
Martin Ziegler
Beata Zielosko

Guide for Autors

Introduction

Technical Sciences is a peer-reviewed research Journal published in English by the Publishing House of the University of Warmia and Mazury in Olsztyn (Poland). Journal is published continually since 1998. Until 2010 Journal was published as a yearbook, in 2011 and 2012 it was published semiyearly. From 2013, the Journal is published quarterly in the spring, summer, fall, and winter.

The Journal covers basic and applied researches in the field of engineering and the physical sciences that represent advances in understanding or modeling of the performance of technical and/or biological systems. The Journal covers most branches of engineering science including biosystems engineering, civil engineering, environmental engineering, food engineering, geodesy and cartography, information technology, mechanical engineering, materials science, production engineering etc.

Papers may report the results of experiments, theoretical analyses, design of machines and mechanization systems, processes or processing methods, new materials, new measurements methods or new ideas in information technology.

The submitted manuscripts should have clear science content in methodology, results and discussion. Appropriate scientific and statistically sound experimental designs must be included in methodology and statistics must be employed in analyzing data to discuss the impact of test variables. Moreover there should be clear evidence provided on how the given results advance the area of engineering science. Mere confirmation of existing published data is not acceptable. Manuscripts should present results of completed works.

There are three types of papers: a) research papers (full length articles); b) short communications; c) review papers.

The Journal is published in the printed and electronic version. The electronic version is published on the website ahead of printed version of Technical Sciences.

Technical Sciences does not charge submission or page fees.

Types of paper

The following articles are accepted for publication:

Reviews

Reviews should present a focused aspect on a topic of current interest in the area of biosystems engineering, civil engineering, environmental engineering, food engineering, geodesy and cartography, information technology, mechanical engineering, materials science, production engineering etc. They should include all major findings and bring together reports from a number of sources. These critical reviews should draw out comparisons and conflicts between work, and provide an overview of the 'state of the art'. They should give objective assessments of the topic by citing relevant published work, and not merely present the opinions of individual authors or summarize only work carried out by the authors or by those with whom the authors agree. Undue speculations should also be avoided. Reviews generally should not exceed 6,000 words.

Research Papers

Research Papers are reports of complete, scientifically sound, original research which contributes new knowledge to its field. Papers should not exceed 5,000 words, including figures and tables.

Short Communications

Short Communications are research papers constituting a concise description of a limited investigation. They should be completely documented, both by reference list, and description of the experimental procedures. Short Communications should not occupy more than 2,000 words, including figures and tables.

Letters to the Editor

Letters to the Editor should concern with issues raised by articles recently published in scientific journals or by recent developments in the engineering area.

Contact details for submission

The paper should be sent to the Editorial Office, as a Microsoft Word file, by e-mail: techsci@uwm.edu.pl

Referees

Author/authors should suggest, the names, addresses and e-mail addresses of at least three potential referees. The editor retains the sole right to decide whether or not the suggested reviewers are used.

Submission declaration

After final acceptance of the manuscript, the corresponding author should send to the Editorial Office the author's declaration. Submission of an article implies that the work has not been published previously (except in the form of an abstract or as part of a published lecture or academic thesis or as an electronic preprint), that it is not under consideration for publication elsewhere, that publication is approved by all authors and tacitly or explicitly by the responsible authorities where the work was carried out, and that, if accepted, it will not be published elsewhere in the same form, in English or in any other language.

To prevent cases of ghostwriting and guest authorship, the author/authors of manuscripts is/are obliged to: (i) disclose the input of each author to the text (specifying their affiliations and contributions, i.e. who is the author of the concept, assumptions, methods, protocol, etc. used during the preparation of the text); (ii) disclose information about the funding sources for the article, the contribution of research institutions, associations and other entities.

Language

Authors should prepare the full manuscript i.e. title, abstract and the main text in English (American or British usage is accepted). Polish version of the manuscript is not required.

The file type

Text should be prepared in a word processor and saved in doc or docx file (MS Office).

Article structure

Suggested structure of the manuscript is as follows:

Title
Authors and affiliations
Corresponding author
Abstract
Keywords
Introduction
Material and Methods
Results and Discussion
Conclusions

Acknowledgements (*optional*)
References
Tables
Figures

Subdivision – numbered sections

Text should be organized into clearly defined and numbered sections and subsections (optionally). Sections and subsections should be numbered as 1. 2. 3. then 1.1 1.2 1.3 (then 1.1.1, 1.1.2, ...). The abstract should not be included in numbering section. A brief heading may be given to any subsection. Each heading should appear on its own separate line. A single line should separate paragraphs. Indentation should be used in each paragraph.

Font guidelines are as follows:
– Title: 14 pt. Times New Roman, bold, centered, with caps
– Author names and affiliations:12 pt. Times New Roman, bold, centered, italic, two blank line above
– Abstract: 10 pt. Times New Roman, full justified, one and a half space. Abstract should begin with the word Abstract immediately following the title block with one blank line in between. The word Abstract: 10 pt. Times New Roman, centered, indentation should be used
– Section Headings: Not numbered, 12 pt. Times New Roman, bold, centered; one blank line above
– Section Sub-headings: Numbered, 12 pt. Times New Roman, bold, italic, centered; one blank line above
– Regular text: 12 pt. Times New Roman, one and a half space,full justified, indentation should be used in each paragraph

Title page information

The following information should be placed at the first page:

Title

Concise and informative. If possible, authors should not use abbreviations and formulae.

Authors and affiliations

Author/authors' names should be presented below the title. The authors' affiliation addresses (department or college; university or company; city, state and zip code, country) should be placed below the names. Authors with the same affiliation must be grouped together on the same line with affiliation information following in a single block. Authors should indicate all affiliations with a lower-case superscript letter immediately after the author's name and in front of the appropriate address.

Corresponding author

It should be clearly indicated who will handle correspondence at all stages of refereeing and publication, also post-publication process. The e-mail address should be provided (footer, first page). Contact details must be kept up to date by the corresponding author.

Abstract

The abstract should have up to 100-150 words in length. A concise abstract is required. The abstract should state briefly the aim of the research, the principal results and major conclusions. Abstract must be able to stand alone. Only abbreviations firmly established in the field may be eligible. Non-standard or uncommon abbreviations should be avoided, but if essential they must be defined at their first mention in the abstract itself.

Keywords

Immediately after the abstract, author/authors should provide a maximum of 6 keywords avoiding general, plural terms and multiple concepts (avoid, for example, 'and', 'of'). Author/authors should be sparing with abbreviations: only abbreviations firmly established in the field may be eligible.

Abbreviations

Author/authors should define abbreviations that are not standard in this field. Abbreviations must be defined at their first mention there. Author/authors should ensure consistency of abbreviations throughout the article.

Units

All units used in the paper should be consistent with the SI system of measurement. If other units are mentioned, author/authors should give their equivalent in SI.

Introduction

Literature sources should be appropriately selected and cited. A literature review should discuss published information in a particular subject area. Introduction should identify, describe and analyze related research that has already been done and summarize the state of art in the topic area. Author/authors should state clearly the objectives of the work and provide an adequate background.

Material and Methods

Author/authors should provide sufficient details to allow the work to be reproduced by other researchers. Methods already published should be indicated by a reference. A theory should extend, not repeat, the background to the article already dealt within the Introduction and lay the foundation for further work. Calculations should represent a practical development from a theoretical basis.

Results and Discussion

Results should be clear and concise. Discussion should explore the significance of the results of the work, not repeat them. A combined Results and Discussion section is often appropriate.

Conclusions

The main conclusions of the study may be presented in a Conclusions section, which may stand alone or form a subsection of a Results and Discussion section.

Acknowledgements

Author/authors should include acknowledgements in a separate section at the end of the manuscript before the references. Author/authors should not include them on the title page, as a footnote to the title or otherwise. Individuals who provided help during the research study should be listed in this section.

Artwork
General points

– Make sure you use uniform lettering and sizing of your original artwork
– Embed the used fonts if the application provides that option

– Aim to use the following fonts in your illustrations: Arial, Courier, Times New Roman, Symbol
– Number equations, tables and figures according to their sequence in the text
– Size the illustrations close to the desired dimensions of the printed version

Formats

If your electronic artwork is created in a Microsoft Office application (Word, PowerPoint, Excel) then please supply ‘as is’ in the native document format

Regardless of the application used other than Microsoft Office, when your electronic artwork is finalized, please ‘Save as’ or convert the images to one of the following formats (note the resolution requirements given below):

EPS (or PDF): Vector drawings, embed all used fonts

JPEG: Color or grayscale photographs (halftones), keep to a minimum of 300 dpi

JPEG: Bitmapped (pure black & white pixels) line drawings, keep to a minimum of 1000 dpi or combinations bitmapped line/half-tone (color or grayscale), keep to a minimum of 500 dpi

Please **do not**:
– Supply files that are optimized for screen use (e.g., GIF, BMP, PICT, WPG); these typically have a low number of pixels and limited set of colors
– Supply files that are too low in resolution
– Submit graphics that are disproportionately large for the content

Color artwork

Author/authors should make sure that artwork files are in an acceptable format (JPEG, EPS PDF, or MS Office files) and with the correct resolution. If, together with manuscript, author/authors submit color figures then Technical Sciences will ensure that these figures will appear in color on the web as well as in the printed version at no additional charge.

Tables, figures, and equations

Tables, figures, and equations/formulae should be identified and numbered consecutively in accordance with their appearance in the text.

Equations/mathematical and physical formulae should be presented in the main text, while tables and figures should be presented at the end of file (after References section). Mathematical and physical formulae should be presented in the MS Word formula editor.

All types of figures can be black/white or color. Author/authors should ensure that each figure is numbered and has a caption. A caption should be placed below the figure. Figure must be able to stand alone (explanation of all symbols and abbreviations used in figure is required). Units must be always included. It is noted that figure and table numbering should be independent.

Tables should be numbered consecutively in accordance with their appearance in the text. Table caption should be placed above the table. Footnotes to tables should be placed below the table body and indicated with superscript lowercase letters. Vertical rules should be avoided. Author/authors should ensure that the data presented in tables do not duplicate results described in figures, diagrams, schemes, etc. Table must be able to stand alone (explanation of all symbols and abbreviations used in table is required). Units must be always included. As above, figure and table numbering should be independent.

References

References: All publications cited in the text should be presented in a list of references following the text of the manuscript. The manuscript should be carefully checked to ensure that the spelling of authors' names and dates of publications are exactly the same in the text as in the reference list. Authors should ensure that each reference cited in the text is also present in the reference list (and vice versa).

Citations may be made directly (or parenthetically). All citations in the text should refer to:

1. Single author

The author's name (without initials, with caps, unless there is ambiguity) and the year of publication should appear in the text

2. Two authors

Both authors' names (without initials, with caps) and the year of publication should appear in the text

3. Three or more authors

First author's name followed by et al. and the year of publication should appear in the text

Groups of references should be listed first alphabetically, then chronologically.

Examples:

"... have been reported recently (ALLAN, 1996a, 1996b, 1999; ALLAN and JONES, 1995). KRAMER et al. (2000) have recently shown..."

The list of references should be arranged alphabetically by authors' names, then further sorted chronologically if necessary. More than once reference from the same author(s) in the same year must be identified by the letters "a", "b", "c" etc., placed after the year of publication.

References should be given in the following form:

KUMBHAR B.K., AGARVAL R.S., DAS K. 1981. *Thermal properties of fresh and frozen fish*. International Journal of Refrigeration, 4(3), 143–146.

MACHADO M.F., OLIVEIRA F.A.R., GEKAS V. 1997. *Modelling water uptake and soluble solids losses by puffed breakfast cereal immersed in water or milk*. In Proceedings of the Seventh International Congress on Engineering and Food, Brighton, UK.

NETER J., KUTNER M.H., NACHTSCHEIM C.J., WASSERMAN W. 1966. *Applied linear statistical models* (4th ed., pp. 1289–1293). Irwin, Chicago.

THOMSON F.M. 1984. *Storage of particulate solids*. In M. E. Fayed, L. Otten (Eds.), Handbook of Powder Science and Technology (pp. 365–463). Van Nostrand Reinhold, New York.

Citation of a reference as 'in press' implies that the item has been accepted for publication.

Note that the full names of Journals should appear in reference list.

Submission checklist

The following list will be useful during the final checking of an article prior to the submission. Before sending the manuscript to the Journal for review, author/authors should ensure that the following items are present:

– Text is prepared with a word processor and saved in DOC or DOCX file (MS Office). One author has been designated as the corresponding author with contact details: e-mail address

– Manuscript has been 'spell-checked' and 'grammar-checked'

– References are in the correct format for this Journal

– All references mentioned in the Reference list are cited in the text, and vice versa

– Author/authors does/do not supply files that are too low in resolution

– Author/authors does/do not submit graphics that are disproportionately large for the content